

https://dspace.org/

Design, construction and calibration of a transonic wind tunnel

Nash, Jonathan

2013-01-31
http://hdl.handle.net/10539/12351

Downloaded from a DSpace repository. https://dspace.org/

DESIGN, CONSTRUCTION AND CALIBRATION OF A TRANSONIC WIND TUNNEL

Jonathan Nash

A dissertation submitted to the Faculty of Engineering and the Built Environment, University of the Witwatersrand, in fulfilment of the requirements for the degree of Master of Science in Engineering.

Johannesburg, 2012

Declaration

I declare that this dissertation is my own, unaided work, except where otherwise acknowledged. It is being submitted for the degree of Master of Science in Engineering at the University of the Witwatersrand, Johannesburg. It has not been submitted before for any degree or examination at any other university.

Signed on this the _____ day of _____

_____

Jonathan Nash

Abstract

A transonic wind tunnel was designed, constructed and calibrated in order to provide a valuable tool for the study of transonic flow phenomena. The wind tunnel makes use of flow properties surrounding the propagation of a shock wave along a tube in order to create the transonic flow. As a result, the wind tunnel is a modified shock tube, with its layout being optimised for maximum flow time. The flow times are dependent on the Mach number of the transonic flow being created, with the longest realistic flow time being approximately sixty milliseconds. The majority of the shock tube was built from commercially available steel construction tubing which was then attached to a pressure vessel of similar cross sectional dimension. A test section containing windows was constructed and placed in a position along the length of the tube to maximise the available test flow time. The position optimisation was calculated based on standard shock wave theory. The incident shock wave, as well as any resulting flow features, were visualised using schlieren photography. The test piece was designed to be set at angles of attack of up to ten degrees, both positive and negative. The main purpose of the testing carried out was to validate the functioning of the wind tunnel rather than obtaining more data on the test piece. An RAE2822 aerofoil was used as the test piece due to the large amount of aerodynamic data available on it, especially in the transonic flow region, thus making it an excellent tool for validation. In addition, the Fluent computational fluid dynamics package made use of the same aerofoil to validate their numerical results when the package was under development. This meant that for any numerical result obtained for the RAE2822 aerofoil using the Fluent package, there was a high degree of confidence. This fact provided a great tool for comparing results obtained experimentally in the wind tunnel with results obtained numerically. The short duration testing time was found to be adequate for establishing semi-steady state flow at any transonic flow Mach number. The bursting of the weak diaphragm at the end of the driven section of the shock tube resulted in the upstream propagation of a disturbance with a much lower velocity than would be seen if the incident shock wave reflected off a solid boundary and thus its arrival at the test section was delayed, resulting in a significant increase in testing time.

The results obtained experimentally compared well to results obtained numerically. Transonic shock waves that were set up on the test piece had very similar shapes, features and chord-wise positions in both experimental and numerical results, showing that the geometric layout of the test section was correct. Furthermore, it was shown that a short duration flow time wind tunnel could be constructed using a shock tube and that accurate results could be obtained through its use.

Acknowledgements

I would like to thank Professor Beric Skews for his excellent supervision, guidance and advice during the research carried out as well as for allowing me to present the research at the International Aerospace Symposium of Southern Africa, 2011.

Dimmy Smith and Marius van Vyk went out of their way to assist in the manufacture and construction of the facilities.

I would also like to thank the National Research Foundation for helping fund my research.

Table of Contents

Declaration ..... **i**

Abstract ..... **ii**

Acknowledgements ..... **iii**

Table of Contents ..... **iv**

List of Figures ..... **vi**

List of Tables ..... **x**

List of Symbols ..... **xi**

1 Introduction **1**

2 Literature Review **8**

2.1 Types of Shock Waves **8**
2.1.1 Normal shock waves 9
2.1.2 The oblique shock wave 12
2.1.3 Transonic shock waves and their resulting features 13

2.2 The shock tube **16**

2.3 Schlieren Imaging Technique **17**

3 Objectives **20**

4 Design of the Transonic Shock Tube **21**

4.1 Design Constraints Based on Existing Resources **21**

4.2 Design of the Partially Open Walls **22**

4.3 Design of the Test Section **24**
4.3.1 The plenum chamber 25
4.3.2 The window and door 27
4.3.3 Test section body 32
4.3.4 Upstream cleanup section 34
4.3.5 Vacuum seal system for the end of the shock tube 36

4.4 Final Test Section Layout and Specifications **37**

4.5 Design of the Test Piece **39**

4.6 Design Optimisation Using Kasimir3 ..... **45**

4.7 Instrumentation **51**

5 Calibration 52

5.1 Diaphragm Thickness versus Pressure Ratio 52
5.1.1 Pneumatic pricker 53
5.1.2 Second diaphragm station 53

5.2 Pressure Ratio versus Mach Number 54
5.2.1 Examining joint losses 55

6 Testing Procedure and Precautions 60

6.1 Test Section Set Up Procedure 60

6.2 Test Piece Set Up Procedure 61

6.3 Shock Tube Set Up Procedure 63

6.4 Optics Set Up 64

6.5 Data Acquisition System Set Up 64

6.6 General Set Up Precautions 64

6.7 Testing Procedure 65

7 Results 67

7.1 Computational Fluid Dynamics 67
7.1.1 Numerical Results 69
7.1.2 Fluent Results Validation 70

7.2 Wind Tunnel Test Results 72
7.2.1 Initial Photographs 74
7.2.2 Testing at Mach 0.83 76
7.2.3 Testing at Mach 0.73 106
7.2.4 Testing at Mach 0.91 110
7.2.5 Predicted versus actual testing time 114

8 Conclusions 118

References 123

List of Figures

Figure 1.1 Aerofoil in free flight....2

Figure 1.2 Aerofoil in a closed wall wind tunnel....2

Figure 1.3 Aerofoil in an open-jet wind tunnel....2

Figure 1.4 Schematic of a typical shock tube wave diagram....5

Figure 1.5 Graph of shock Mach number versus flow Mach number....6

Figure 2.1 Normal shock wave with different reference frames....9

Figure 2.2 Oblique shock wave....12

Figure 2.3 Normal shock wave without boundary layer separation....14

Figure 2.4 Normal shock wave with boundary layer separation....15

Figure 2.5 Schematic layout of a shock tube before (a) and after (b) diaphragm rupture....16

Figure 2.6 Typical Z-shape schlieren system layout bent through 90˚....18

Figure 4.1 CFD of perforated wall concept at Mach 0.83 over half of a diamond shaped aerofoil 23

Figure 4.2 Plenum chamber concepts, with solid and bar slots....25

Figure 4.3 Plenum chamber with 10% open and 50% open wall slots....26

Figure 4.4 Plenum chamber with 50% open walls showing supports....26

Figure 4.5 Original high optical quality window frame....27

Figure 4.6 New Perspex window mounting system....28

Figure 4.7 Door clamping system....30

Figure 4.8 Step machined into the perspex window....31

Figure 4.9 Outside view of door frame with hinge system....32

Figure 4.10 Side wall with door recess and mounting holes 33

Figure 4.11 O-ring grooves, dowel and bolt holes for alignment and sealing 34

Figure 4.12 Cleanup section with channel sides and plate top and bottom 35

Figure 4.13 Final test section with wall removed for clarity 37

Figure 4.14 Basic dimensions of the final test section 38

Figure 4.15 Test section after manufacture 38

Figure 4.16 RAE 2822 Profile 39

Figure 4.17 Proposed method of mounting the aerofoil 41

Figure 4.18 Test piece mounting layout 42

Figure 4.19 Aerofoil with wedge cut-outs for the uprights 43

Figure 4.20 Final test piece layout for upper and lower surface testing 44

Figure 4.21 Test piece mounted into the test section with 50% open walls 45

Figure 4.22 3.4 meter driver at a flow Mach number of 0.83 46

Figure 4.23 9.4 meter driver at a flow Mach number of 0.83 47

Figure 4.24 15.4 meter driver at a flow Mach number of 0.83 47

Figure 4.25 Theoretical testing time 49

Figure 5.1 First shock wave image 58

Figure 6.1 Schematic layout of the control board 65

Figure 7.1 Layout of mesh 68

Figure 7.2 CFD at Mach 0.88 at 0º, 2.79º and 5º angle of attack 69

Figure 7.3 CFD at 2.79º at Mach 0.73, 0.83 and 0.93 70

Figure 7.4 Comparison of numerical and experimental pressure coefficient by Fluent 71

Figure 7.5 Mach 0.73 and 2.79˚ angle of attack 72

Figure 7.6 Shock tube start-up process 74

Figure 7.7 Pressure trace produced during testing at Mach 0.91 75

Figure 7.8 Example of joined image 76

Figure 7.9 Mach 0.83 at 2.79º with open walls 78

Figure 7.10 CFD at Mach 0.83 and 2.79º angle of attack 80

Figure 7.11 CFD Mach 0.83 overlaid onto experimental Mach 0.83 81

Figure 7.12 Overlay of different CFD Mach numbers onto Mach 0.83 experiment at 2.79º angle of attack 82

Figure 7.13 CFD at Mach 0.88 compared to experiment at 2.79º angle of attack (9-24ms) 83

Figure 7.14 CFD at Mach 0.88 compared to experiment at 2.79º angle of attack (27-45ms) 84

Figure 7.15 Mach 0.83 at 2.79º angle of attack with closed walls 86

Figure 7.16 Comparison of Mach 0.88 CFD to results at 10% and 50% open wall (5º angle of attack) 87

Figure 7.17 Pressure trace at Mach 0.83 and 2.79º angle of attack with open and closed walls ... 88

Figure 7.18 Mach 0.83 at 5º angle of attack with open walls 89

Figure 7.19 CFD at Mach 0.88 and 5º angle of attack 91

Figure 7.20 Overlay of different CFD Mach numbers onto Mach 0.83 experiment at 2.79º angle of attack 92

Figure 7.21 CFD at Mach 0.88 compared to experiment at 5º angle of attack 93

Figure 7.22 Mach 0.83 at 5º angle of attack with closed walls 96

Figure 7.23 Comparison of Mach 0.88 CFD with results at 10% and 50% open wall (5º angle of attack) 98

Figure 7.24 Pressure trace at Mach 0.83 and 5º aoa for open and closed walls 99

Figure 7.25 Mach 0.83 at 0º angle of attack with open walls 100

Figure 7.26 High contrast image showing wake region and lambda shock systems 101

Figure 7.27 CFD at Mach 0.88 and 0º angle of attack 102

Figure 7.28 Overlay of different CFD Mach numbers onto Mach 0.83 experiment at 0º angle of attack 103

Figure 7.29 CFD at Mach 0.88 compared with experiment at 0º angle of attack 104

Figure 7.30 Mach 0.73 at 2.79º angle of attack with open walls 106

Figure 7.31 CFD at Mach 0.75 and 2.79º angle of attack 107

Figure 7.32 Overlay of different CFD Mach numbers onto Mach 0.73 experiment at 2.79º angle of attack 108

Figure 7.33 CFD at Mach 0.75 compared to experiment at 2.79º angle of attack 109

Figure 7.34 Mach 0.91 at 2.79º angle of attack with open walls 111

Figure 7.35 Pressure trace overlay for testing at M0.91 and M0.83 113

Figure 7.36 Pressure trace for flow at M0.91 115

List of Tables

Table 4.1 Test section position versus driven section length 50

Table 5.1 Pressure ratio required to achieve a theoretical test Mach number 54

Table 5.2 Comparison of Mach numbers across joints 57

Table 7.1 Available CFD tests 68

Table 7.2 Summary of testing carried out 73

Table 7.3 Theoretical and experimental testing times 116

List of Symbols

M	Mach Number
v	Velocity (m/s)
p	Pressure (Pa)
T	Temperature (K)
ρ	Density (kg/m^3)
γ	Ratio of specific heats
V_s	Velocity of the shock wave (m/s)
M_s	Mach number of the shock wave
a	Local speed of sound (m/s)
R	Universal gas constant (kJ/kg K)
h	Specific enthalpy (kJ/kg)

1 Introduction

Wind tunnels have been used in various applications for many years. They range from extremely simple low speed to highly complex hypersonic versions, each having a specific purpose and specific limitations.

The vast majority of wind tunnels are in existence to recreate the flow of air expected around a body or object in a controlled environment. The purpose of wind tunnel testing is to better understand flow phenomena and forces that can be expected around that body when it is subjected to the conditions for which it is designed.

There are a wide variety of forms that wind tunnels can take, with each form providing specific advantages and disadvantages. However, with most wind tunnels a key objective in their design is to try and reproduce unbounded airflow such as that found when a body is exposed to airflow without nearby solid boundaries. In such a case, the streamlines around the body would bend and only become straight again at a theoretical infinite distance away. In a laboratory where space is limited there has to be a wind tunnel wall or some similar boundary at some finite distance from a test model which forces the streamlines to become straight again. As a result, a large amount of effort needs to be applied to wind tunnel design to ensure that these artificial boundaries have a minimal effect on the flow around the test piece and the data being collected.

Various methods have been used to achieve this result, although each method comes with related shortfalls.

Two types of wind tunnels, with different effects on the streamlines, are the closed wall wind tunnel and the open jet wind tunnel.

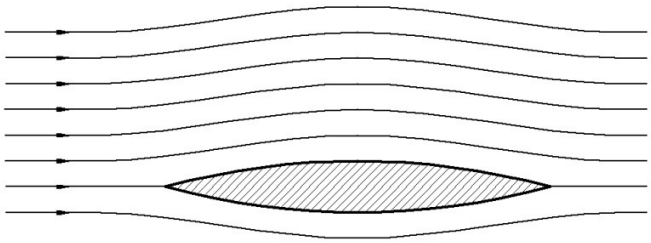


Figure 1.1 Aerofoil in free flight

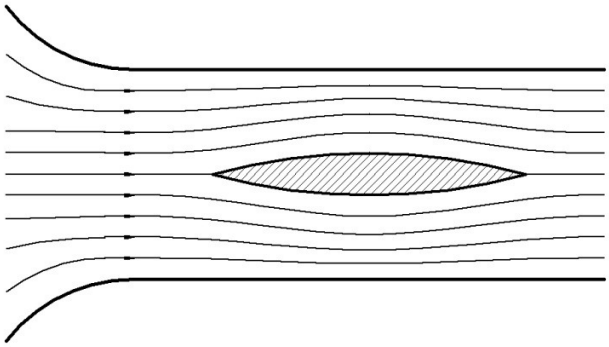


Figure 1.2 Aerofoil in a closed wall wind tunnel

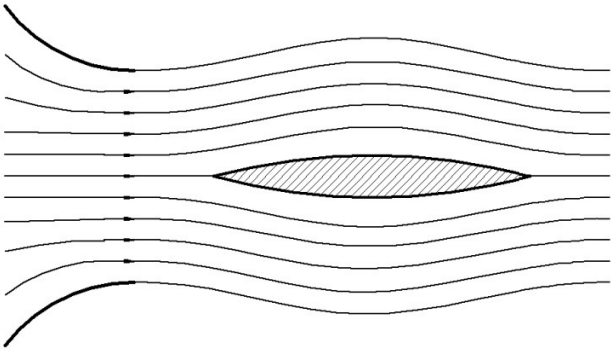


Figure 1.3 Aerofoil in an open-jet wind tunnel

In the case of the closed wind tunnel (Figure 1.2), streamlines around the body are forced to straighten out much faster because of the presence of the wall. At subsonic velocities this has an additional effect of increasing the flow velocity around the body, causing the need for a velocity correction to be used.

In the case of an open jet wind tunnel (Figure 1.3), the undisturbed free stream pressure is reached at the boundary of the jet which again happens much closer to the body than in the free flight condition. This tends to add extra curvature to the streamlines (Goethert, 1961).

The possibility of recreating the free flight streamlines with the correct shape in the wind tunnel arises by combining the two types to form a partially open wind tunnel

One way of achieving a partially open wind tunnel is by taking a closed wind tunnel and cutting slots into its walls. Through careful arrangement of the open and closed wall sections, the velocity correction and flow distortion resulting from the tunnel walls can be minimised, and possibly even eliminated all together. Slotted walls also help eliminate choking of the wind tunnel near Mach 1 (Goethert, 1961).

The number of open and closed sections (open area ratio), and thus slot width, must be chosen carefully depending on the cross sectional shape of the wind tunnel, as well as the type of model to be placed in the test section. It has been shown that a large number of thin slots provide an advantage over a small number of wide slots, but only to a point (Goethert, 1961).

In both the slotted and perforated wall case, there needs to exist a region of open space on the other side of the boundary in order to allow the shock cancellation effects to take place. This open region is known as the plenum chamber. It in effect creates an open test section where expansion waves can be formed in order for shock cancellation to take place. The plenum chamber is also responsible for effectively increasing the wind tunnel cross sectional area around the test piece and thus ensuring that the presence of the test piece does not result in the wind tunnel choking at high subsonic Mach number testing.

During wind tunnel testing at high subsonic, sonic, or supersonic flow velocities, shock waves can be formed. These shock waves can interfere with the flow around a model in a wind tunnel because they can reflect off the nearby wind tunnel wall. If the model is sufficiently short and the Mach number sufficiently high, the reflected wave will miss the model and only influence the downstream flow, but if the reflected wave does interact with the model, a non true to free flight condition arises.

This fact becomes a problem, especially around the region of Mach 1, and thus is of concern when dealing with transonic flow. At a Mach number of 1, the shock waves formed off a model will form at 90 degrees to the flow, and thus will extend to the wall and reflect back onto the model. Cancellation of this wave is necessary for accurate data to be obtained. An equal but opposite expansion wave must be formed at the boundary such that the interaction between the two cancels the reflected wave altogether. One way of achieving this is either by means of a slotted wall, as previously described, or a perforated wall. Both perforated walls and slotted walls have advantages and disadvantages, and it is thus necessary to design the wall with the type of operation of the wind tunnel in mind. From previous experimentation, it has been shown that slotted walls are effective in creating zero reflection, but a given wall geometry is only effective for a given operating condition. Perforated walls on the other hand, have been shown that for a given layout, zero reflection still occurs over a large operating window. The perforated walls effectiveness is however sensitive to boundary layer thickness, and so this factor must be taken into account. Slotted walls also have the advantage of reducing the need for velocity correction in wind tunnels as well as relieving the effects of choking. Since choking is a feature that is prominent during high Mach number testing, the slotted walls allow a model with a greater frontal area to be tested, thus reducing the limitations on model size slightly (Goethert, 1961).

Creating the flow in a wind tunnel can be achieved using various means, the most common of which is a fan driven by a large motor. As expected however, the greater the velocity of the desired flow generally translates into more power required from the motor and thus greater expense in manufacturing and running the system.

One possibility is making use of the velocity induced in stationary air by means of the passage of a shock wave. Instinctively, this option would mean extremely short duration testing times but at a significantly reduced cost when compared to more traditional means.

A shock tube is one of the more practical apparatus for creating shock waves safely in an environment where their properties and associated flow characteristics can be studied.

Since the reduced testing time of a wind tunnel created from a shock tube is the obvious drawback to the method, understanding what testing time can be obtained is desirable. A wave diagram of the operation of a shock tube is capable of providing a large amount of information including the theoretical testing time available when attempting to use it as a wind tunnel. Figure 1.4 shows the typical features of a shock tube wave diagram.

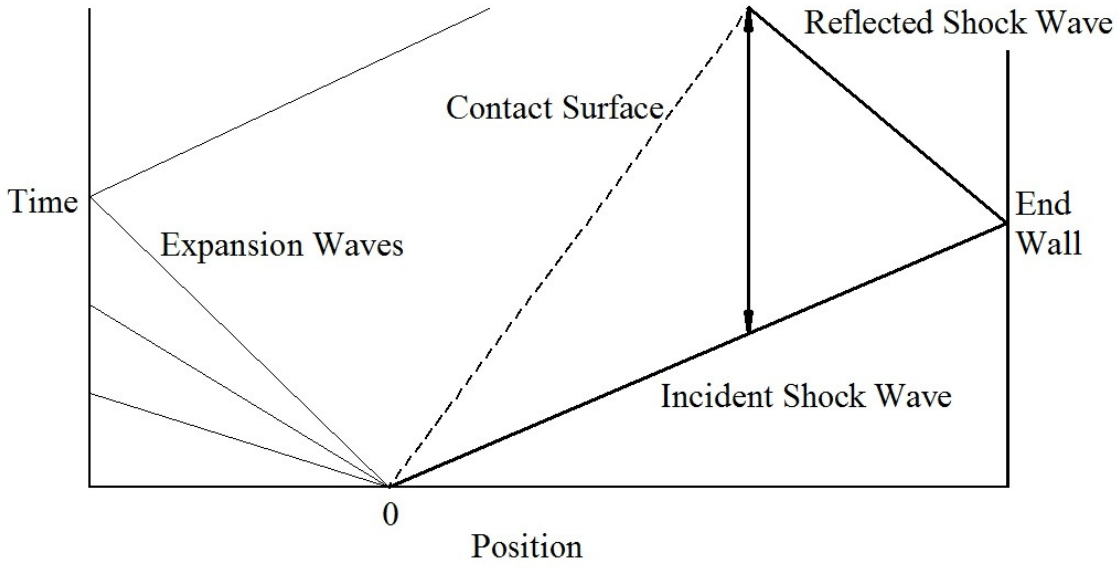


Figure 1.4 Schematic of a typical shock tube wave diagram

Upon activation of the shock tube, a shock wave propagates from the "0" position towards the downstream end of the shock tube. At the same time a contact surface follows the incident shock wave, but at a lower Mach number. Expansion waves propagate from the "0" position towards the upstream end of the shock tube. After some amount of time, the incident shock wave will reflect off the downstream end of the shock tube and start propagating upstream towards the contact surface and the expansion waves. The point of first interaction between these features will be at the position of maximum testing time, since it relates to the position where the flow behind the incident shock wave has the greatest amount of time before being interfered with by the aforementioned features. The theoretical maximum testing time is the difference between the time at which the reflected wave interacts with the contact surface or expansion waves and the time at which the incident shock wave passes the position of maximum testing time. This time is shown by the arrow in Figure 1.4. More details about the operation of a shock tube can be found in section 2.2.

In the event that a weak diaphragm is used at the end of the driven section of the shock tube to allow a vacuum to be drawn, while at the same time, allowing the high pressure gas to escape after bursting, an interesting feature can result. If, after the incident shock wave hits the diaphragm, the reflected wave raises the pressure above the ambient pressure, the diaphragm will burst outward, resulting in an expansion wave propagating back upstream toward the test section.

This expansion wave will propagate at a much lower velocity when compared to the velocity that would be seen if the reflected wave were produced by the incident shock wave reflecting off a solid wall. This fact would result in an increase in testing time since the arrival of the disturbance at the test section would be significantly delayed. At the same time, due to the venting of the shock tube by the bursting of the diaphragm, a reflected shock wave would also be weakened, and it too would result in an increase in the available testing time.

If the end of the shock tube is open to the atmosphere, the reflection takes the form of an expansion wave which propagates upstream at the local sound speed. This would have the effect of increasing testing time over that predicted where the reflection of the incident shock wave occurs off a solid boundary, as discussed previously.

Figure 1.5 shows the incident shock wave Mach number required to produce a flow of a given Mach number. Of particular interest is the shock wave Mach numbers that result in flow Mach numbers falling within the transonic Mach range. The dotted lines on the graph indicate the upper and lower shock wave Mach numbers to induce flow Mach numbers in the upper and lower limits of this range.

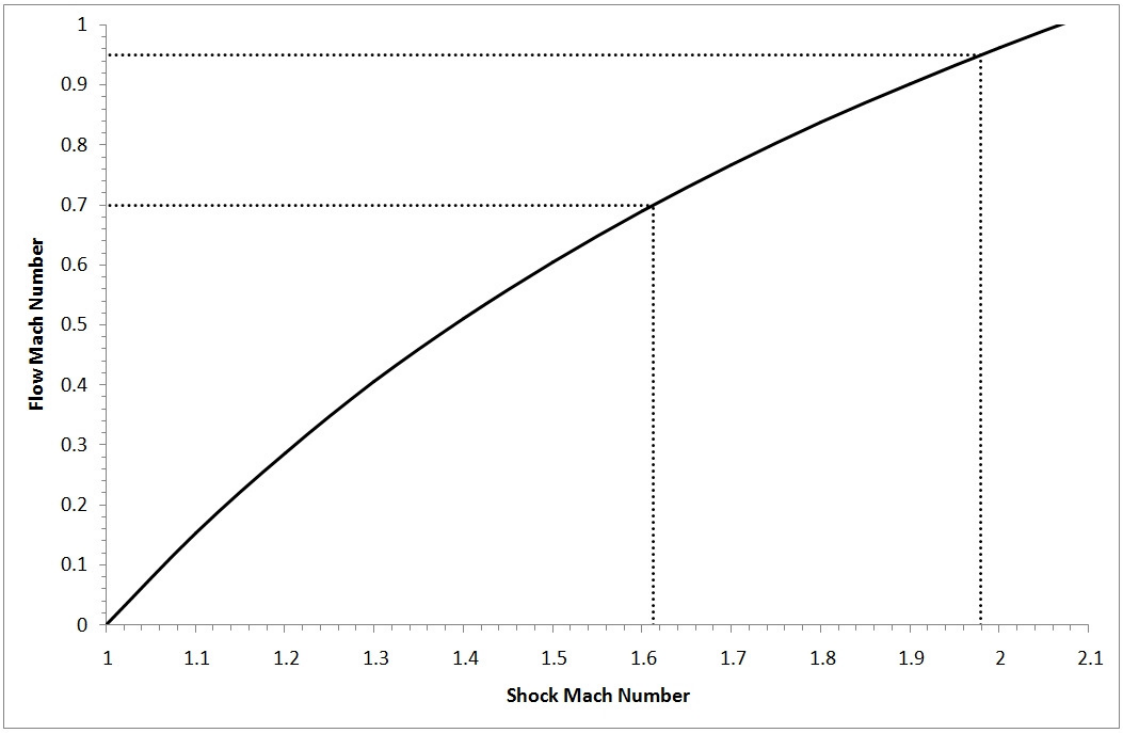


Figure 1.5 Graph of shock Mach number versus flow Mach number

While shock tubes have been used before for the purpose of creating a short duration wind tunnel, the amount of testing time being produced in the current work is greater than that previously seen. Thus, the study explored the production of the new facility as well as all the problems, procedures and results associated with it. The results presented are of little interest from a research point of view, but provide proof that the facility is operating correctly, as well as demonstrating the limitations surrounding its use.

Section 2 of this dissertation outlines the properties of shock waves as well as common methods of recreating them in a laboratory. A review of literature applicable to the research is also presented and an introduction into the techniques used to visually study the shock waves and their associated flow features is provided. Finally, the objectives of the research are presented in section 3.

Section 4 details the design of the new facility and explores the physical constraints of the design. Specific emphasis is given to the design of the test section and its associated features, ending in the final specification and layout of the test section. The details of the design of the test piece are also presented, along with the optimisation process to ensure optimal operation of the wind tunnel.

Section 5 examines the initial running and calibration of the wind tunnel as well as some of the problems associated with the layout and how those problems were dealt with. The procedure for carrying out safe and accurate testing using the facility is then detailed in section 6.

The results from both the experimental and numerical testing are presented in section 7 with specific emphasis on the comparison between the two, as well as those details that provide insight into the functioning of the facility. Finally, specific conclusions relating to the objectives originally laid out are detailed in section 8, along with recommendations on the further improvement of the facility and its ability to reproduce transonic flow accurately.

2 Literature Review

Shock waves occur frequently in nature and are formed by a variety of sources. Lightning bolts superheat the air around them causing explosive expansion of the air and a shock wave to form, creating the loud bangs associated with them. Explosions result in a similar scenario.

Manmade objects are also capable of creating shock waves. The popping of a balloon or the cracking of whip both result in shock wave formation. The passage of aircraft through air at velocities around seventy percent of the local speed of sound and higher cause shock waves to form around the craft. The strength of these shock waves depends on the velocity and shape of the aircraft and its components.

2.1 Types of Shock Waves

Shock waves can take a variety of forms, but generally speaking, they are considered to be a discontinuity in flow across which the properties of temperature, pressure and density of the fluid change over an effectively infinitely small distance. A true discontinuity of course cannot exist, but the fact that a shock wave is of the order of a few molecular mean free paths in thickness, this assumption is adequate.

An aircraft flying at low subsonic velocities (M < Mach 0.7) will generally not experience any shock wave formation over it since the local velocities of the flow remain in the low subsonic region. However, once the aircraft enters the transonic region (Mach 0.7 < M < Mach 1) its shape potentially can cause the airflow over it to go sonic or even supersonic in small regions around it. This causes transonic shock waves to form around the areas causing the disturbance. Upon the velocity of the aircraft becoming sonic (M = 1) a normal shock wave or a bow shock wave forms, depending on the shape of the body while at velocities above the local speed of sound (M > 1) an oblique shock wave or a stronger bow shock wave will occur.

Normal and transonic shock waves are relevant to the study and their properties are discussed in greater detail below.

2.1.1 Normal shock waves

A normal shock wave is one where the wave front lies ninety degrees to the direction of travel, as shown in Figure 2.1.

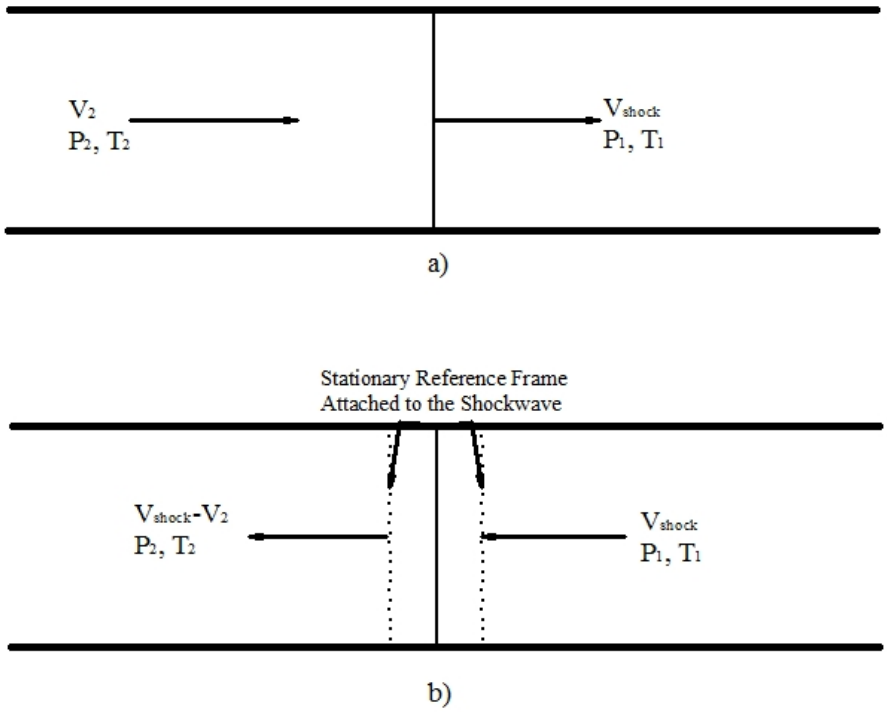


Figure 2.1 Normal shock wave with different reference frames

As stated previously, the properties of the fluid change discontinuously across the shock wave. In Figure 2.1 the properties with a subscript of 1 and 2 refer respectively to the effects before and after the shock wave has had an effect.

Because the shock wave is occurring in a 1 dimensional ideal gas, the equations of continuity, momentum and energy must be satisfied. The following equations apply for frictionless, adiabatic flow.

For continuity: $$\rho_1 V_1 = \rho_2 V_2 \tag{2.1}$$

Momentum: $$\rho_1 V_1^2 + p_1 = \rho_2 V_2^2 + p_2 \tag{2.2}$$

Energy: $$h_1 + \frac{V_1^2}{2} = h_2 + \frac{V_2^2}{2} \tag{2.3}$$

But because the medium is an ideal gas:

$$P = \rho R T \tag{2.4}$$

$$a^2 = \gamma RT \tag{2.5}$$

$$h = \frac{\gamma}{\gamma - 1} RT \tag{2.6}$$

$$M = \frac{V}{a} \tag{2.7}$$

The following useful equations result from manipulating the above:

$$\frac{P_2}{p_1} = \frac{\left(1 + \gamma M_1^{\,2}\right)}{\left(1 + \gamma M_2^{\,2}\right)} \tag{2.8}$$

$$\frac{T_2}{T_1} = \frac{\left(1 + \frac{\gamma - 1}{2} M_1^{\,2}\right)}{\left(1 + \frac{\gamma - 1}{2} M_2^{\,2}\right)} \tag{2.9}$$

$$M_2 = \left(\frac{\frac{2}{\gamma-1} + M_1^2}{\frac{2\gamma}{\gamma-1} M_1^2 - 1} \right)^{1/2} \tag{2.10}$$

Furthermore, the stagnation properties of pressure and density can be defined as follows:

$$\frac{p}{p_0} = \left(1 + \frac{\gamma-1}{2} M^2 \right)^{\frac{\gamma}{\gamma-1}} \tag{2.11}$$

$$\frac{\rho}{\rho_0} = \left(1 + \frac{\gamma-1}{2} M^2 \right)^{\frac{1}{1-\gamma}} \tag{2.12}$$

The choice of reference frame will influence the stagnation properties of the fluid while the static properties of pressure, temperature and density are independent of the reference frame. The equations derived above apply to the stationary reference frame as shown in Figure 2.1 b) where the observer is seen to move with the shock wave rather than the case where the shock wave moves into stationary fluid (Figure 2.1 a)

In order to study shock waves in a controlled environment like a laboratory, we need to be able to reproduce them safely and predictably. One of the best ways of achieving this is by means of a shock tube as described in section 2.2.

Manipulation of the above equations as well as a change into the stationary observer reference frame yields the following pertinent equations that are especially relevant when it comes to the operation of a shock tube:

$$\frac{p_4}{p_1} = \frac{2\gamma_1 M_s^2 - (\gamma_1 - 1)}{\gamma_1 + 1}\left(1 - \frac{\gamma_4 - 1}{\gamma_1 + 1}\frac{a_1}{a_4}\left(M_s - \frac{1}{M_s}\right)\right)^{-2\gamma_4/(\gamma_4 - 1)} \tag{2.13}$$

$$M_2 = \frac{2(M_s^2 - 1)}{\left(2\gamma M_s^2 - (\gamma - 1)\right)^{0.5}\left((\gamma - 1)M_s^2 + 2\right)^{0.5}} \tag{2.14}$$

Subscripts numbered 4 denote the region of the driver gas, while subscripts of 1 denote the region of the driven gas. M_2 denotes the Mach number of the flow induced by the shock wave and M_s denotes the Mach number of the shock wave itself.

2.1.2 The oblique shock wave

The oblique shock wave differs from a normal shock wave in that it does not lie at 90 degrees to the flow, but can lie at some acute angle to it instead. As before, the properties of the fluid on either side of the oblique shock wave will change discontinuously, however they will not change with the same magnitude as before.

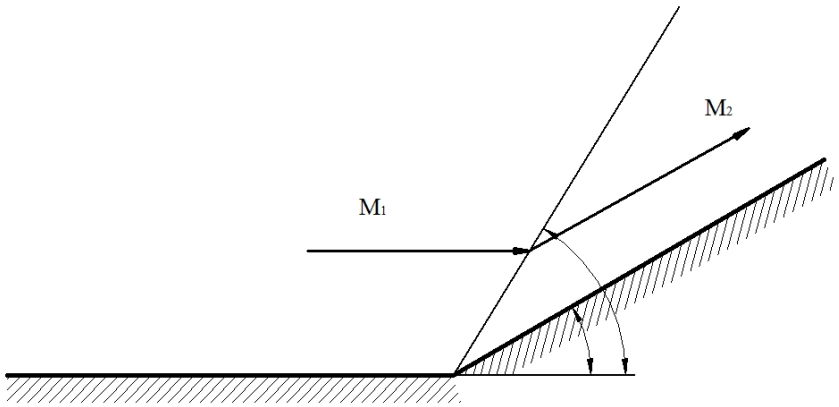


Figure 2.2 Oblique shock wave

Oblique shock waves occur in supersonic flow and are the result of the flow being required to turn through some angle by the presence of a corner. Since the flow is required to turn into itself, the shock wave is considered to be a compressive wave and creates a rise in static temperature

and pressure, but a drop in Mach number. Unlike the normal shock wave, the drop in Mach number caused by an oblique shock does not cause the flow to become subsonic. (Ben-Dor, Igra, & Elperin, 2001)

2.1.3 Transonic shock waves and their resulting features

Particularly relevant to the research being undertaken is the occurrence of transonic shock waves with specific emphasis on those occurring on an aerofoil shaped body exposed to transonic flow.

When an aerofoil (or other body) is exposed to flow with a Mach number in the transonic region, depending on the shape and relative dimensions of the aerofoil, there is a possibility for the flow in certain regions around the aerofoil to go locally supersonic. This locally supersonic flow cannot remain supersonic throughout the flow region around the aerofoil and so at some point, needs to become subsonic once again. The transition from supersonic to subsonic takes place by means of a shock wave through which the properties of the flow in question will change discontinuously as stated previously.

The normal shock wave discussed is the same as the normal shock wave described in section 2.1.1, however, the shock wave does not have to take the form of a straight line but can contain curvature. The reason it is still considered a normal shock wave is because the streamlines entering the shock wave will do so at 90 degrees to the shock front. (Skews, 2007)

As for the case of an aerofoil being exposed to subsonic flow, a boundary layer will form along the upper and lower surface. In the case where the flow Mach number and aerofoil shape create locally supersonic regions on the aerofoil, a transonic shock wave will form. This shock wave will interact with the boundary layer at the point where the two meet. This interaction is complex and beyond the scope of the research in question. However, the result of the interaction is of interest.

Two types of interaction are possible:

Normal shock wave without boundary layer separation:

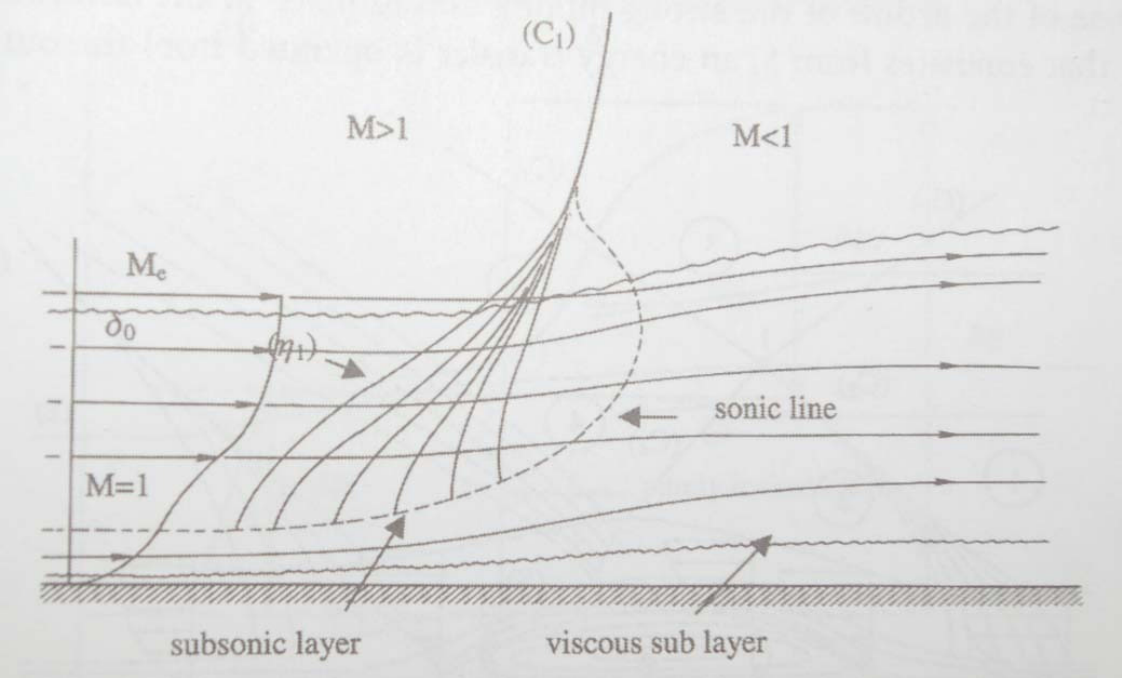


Figure 2.3 Normal shock wave without boundary layer separation
(Ben-Dor, Igra, & Elperin, 2001)

Since the boundary layer attached to the surface of the aerofoil is moving at an ever slower velocity as it approaches the surface, at some point in the boundary layer the flow will become subsonic. At the position where the normal shock wave and the boundary layer meet, the pressure rise associated with the shock wave is able to be transmitted a small distance upstream through the subsonic boundary layer. This transmitted pressure rise results in compression waves forming which ultimately coalesce to form up with the normal shock wave.

The compression in the lower part of the shock wave boundary layer interaction is very close to isentropic, thus the entropy level of the flow is less than that found at some distance away from the wall, behind the normal shock wave. This fact results in a region close to the wall where the Mach number is higher than that found trailing the shock, and is in fact still supersonic. This region is visible in Figure 2.3.

Normal shock wave with boundary layer separation (the lambda shock system):

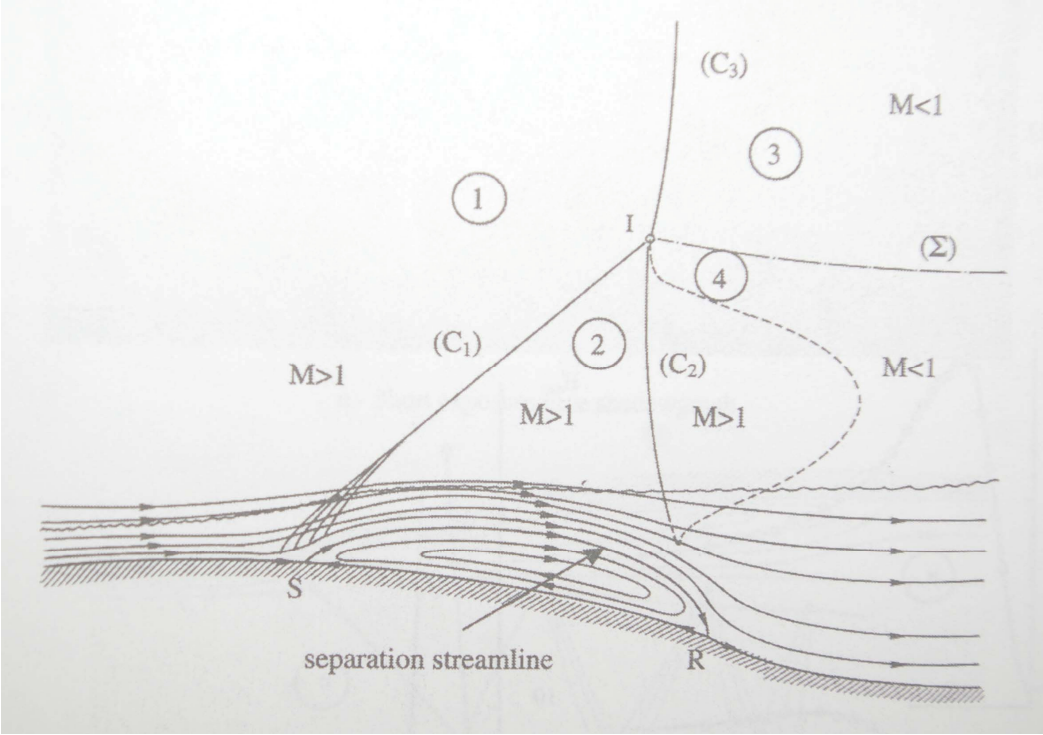


Figure 2.4 Normal shock wave with boundary layer separation
(Ben-Dor, Igra, & Elperin, 2001)

In the case where the boundary layer separates, a separation bubble forms in the boundary layer. The nature of this formation is beyond the scope of the research in question, however, it is directly related to the strength of the shock wave interacting with the boundary layer. Of course, the strength of shock wave is a direct result of the free stream Mach number.

In the event that a separation bubble forms, as seen in Figure 2.4, an oblique shock wave forms off the upstream section of the bubble, due to the fact that the supersonic flow is required to undergo a compressive change of direction, as described in section 2.1.2. This oblique shock wave meets up with the normal shock wave. Downstream of the oblique shock wave, the flow is still supersonic. In order to satisfy compatibility conditions, the formation of a trailing shock wave is required. This downstream oblique shock wave can lead to a situation where the flow is very low supersonic downstream of the trailing shock. This region is known as the supersonic tongue, the size of which is dependent on the local and downstream boundary conditions.

This arrangement of shock waves and flow features is known as a lambda shock pattern and is common in transonic flow where the normal shock wave induces boundary layer separation.

2.2 The shock tube

A shock tube is a device used to create shock waves in a controlled environment, like a laboratory, for the purpose of studying phenomena surrounding their passage through a medium.

The shock tube in its simplest form shown in Figure 2.5, is a device capable of dividing a high pressure region of gas (driver) from a low pressure region of gas (driven). The separation of the two regions is made possible by a thin diaphragm of either plastic or metal sheeting. Upon rupture of the diaphragm, the high pressure gas expands rapidly into the low pressure gas. This expansion does not immediately result in the formation of a shock wave however.

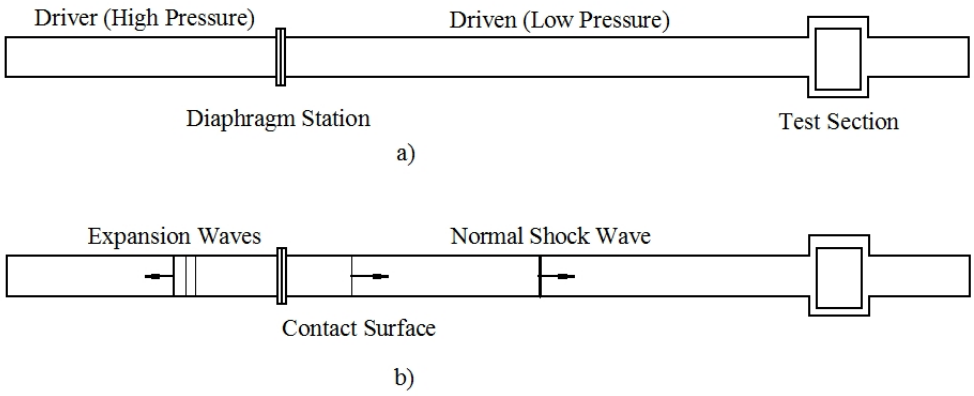


Figure 2.5 Schematic layout of a shock tube before (a) and after (b) diaphragm rupture

Initially, upon rupture of the diaphragm, a succession of compression waves propagate into the low pressure region, each wave travelling at the local speed of sound for the region into which it is propagating. As the first compression wave moves, it raises the temperature of the gas behind it, which in turn raises the local speed of sound in that region. The following compression wave then travels slightly faster than the preceding wave and will, after some time, catch it. This

process occurs with all of the compression waves that follow and they ultimately coalesce and steepen to form a shock wave.

At the same instant that the diaphragm ruptures, expansion waves move into the high pressure region. Due to the cooling effect that they have on the gas, they do not catch up with each other to form a shock wave.

Following the compression waves is a contact surface which, like a shock wave, is a discontinuous fluid region, but it is only discontinuous in density and temperature. The contact surface is a direct result of the two regions being separated from one another prior to the rupturing of the diaphragm. The pressure remains constant across the contact surface.

Built into the shock tube at some distance greater than the distance required for the compression waves to form a shock wave, will be a test section where the phenomena of interest can be studied.

The strength and Mach number with which the shock wave propagates is related to the pressure ratio across the diaphragm separating the high from the low pressure regions. As a result, the equations listed in section 2.1 can be used to estimate the flow properties that result from a given pressure ratio across the diaphragm. Of particular interest to the study in question, is the ability to predict the Mach number of the flow behind the shock wave since a high enough pressure ratio will create flow with a Mach number that falls into the transonic region (Glass, 1959).

2.3 Schlieren Imaging Technique

Due to fact that the features observed are difficult to see with the naked eye, as well as the high speed of the shock wave and short duration for which the features exist, a method of capturing the features at a given instant in time was required.

The method used is known as schlieren imaging and it allows a user to pick up the slightest variation in density in a transparent medium which would otherwise be largely invisible to the unaided eye. It converts density variations in a transparent medium into light variations which can easily be seen by the human eye.

A common layout of optical components required to achieve the technique is shown in Figure 2.6.

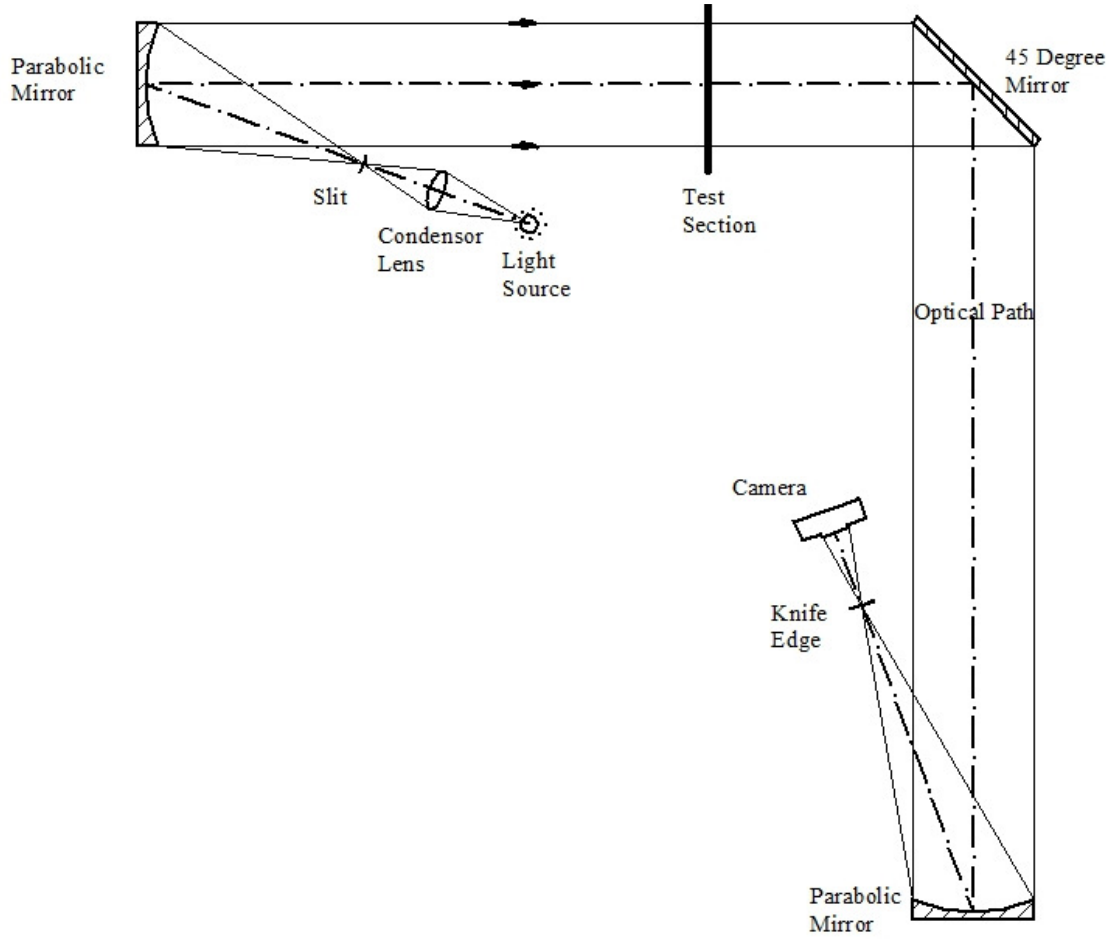


Figure 2.6 Typical Z-shape schlieren system layout bent through 90˚

A point source of light is cast upon a parabolic mirror originating at the focal point of the mirror, resulting in a parallel beam of light being reflected from the mirror. This parallel beam then passes through a region of interest (shock tube test section) and is reflected by another parabolic mirror. A knife edge is placed at the focal point of the second mirror and is used to control the amount of light being received by either a camera, human eye, or some other optical device. Any deviation in the parallel beams caused by some change in density in the test region will alter that portion of the light rays path to the knife edge. If the deviation causes the light rays to miss the knife edge, that area of the test region will appear lighter than the rest. Deviation causing the light

rays to intercept the knife edge will be blocked from reaching the final optical device and so that area in the test region will appear darker.

The deviation in the light path caused by the difference in densities of the medium in question is directly related to the refractive indices of the various areas in the test region. The refractive indices differ according to properties such as density of the medium and the wavelength of light causing illumination.

Varying the degree to which the knife edge cuts off the light path changes the sensitivity of the schlieren setup.

Settles describes in detail the mathematics to fully understand the optical processes involved in creating the schlieren setup. (Settles, 2001)

In order to capture an instant in time during a short duration event like that experienced in shock wave studies, a trigger system attached to pressure transducers is used. The pressure transducers register the steep change in pressure caused by the passage of the shock wave and send a signal through a delay box to trigger the light source. The light source illuminates the test region for an extremely short time and that illumination is recorded onto a camera or other optical device capturing that specific instant in time.

3 Objectives

The key objectives are:

- To design, manufacture, and calibrate a transonic wind tunnel using an existing shock tube
- To test transonic flow over a test piece
- To make a comparison between the experimental results and numerical results in order to verify the accuracy of the flow produced in the wind tunnel

4 Design of the Transonic Shock Tube

The design of the various components making up the transonic shock tube is detailed below. Specific emphasis is given to the test section and the reasons behind the selection of the various components and their particular layouts.

4.1 Design Constraints Based on Existing Resources

Due to the large cost of materials when creating a new facility, it is always advantages to make use of existing materials and components.

Tube lengths:

As part of an MSc completed previously Graeme Doyle was tasked with designing a new 100ms shock tube to study the effects of shock waves on particles. As a result of the relatively long testing time of 100ms, the shock tube needed to extend approximately 50 meters across the laboratory. With the study complete, a large number of lengths of piping were available to create a new facility. Thus, in order to keep costs down, and relieve some workload on the laboratory staff, the lengths would form the basis of the tubing required for the transonic wind tunnel, which would be positioned in the same portion of the laboratory (Doyle, 1998).

The lengths from the driven section were standard, industrial welded seam, rectangular steel tubing with outer dimensions of 177 x 127mm and a wall thickness of 10mm. The sections were made up of thirteen 2 meter long sections, two 1 meter long sections and a single 0.6 meter section. Each section had a flange welded to it and the flanges each contained two dowel pin holes to ensure accurate alignment once assembled.

The driver section was an Arlec Engineering pressure vessel made from three lengths of circular steel tubing with an outer diameter of 168.3mm and wall thickness of 7.11mm. Two lengths of 6 meters and one length of 3.4 meters made up the vessel. The total length of 15.4 meters had been

pressure tested and certified for a working pressure of 4 bar. The 3.4 meter section had a larger diameter flange welded to it to allow for connection to the driven section described above. One of the 6 meter sections had a blanking flange to close the section off.

Due to the large shock wave Mach numbers required to produce the transonic flow, the pressure vessel had to be recertified to a higher working pressure. The largest compressor available in the laboratory was capable of producing a pressure of 15 bar , and so the connecting flanges on the driver were upgraded to allow the vessel to be certified for a 15 bar working pressure.

Stands had been manufactured previously to support the assembled tube, with special stands to ensure that the driver section was able to be moved. Unfortunately, during the time that the existing shock tube lay disassembled, these stands were redistributed and as a result some new ones needed to be fabricated.

Windows:

The sensitive schlieren optical setup requires that the test section windows be made from an optically clear medium. High quality glass is commonly used but is very expensive, and so it was decided that the new transonic test section should be designed such that the windows and doors could be interchanged with another recently redesigned shock tube test section.

These requirements set up some basic but rigid constraints on the design with the most key constraint being that the test section would need to have inner dimensions matching those of the driven section tubing. The reason for matching the dimensions was to minimise energy losses during the transition from one cross section to another.

4.2 Design of the Partially Open Walls

As described previously, one of the most important features that the test section required is the ability to both cancel any reflected shock waves off the walls as well as minimise blockage effects in the wind tunnel.

Studying literature on the way in which this has been achieved in larger scale wind tunnels revealed a predominance in a slotted wall type layout. However, theory predicted that using a perforated wall type boundary had the most advantages.

Slotted and perforated walls each have advantages and disadvantages as described briefly in section 1.

Unfortunately due to the lack of numbers of transonic wind tunnels based on a shock tube, no literature was found to aid in the decision as to which layout was best. Consequently, some basic 2-dimensional computational fluid dynamic simulations were run to see if either method had an obvious advantage over the other.

Computational Fluid Dynamics:

The Fluent computational fluid dynamics package was used to create a shock wave upstream of a 'test section', with a short distance to propagate along, in order to ensure shock uniformity and proper formation when it reached the test section. It was then allowed to pass through the section and out the other side so that the resulting flow features could be visualised.

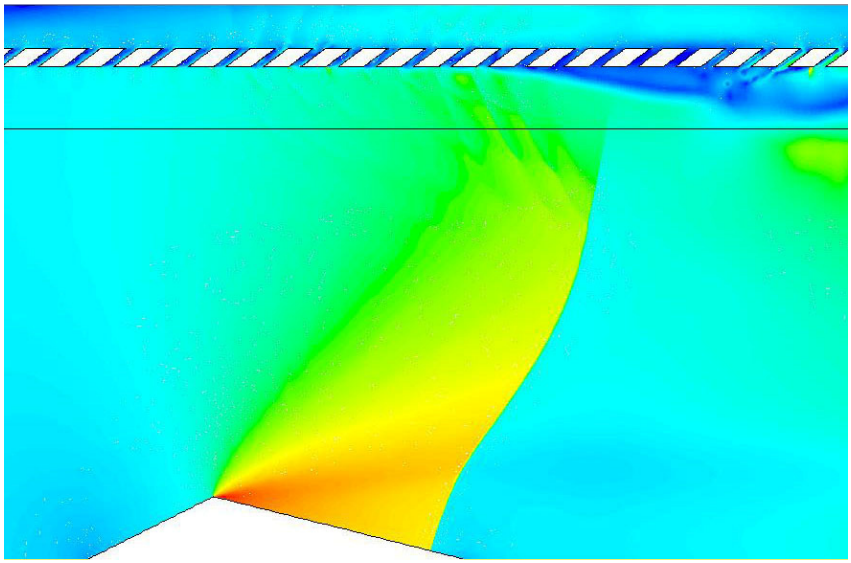


Figure 4.1 CFD of perforated wall concept at Mach 0.83 over half of a diamond shaped aerofoil

Figure 4.1 shows that the perforated wall concept tended to produce small perturbations in the flow and as such each perforation created a disturbance that propagated downstream as well as away from the wall. This is extremely undesirable since each of the disturbances would propagate outwards from the wall and into the flow features or onto the model in question.

The complexity of manufacture as well as the difficulty in predicting the correct size and spacing of the perforations as well as the possible interference it might create meant that the concept was deemed unsuitable.

The lack of literature and thus the requirement for a flexible layout meant that the slotted wall option was much more practical from a manufacturing and testing point of view. The likelihood of meeting the flow requirements was also high and as a result, design continued with only this option in mind.

4.3 Design of the Test Section

A key feature of the test section was the need to have the option of varying the layout of the components, thereby allowing different layouts to be tested, in the hope that one would be found to have minimal model interference while providing the most accurate results.

With the slotted wall layout decided upon, it became necessary to decide how the slots should be laid out and fitted into the test section, as well as the slot dimensions. All of these aspects were relatively unknown, except that an open area ratio of approximately 50 percent for shock wave cancellation seemed to be reasonable.

The basic design concept began with two jig-like walls which would be capable of holding the various components together at the required spacing. The walls were designed such that the doors from the original shock tube would fit and operate correctly as well as being able to house the new doors holding the perspex windows. The plenum chamber concepts were then fitted, along with the mounting for a test piece and the required connections to the rest of the shock tube.

The details of each phase of the design are described below.

4.3.1 The plenum chamber

A key component of the shock wave reflection cancellation is that an open space of some kind needed to be in place on the other side of the boundary. This is the region into which the equal strength expansion wave could expand.

Due to this requirement, as well as the need to have an extremely variable test section layout, a separate plenum chamber was conceptualised.

A few concepts were created:

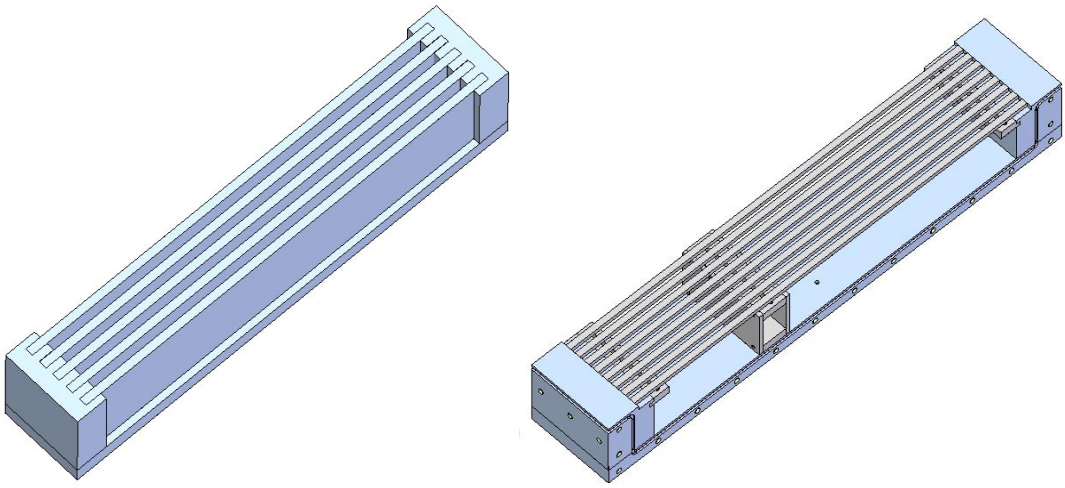


Figure 4.2 Plenum chamber concepts, with solid and bar slots

Figure 4.2 shows two concepts that were considered. The first concept contained solid slats to create the slotted wall feature. This concept had the disadvantage that changing the slot width and thus open area ratio would mean a large amount of disassembly of the test section. Changing the plenum chamber depth if needed would also not prove to be a simple task.

The second concept with thin bar slots was chosen due to the ease with which the slot width, depth and number could be varied. Another favourable aspect of the chosen layout was the ability to make the changes without any disassembly of the test section itself. The second concept was thus favoured over the first and developed further.

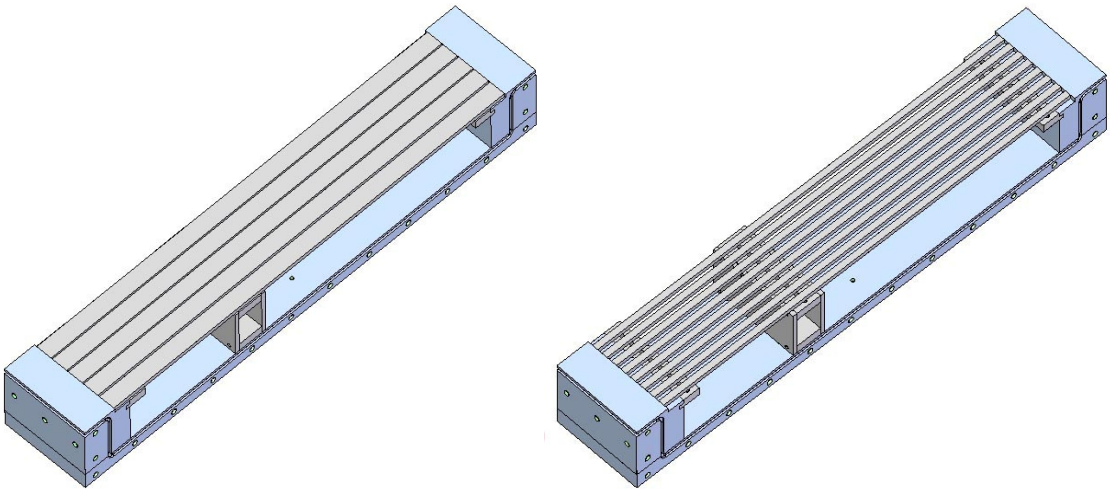


Figure 4.3 Plenum chamber with 10% open and 50% open wall slots

Due to slenderness of the slotted members, supports needed to be put in place to ensure that they did not vibrate or bend during testing. These supports also doubled as clamping regions to ensure that the spacing between the slots could be accurately maintained. Figure 4.4 shows the support offset from the centre of the plenum chamber to allow space for the mounting of the test piece. Each end of the slotted insert was also supported to maintain slot spacing accurately.

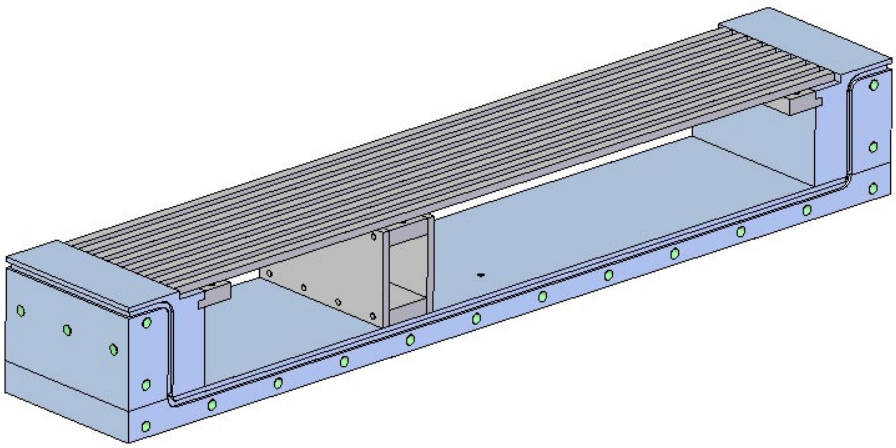


Figure 4.4 Plenum chamber with 50% open walls showing supports

Each slot making up the slotted wall could be bolted onto the three supports using short, M4 cap screws. The supports shown in Figure 4.4 incorporated a slotted guide thus allowing the spacing

of the slots to be altered as well as allowing different width slots to be used with the same support structure. This had the effect of simplifying manufacture and replacement of the slotted sections.

4.3.2 The window and door

As stated previously, the test section needed to be designed such that the windows could be interchanged with a shock tube that had been recently upgraded. The window of the upgraded shock tube can be seen in Figure 4.5.

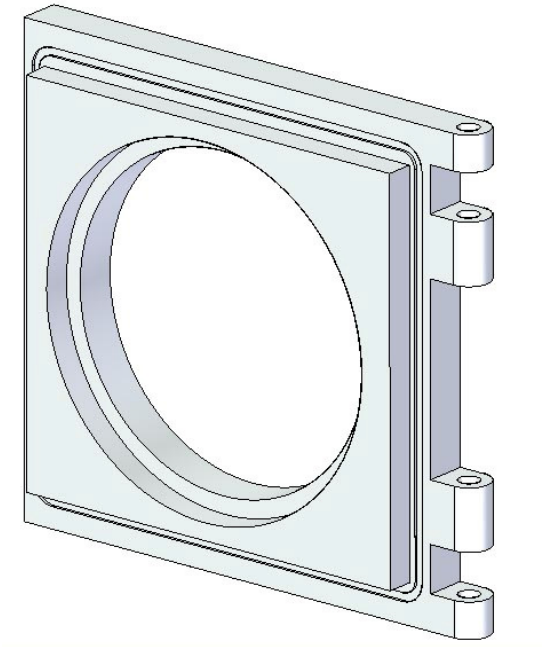


Figure 4.5 Original high optical quality window frame

In order to make the original door fit the test section, the basic test section shell was designed around it. At the same time, a similar door and window system was designed to be capable of housing a much cheaper perspex window. As a result, tests could be run with a lower optical sensitivity on the new transonic shock tube, and then in the event a higher sensitivity was required, the doors would be swapped.

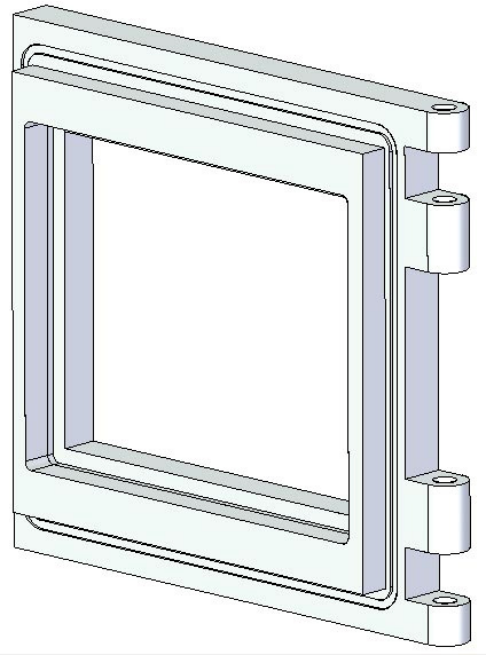


Figure 4.6 New Perspex window mounting system

The door was designed to have the largest possible Perspex window, which under the expected test pressures would not bend significantly. Any bending of the windows effectively increases the cross sectional area of the test section at that point and would thus tend to alter the flow velocities through the test section.

At the same time when Perspex is stressed beyond a certain limit, it has a tendency to craze, whereby tiny cracks form on the surface, decreasing both its strength and its optical quality. It is recommended that the maximum stress be limited to 10% of the yield stress to avoid crazing. This became a key factor in choosing the window thickness.

Of course, due to the optical layout shown in section 2.3, the size of what is visible through the schlieren system is limited by the size of the parabolic mirrors used. Since 10 inch diameter mirrors were available, and it was unlikely that larger mirrors would ever be used on the new shock tube, it was decided to limit the window size to 200 by 250mm, with the larger dimension running parallel to the flow direction. This size is more than adequate to visualise the entire height of the test section (107mm) while including a portion of the plenum chamber.

Based on these dimensions and the fact that the driver pressure was limited to 15 bar, the window thickness could be estimated making use of Bruhn (1973). It was found that 25mm thick perspex

would ensure that no crazing occurred, and would result in minimal deformation. Both of these features are highly desirable.

With the window size known, the frame could be designed. In order to ensure that the window and frame from the existing tube were able to fit correctly, modification of the existing components was all that was required. The basic design concept was kept and only the window cut-out dimensions were altered from the original round windows to the new rectangular ones.

An O-ring groove was also included to ensure that the doors sealed correctly under both positive pressure as well as vacuum. The O-ring groove and required O-ring material was sized to create the required squeeze on the O-ring while ensuring that none of the material was pinched in the process. A 4mm groove width with a 2mm depth was specified. Thus a 3mm O-ring would be squeezed the required amount and the 4mm width would allow the O-ring the required expansion. A layout of the inner section of the door can be seen in Figure 4.6.

Locking system:

A simple locking system (Figure 4.7) was then designed that would be easy to manufacture and use, and would be capable of being used on both the new and existing doors. The system holds both doors on either side of the test section in position simultaneously with the upper and lower clamps, while the single side clamp is specific to each door system. The system allows the doors to be unclamped very quickly while still providing the required clamping force during testing.

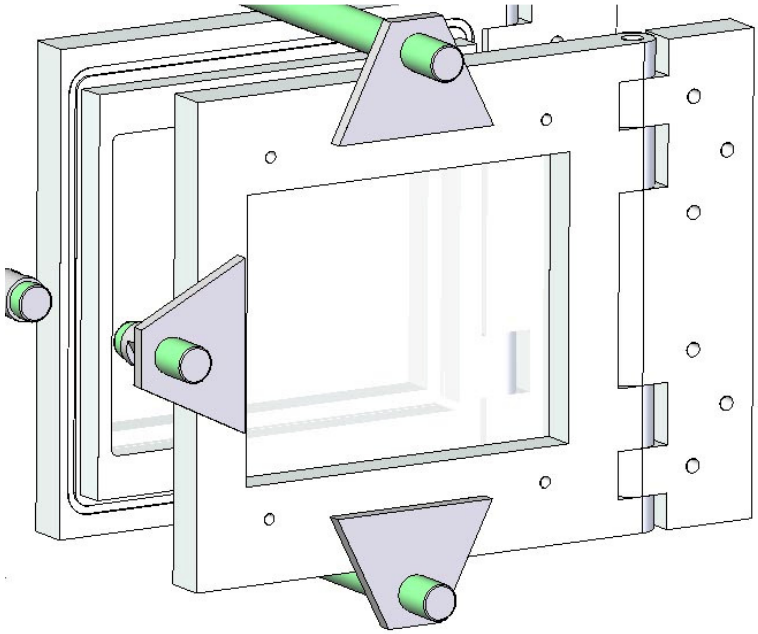


Figure 4.7 Door clamping system

Window clamping method:

Due to the window experiencing both positive pressures and vacuum, the window and window clamping system were designed to ensure this would not cause problems. A further requirement for flow uniformity in the test section was to ensure that the inner surface of the door, and more especially, the region where the door and window met was as smooth as possible with a minimal step and gap. This meant that clamping the window in place to prevent it being pulled inwards when the test section was under vacuum was not achievable by simply bonding the window to its frame. This was overcome by a machined step as shown in Figure 4.8. The inner support frame has been removed in the figure for clarity. This frame has a corresponding step in it to ensure no gaps between the window and frame exist.

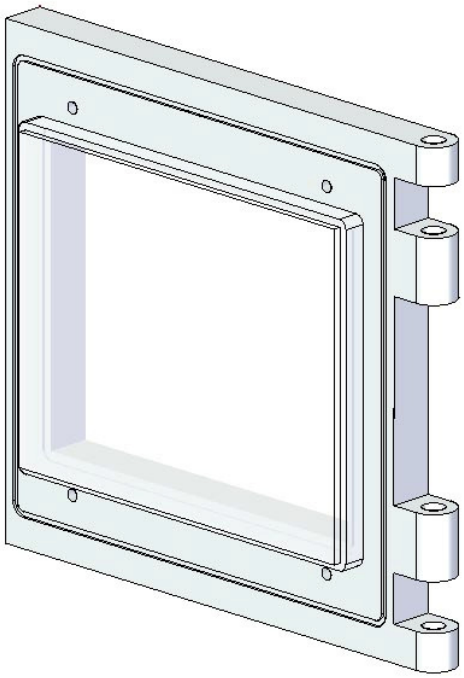


Figure 4.8 Step machined into the perspex window

To ensure that no air was capable of moving through the joint between the window and the door, an O-ring was included.

To further seal the joint, and to take up any play in the seating of the window created during the machining process, the joint was filled with Sikaflex. Sikaflex is safe to use with Perspex and creates a tight seal but does not set hard and thus allows for small amounts of expansion and contraction due to temperature changes, thus preventing overstressing the perspex window.

Door frame:

The door frame was made from 30mm aluminium plate (Figure 4.9). This was to ensure adequate rigidity under the various pressure loadings since the locking plates covered a relatively small area. O-ring grooves were included in the door frame to ensure that no gas could move through the joint created when the door was closed and locked onto the outer walls of the test section. The hinge system was manufactured to be identical to that of the existing door and so interchanging the two would involve removing the hinge pin only.

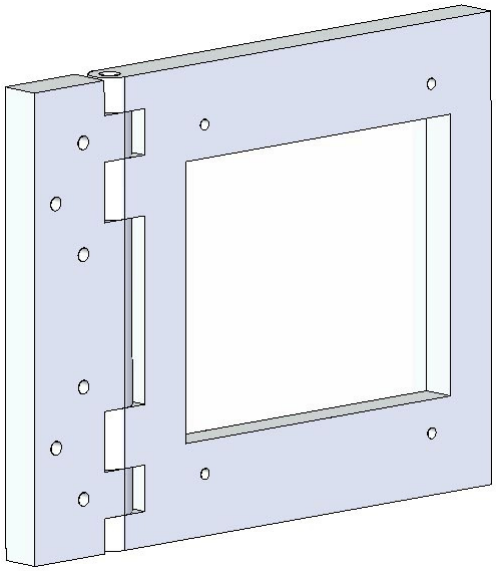


Figure 4.9 Outside view of door frame with hinge system

Replacement of the window in the event of damage is done by removing the door, and then the inner window frame, making the setup quite user friendly.

4.3.3 Test section body

With the layout largely designed, a housing was then required to make up the body of the test section. From a manufacturing point of view, plate steel was used due to its ability to be machined relatively easily, as well as the ease with which a good surface finish could be achieved.

With the window and door requiring an exact fit to prevent any small steps or gaps along the side walls, the plate needed to be an exact thickness. At the same time the surface finish of the plate needed to be very smooth with no dents or notches. Commercially available inexpensive steel plate generally has a lot of surface imperfections and the thickness can vary within quite a large tolerance limit. It was therefore decided that commercial plate would be purchased and ground to an acceptable surface finish. Unfortunately the grinding process and thus plate thickness is only accurate to within approximately one millimetre, and so the window and door could potentially have a one millimetre gap once correctly tightened. Therefore it was decided to oversize the

thickness of the original plate, and allow the plate to be ground oversized. Final machining of the area where the door and hinge mounts would then take the plate to the exact thickness in that region, allowing the door to fit exactly. The required recess can be seen in Figure 4.10, with the actual depth of the recess being dependant on the final ground thickness of the plates.

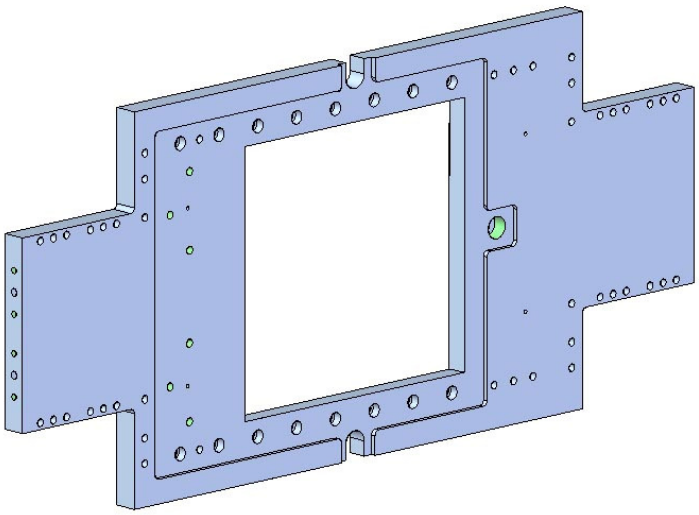


Figure 4.10 Side wall with door recess and mounting holes

All plates making up the main body were specified to be 20mm thick to allow M8 bolt holes to be drilled edge on without being too close to any edges. The plates would also require a 4mm O-ring groove to be machined into the edges to ensure proper sealing, especially under vacuum.

It was decided the side walls would be the main support components for everything that would be attached to the test section. As a result, they were designed larger than was required to ensure that all the components could fit in the space allowed.

It was decided that the test section would extend 900 mm in order to ensure that there was enough space for the various components. This also allowed a reasonable amount of space to mount the window and door and at the same time provide adequate area upstream and downstream of the test piece for flow features to be established. It also had the additional benefit of adding extra length which was required to maximise the transonic flow time.

Every joint had an O-ring groove machined into it and all bolted joints included at least two 8mm dowel pins to allow for accurate alignment during assembly. All major joints were laid similarly to that shown in Figure 4.11.

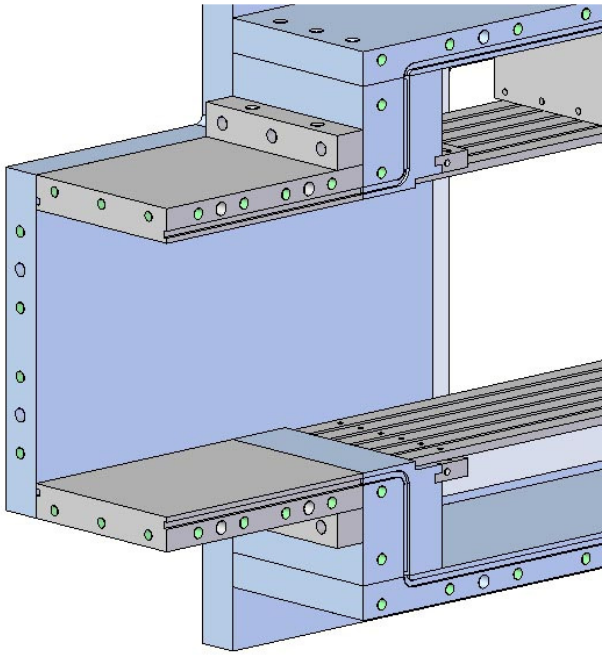


Figure 4.11 O-ring grooves, dowel and bolt holes for alignment and sealing

A flange matching those from the original driven section tubing was fitted to either end of the test section, each containing two dowel pin holes to ensure accurate alignment upon assembly.

4.3.4 Upstream cleanup section

It was decided that due to the rough nature of the inside of the industrial steel tubing, a cleanup section would be required just upstream of the test section. The purpose of this section would be to ensure that the shock wave arriving at the test section is uniform, as plane as possible, and that any flow features set up due to the change in cross section from the tubing to the machined section would occur far away from the test section.

At the same time, pressure transducers needed to be installed upstream of the test section to allow for triggering of the optical system for imaging the flow features. This section provided an ideal place to install them.

A few concepts were created:

Firstly, a simple box shape assembled from 20mm, cold rolled steel plate would provide the inner surface finish required and could be bolted together with ease. Upon pricing the cold rolled sections, the idea was modified.

Due to the inner cross section of the test section being the same as that of the industrial tubing (157.7mm x 107mm), the cleanup section would need to match these dimensions. It was decided that in order to save money, at least half of the cold rolled plating could be replaced with standard tapered flange channel section. The standard size of these sections does not come in either 107mm or 157.7mm widths, however a 160mm width is available which has a flange thickness of approximately 8mm. The surface finish of channel section is rough, but since it is oversized at 160mm, it could be ground down. It was decided to grind the thickness of the channel to 157.7mm with the web being ground smooth in the process. Even with the grinding required, the sections worked out to be much cheaper than the cold rolled steel sections. The cleanup section was laid out as shown in Figure 4.12.

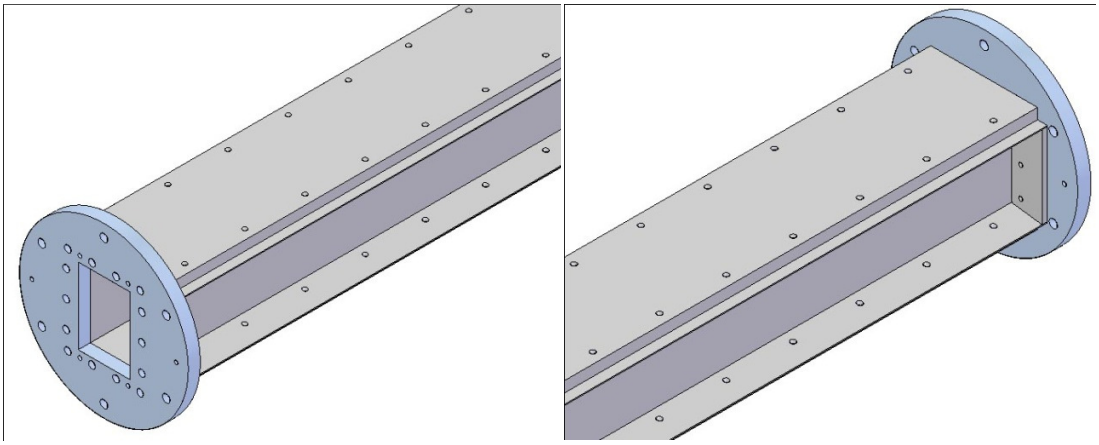


Figure 4.12 Cleanup section with channel sides and plate top and bottom

Steel sections come standard at six meters long, and so it was decided to make the cleanup section three meters long, from an assembly and cost point of view. Three meters is also adequate to ensure that the shock wave is uniform, and it has the added advantage of adding an extra three meters to the overall length of the tube, thus helping maximise the testing time.

The layout also ensured that the corners of the section were at exactly 90 degrees to one another, which is how they would be in the test section, and so no losses would occur during transition from one section to the next.

Machining O-ring grooves along the three meter length was not practical and so the joint created between the channel flange and the cold rolled plate was sealed using Loctite number 3 gasket sealer. Care was taken, once the sections were bolted together, to ensure that no Loctite was squeezed into the corner of the section and where it had occurred, it was quickly removed.

The pressure transducer holes were machined such that the transducers would be flush with the upper inner surface of the section. The transducers were placed exactly 300mm apart and 680mm from the centre of the test section. The 300mm distance is critical because it is used to determine the shock Mach number, while the distance to the centre of the test section is simply used to estimate a trigger time delay for the optical system.

Again, flanges were fitted to each end of the section to allow for assembly with both the original driven tubes and the new test section. These flanges have O-ring groves and 8mm dowel holes machined into them to ensure a good seal and accurate alignment between the flange and the ends of the cleanup section.

4.3.5 Vacuum seal system for the end of the shock tube

Due to the requirement of vacuuming the driven section to increase the shock wave Mach number, the driven section needed to be sealed off from the atmosphere. The end of the driven section vents straight into atmosphere. For tests that do not require vacuum, this is acceptable, but for tests requiring vacuuming, the end either needed to be closed off with a blanking flange or a with a valve system of some kind. Simply putting a blanking flange in place meant that the reflected incident shock wave off the end of the tube would be stronger than if the tube could vent and would thus reduce testing time slightly.

To overcome the problem it was decided that placing a very weak diaphragm at the end of the tube was the best solution. The diaphragm needed to be thick enough to hold the pressure ratio caused by the vacuum, but would burst upon contact with the incident shock wave.

An existing driven section tube, having been cut for other purposes, was used along with 80 micron plastic sheeting clamped between the two flanges making up the joint in the tubing. This system proved to be more than adequate for the purpose with the only disadvantage being that it needed replacing after every test requiring vacuum.

4.4 Final Test Section Layout and Specifications

The final test section was laid out as follows:

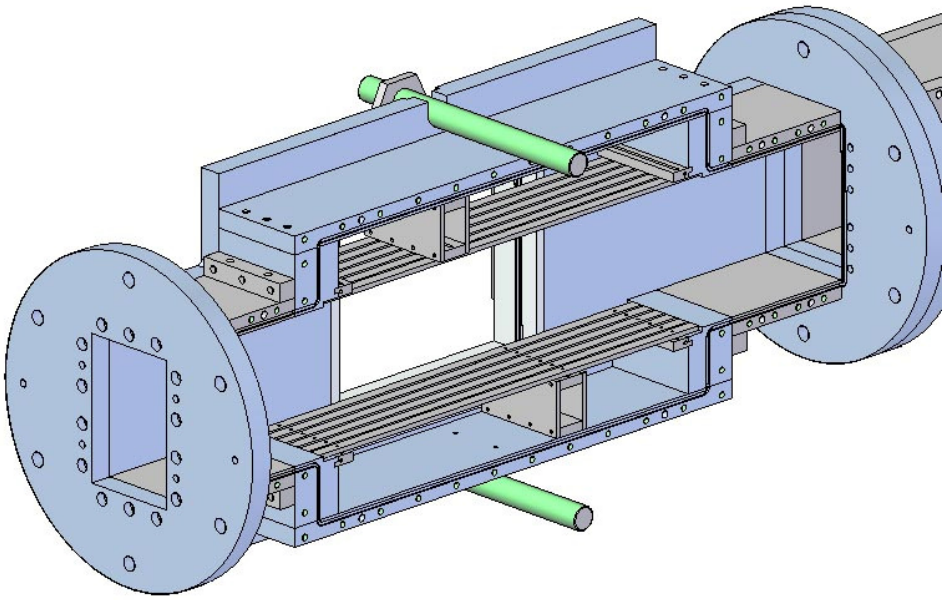


Figure 4.13 Final test section with wall removed for clarity

The test section had the basic dimensions as shown in Figure 4.14.

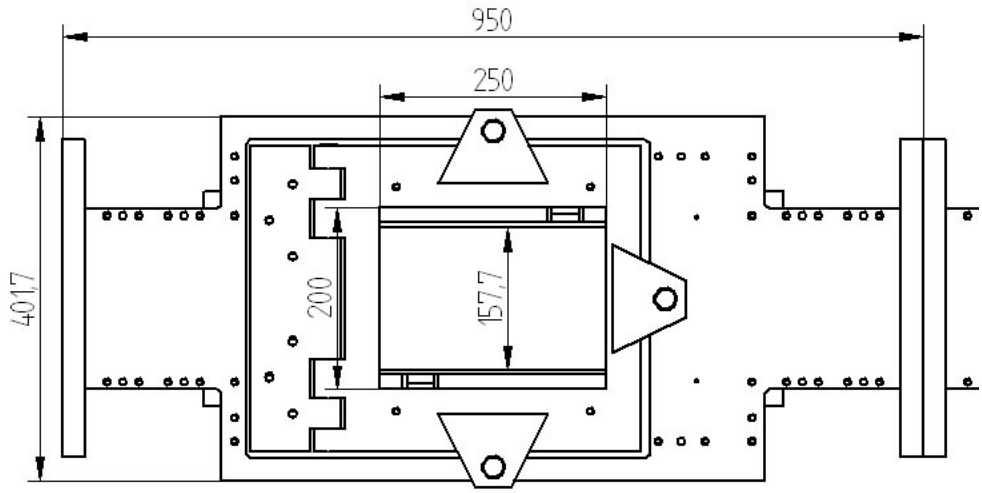


Figure 4.14 Basic dimensions of the final test section

Ultimately, the test section ended up as shown in Figure 4.15.

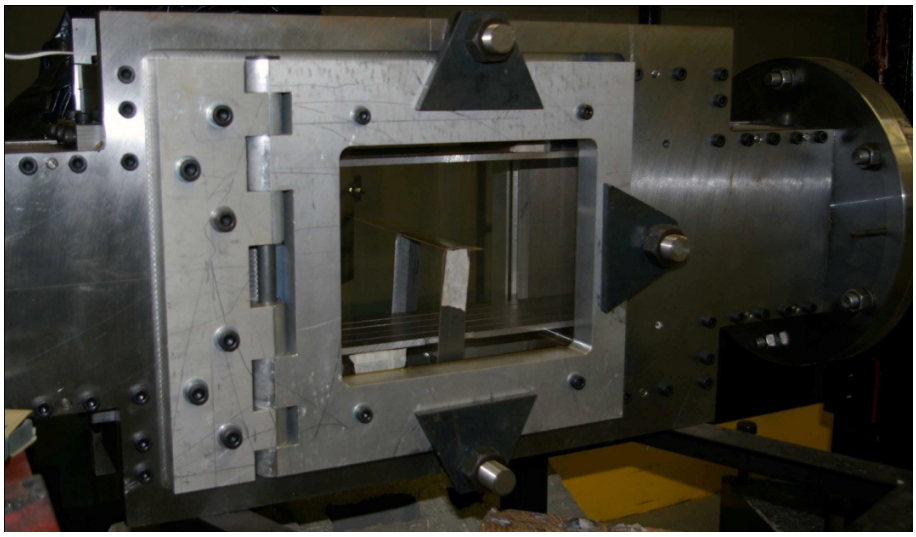


Figure 4.15 Test section after manufacture

The test section itself contained no sensors or instrumentation of any kind since the current study involved getting the apparatus to operate in a satisfactory manner as a transonic wind tunnel. However for future work and further development of the facility, it is essential that

instrumentation is used to gain a better understanding of the flow produced in the test section. Further details can be found in section 8.

4.5 Design of the Test Piece

With the test section designed, a test piece was then required in order to prove that the shock tube was functioning as expected and that the required transonic flow was being established.

Due to the fact that results from the testing would contain very little data, and would be made up largely of pictures of flow features, it was decided that an aerofoil with a large amount of known data be used.

The Fluent computational fluid dynamics program made use of an RAE 2822 supercritical aerofoil in order to validate numerical results obtained from the program. As a result, the designers of the program took a known aerofoil with a large amount of data available, and ensured that the numerical results the program was producing matched the data that was already known. As a result of this fact, numerical results obtained with the Fluent package for the RAE 2822 aerofoil were very accurate. This confidence in accuracy meant that from a visual point of view, the transonic shock positions and shapes for the aerofoil, when subjected to transonic flow, would be a good representation of reality. This fact meant that a good comparison existed if the aerofoil was tested in a wind tunnel, and so the RAE 2822 was chosen as a good test piece to validate the flow in the transonic wind tunnel. The profile of the RAE 2822 can be seen in Figure 4.16.

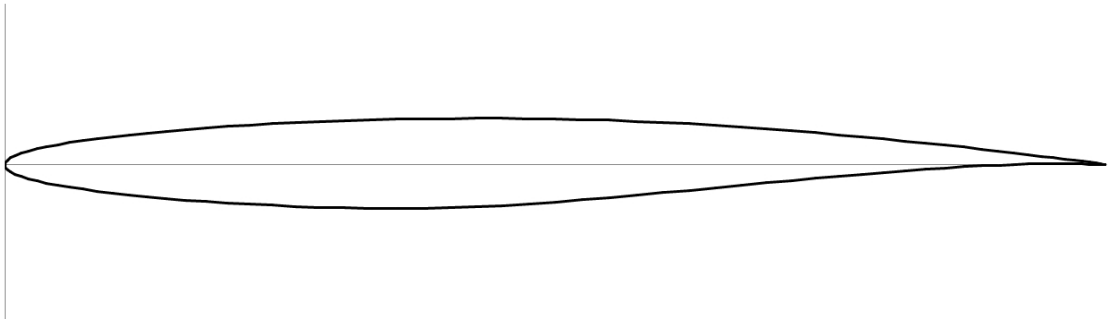


Figure 4.16 RAE 2822 Profile

Due to the nature of the testing required, the aerofoil would span the full width of the test section such that effectively 2-dimensional flow would exist.

Ordinarily test pieces of this nature would be supported by simply clamping them between the two windows on either side of the section. However, due to the fact that Perspex had been chosen for the windows, it became clear that the test piece would likely scratch the windows, and potentially locally distort them from the clamping force. Any distortions would be clearly visible with the sensitive optical system used and so would interfere with the results. Another concern was the relatively high lift and drag loads that would be produced at transonic velocities, and so it was doubtful that simply clamping the piece would hold it in place.

A simple way around the clamping problem, aided by the fact that perspex windows were being used was that holes could be drilled into the perspex to mount the test piece securely. This of course meant that the perspex windows would only be useable with one model, and one angle of attack. If the windows were replaced with the glass ones, as would be expected at some point, a new system would have to be used anyway.

Mounting the test piece with a sting type system meant that it would interfere with the flow around the model and create unnecessary complexity in the design.

With the optical system expected to be used, a solid object like a test piece would appear solid black. This meant that anything attached to the test piece would also appear black and potentially block interesting flow features from view.

As a result of the above, it was decided to mount the test piece with vertical uprights at each end.

This method has a few advantages and disadvantages.

Advantages:

- It would allow stable and secure mounting of the test piece
- Angle of attack would be easy to change
- No damage to the windows
- No interference with flow visualisation on one surface of the test piece

Disadvantages:

- Only one surface of the test piece would be visible
- A full test of the test piece would involve running the wind tunnel twice since the upper and lower surface would need to be tested separately
- Slight flow interference on the surface between the uprights

With these facts in mind, it was decided that the upright mounting method was most practical, easy to achieve, safe and likely to succeed.

Due to only a single surface of the model being tested at one time, it was then decided that two different sets of uprights be manufactured: one set for testing the upper surface and one for the lower. This meant that a single test aerofoil could be manufactured which would be suitable for both upper and lower surface testing.

The proposed layout is shown in Figure 4.17.

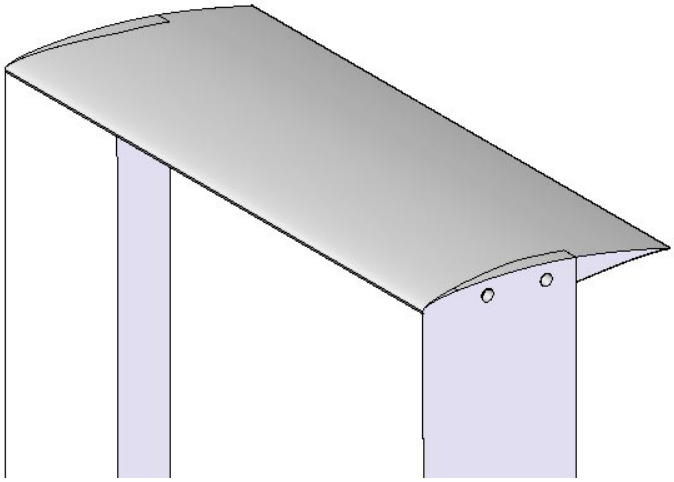


Figure 4.17 Proposed method of mounting the aerofoil

As can be seen, the uprights would extend all the way to the surface in question, and would have an identical profile to that surface. Thus flipping the test piece over and replacing the uprights would allow the other surface to be tested.

It was then decided that changing the angle of attack of the test piece would allow for much greater testing flexibility and improve the results of the study.

The requirement to change the angle of attack during testing of the upper and lower surfaces of the aerofoil meant that the mounting system needed to be capable of positive and negative angles of attack. It was also desirable to be able to adjust the angle by very small increments. The mounting scheme shown in Figure 4.18 was thus conceptualised. The slotted bolt holes allow the uprights to be rotated continuously from -10º to +10º angle of attack.

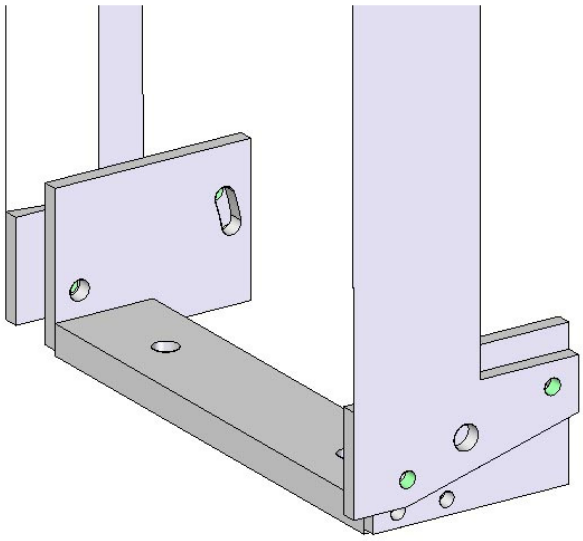


Figure 4.18 Test piece mounting layout

With the layout of the mounting and the type of aerofoil chosen, final dimensions needed to be decided upon. A total blockage of six percent was chosen for the test piece and its mounting system based on wind tunnel testing standards and recommendations.

With the test section area: 157.7mm x 107mm = 16 873.9mm^2

6% = 1012.43mm^2

Making use of the RAE 2822 aerofoil with a 12% thickness and mounting uprights of 3mm thick steel plates, a thickness of 5mm and chord length of 42mm was chosen. The span of the test piece was 107mm. The mounting attachments to the test section body were not included in the blockage calculation because they lie below the slotted wall and so do not form part of the blockage.

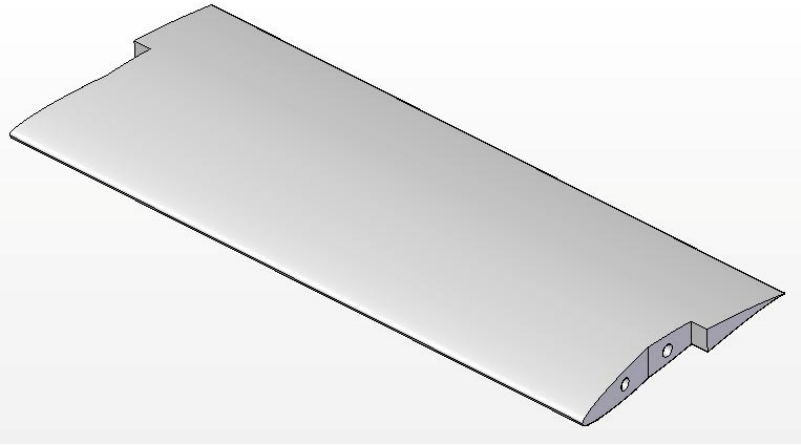


Figure 4.19 Aerofoil with wedge cut-outs for the uprights

The test piece was designed to be mounted in the centre of the test section such that at zero degrees angle of attack, it is in the centre of the windows.

The aerofoil section was machined from brass, while the uprights were mild steel plate. The uprights had a ten degree wedge machined into their leading edge to ensure that they interfered as minimally with the flow between them as possible. The wedge shape also ensures that minimal vibration would occur as the high velocity flow moves past. The wedge shape was also machined into the test piece as shown in Figure 4.19.

The final layout of the test piece mounted for upper and lower surface testing can be seen in Figure 4.20.

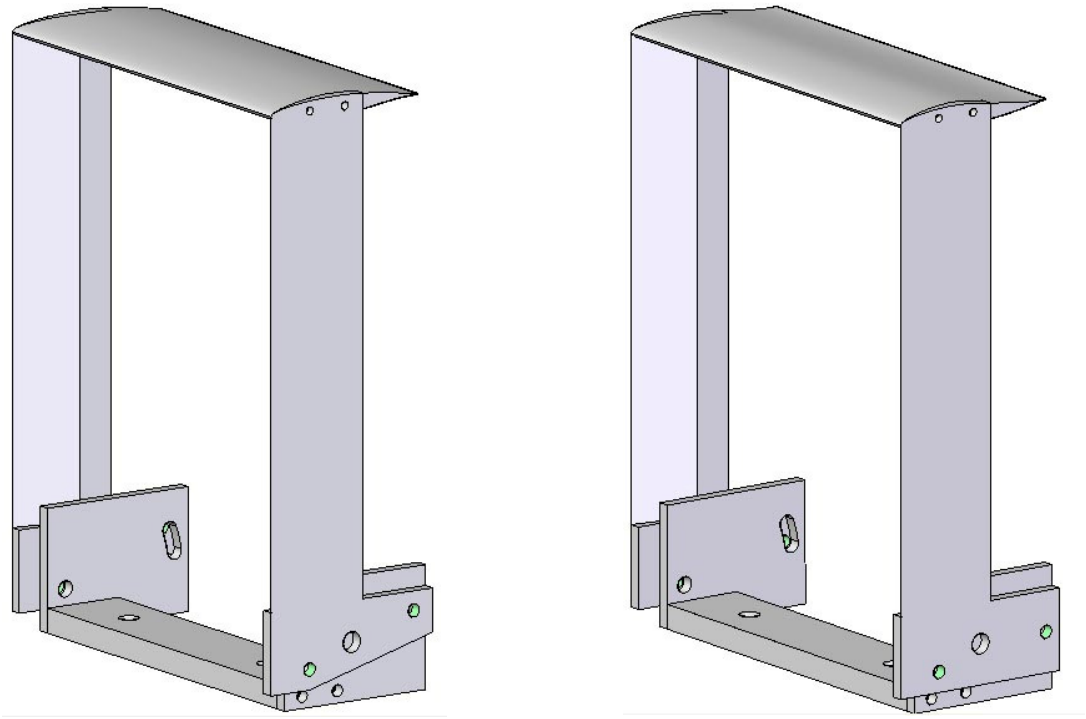


Figure 4.20 Final test piece layout for upper and lower surface testing

The final layout of the test piece within the test section can be seen in Figure 4.21. Again the side of the test section has been removed for clarity. The test section has the 50% open wall layout installed and the test piece is configured for testing the upper surface of the aerofoil at zero degrees angle of attack.

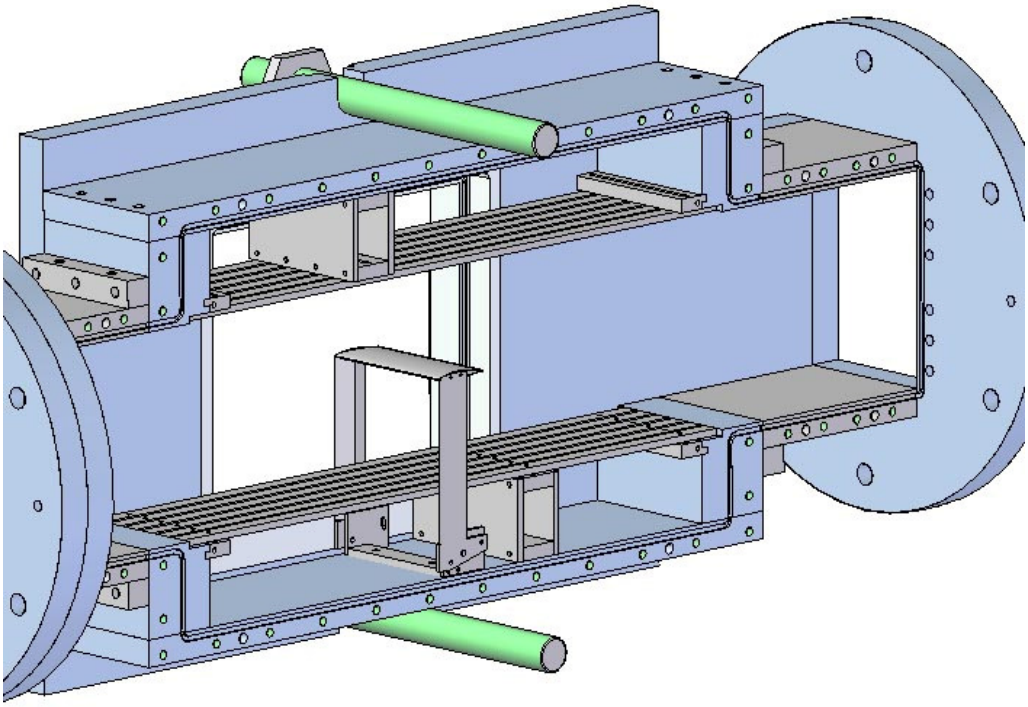


Figure 4.21 Test piece mounted into the test section with 50% open walls

4.6 Design Optimisation Using Kasimir3

Due to the relatively short flow times expected when making use of a shock wave to create transonic flow, maximising the testing time is very important.

The Kasimir3 computer program is capable of taking the standard shock wave equations and producing a graphical output of their results in a form that makes understanding and analysing them extremely simple. The results displayed specifically relate to a shock tube layout that has been input into the program, and takes the form of a wave diagram. As a result it is an invaluable tool in the design of any shock tube. Due to the visual nature of the output, understanding where the various waves will be as well as the fluid properties at any stage, becomes simple.

Once the test section and its upstream cleanup section were designed, the available length of the complete shock tube was known, and thus, an optimum test section position could be found.

First of all, the driver length needed to be decided upon. With the full 15.4 meters available for use in two 6 meter sections, and one 3.4 meter section, a small amount of flexibility existed in its layout. A driver length of either 3.4, 9.4, or 15.4 meters could thus be used since the 3.4m section was required.

A wave diagram was set up using the full driven and variable driver sections available to see how the waves behaved in both sections. The incident and reflected shock waves are displayed in red, while white indicates expansion waves. The contact surface is displayed by the black dashed line.

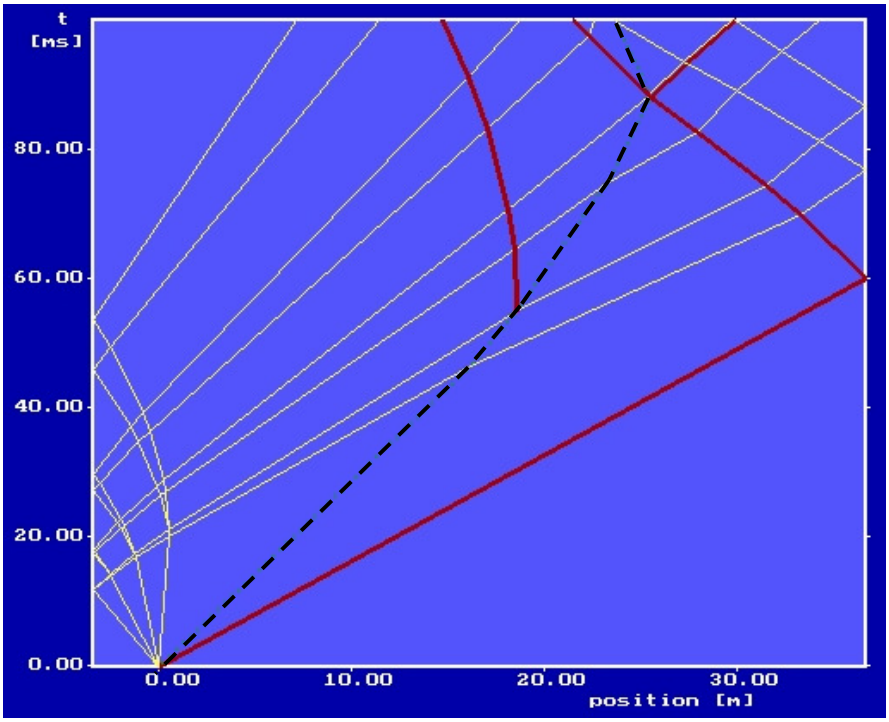


Figure 4.22 3.4 meter driver at a flow Mach number of 0.83

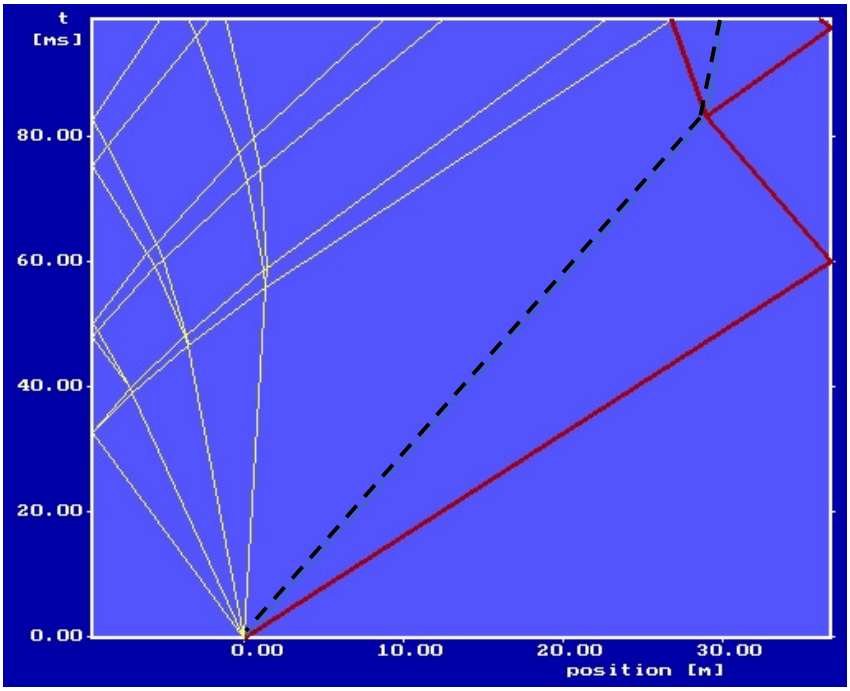


Figure 4.23 9.4 meter driver at a flow Mach number of 0.83

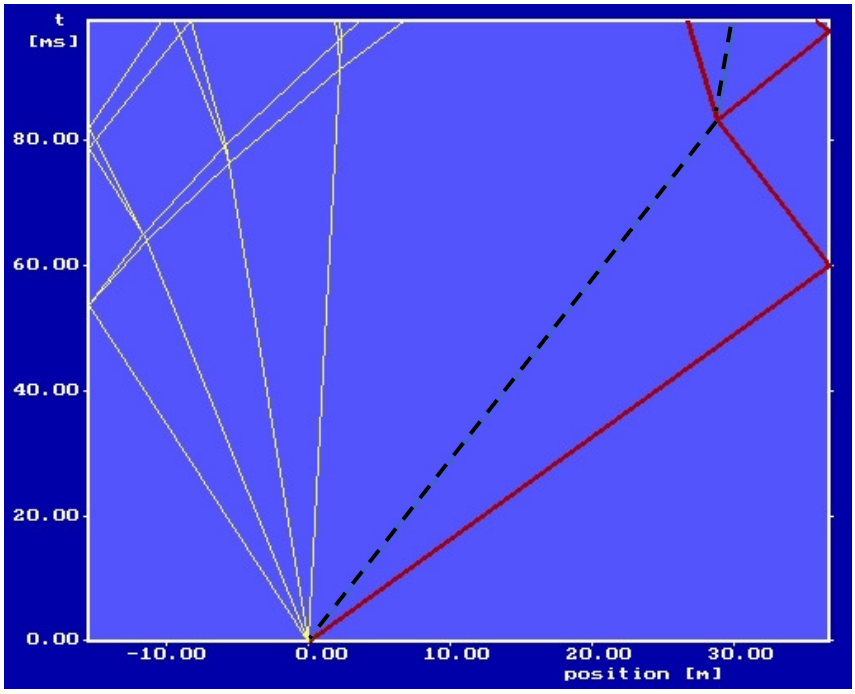


Figure 4.24 15.4 meter driver at a flow Mach number of 0.83

Clearly, in Figure 4.22 the expansion waves actually catch the contact surface as it propagates down the shock tube and ultimately end up shortening the available testing time significantly.

It can be seen that with a longer driver (Figure 4.24), all that is occurring is the delay of the reflected expansion wave off the back of the driver. However, with the available lengths of driven tubing this delay is too long and, as a result, using the 15.4 meter long driver is simply occupying valuable space that could be used to lengthen the driven section and thus delay the return of the reflected shock wave. At the same time, using a 3.4 meter long driver does not provide enough of a delay and the reflected wave interacts with the contact surface too early. The driver length was then fixed at 9.4 meters (Figure 4.23) where the expansion waves enter the test section shortly after the contact surface.

The driver length discussion is only valid for the case of a theoretical flow Mach number of 0.83. However, since Mach 0.83 is approximately in the middle of the testing Mach range, it forms a good basis for developing a compromise for driver length across the Mach range.

With the final dimensions of the entire shock tube known, it became possible to approximate the best position of the test section.

Theoretically the tube can be considered optimised for maximum flow time when the test section is positioned at the point where the contact surface, reflected incident shock wave and reflected expansion wave all meet. Of course for a given shock wave Mach number, there exists only one driver length to driven length ratio that would allow all three of these features to meet at a single point. Since transonic flow covers a Mach range of about 0.7 to 0.9, optimising the shock tube becomes an exercise in compromise.

It was decided that a large portion of the testing to be done would be at a flow Mach number of 0.83 which falls approximately half way between the upper and lower testing limits. The optimising process was therefore performed at Mach 0.83.

Since the driver length had been fixed at 9.4 meters, it became quite difficult to ensure that the reflected expansion wave met the contact surface and reflected incident shock wave at the same point. Thus the point where the contact surface and the reflected incident shock wave met have been used to place the test section. At this point, the theoretical testing time could be calculated based on the time taken for the incident shock wave to pass, and then return. Figure 4.25 shows the theoretical testing time along the thick black line. As before, the incident and reflected shock

waves are shown in red with white lines representing the expansion waves and the black dashed line showing the contact surface.

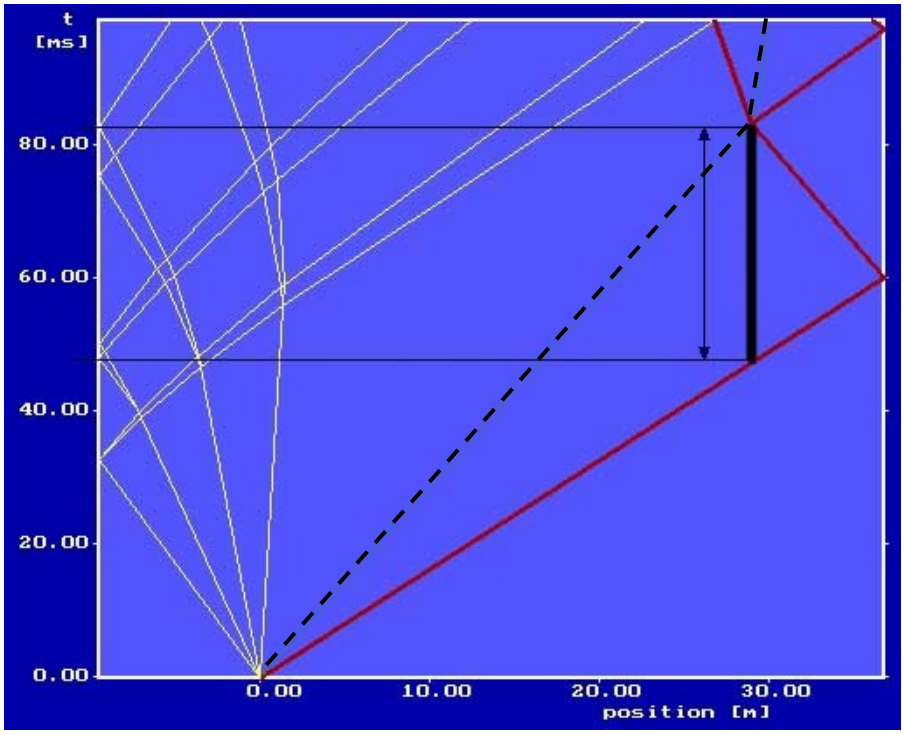


Figure 4.25 Theoretical testing time

This theoretical testing position makes the assumption that all of the flow features do not lose any energy while travelling the length of the tubing which, as it will be shown in section 0, is not true.

Other factors such as walls and practical positioning of the optical system needed to be considered before a final test position was decided upon. The fact that its position could only be achieved to within 0.6 meters, due to availability of tube sizes also needed to be considered.

Since not all of the space in the laboratory had been occupied by the driven section, it was apparent that an increase in available testing time was still possible. An exercise was carried out to establish what gain was possible if an additional 4 meters of driven tubing was attached to the end of the shock tube. At the same time, the optimal testing position needed to be established for the varying lengths of driven tubing. Table 4.1 shows the details for a variety of Mach numbers across the transonic test range.

Table 4.1 Test section position versus driven section length

Mach No	Optimal Test Position at 36.6m (m)	Optimal Testing Time at 36.6m (ms)	Optimal Test Position at 40.6m (m)	Optimal Testing Time at 40.6m (ms)
0.73	27.5	43	30.5	47.9
0.83	28.6	34.7	32.3	39
0.91	30	28.5	33.4	31.6
Average	28.7		32.1	

From Table 4.1 it is apparent that while the addition of 4 meters onto the available tube lengths would increase the testing time, the gains are not huge. At the same time, the optimal testing position shifts a further 3 meters downstream. It is clear that a compromise based on testing time for the various Mach numbers, available tube lengths and laboratory space layout is required.

Since a wall exists at approximately 30 meters from the diaphragm station, and the fact that testing in the room upstream of this wall was highly impractical, it was decided that testing in the room downstream of the wall would be ideal. A test section position of 31.5 meters from the diaphragm station, and 5.1 meters from the end of the tube was chosen for the available tube length of 36.6m. Clearly the optimal testing time is reduced for this position. However, based on the fact that it was highly likely in the future that additional lengths would be added onto the end of the shock tube, this testing position was a good compromise between what was available and what would become available later. In addition, approximately a meter was required between the wall mentioned and the test section to allow practical operation of the shock tube and the set up of the optical system required for visualising the features.

In addition to the aforementioned facts, it will be shown that the theoretically predicted behaviour of the shock tube on which the theoretical test position and thus testing time is based, differs significantly from the actual behaviour of the shock tube. As a result, the theoretical testing position and testing time is simply a guide for an initial position for the test section with the actual position best determined experimentally.

4.7 Instrumentation

The instrumentation detailed provides a guide as to the type of instrumentation required. However, the exact make and model numbers do not need to be matched and as a result these details will be omitted.

Generally speaking, the instrumentation is composed of two, fast response, PCB piezoelectric pressure transducers connected to an amplifier. A delay box and data acquisition system is also required.

The amplified signals from the pressure transducers were sent to the data acquisition system for logging of the data. The upstream pressure transducers' signal was split just before entering the data acquisition system with the second part of the signal connected to the delay box in order to trigger the light source at a given time delay. The data logged by the data acquisition system was used to calculate the Mach number of the shock wave as it propagated down the shock tube.

Details of the procedure required for the correct set up of the instrumentation can be found in section 8.

5 Calibration

With the design and construction complete, calibration of the shock tube could be carried out.

5.1 Diaphragm Thickness versus Pressure Ratio

It is possible to estimate the thickness of the diaphragm material required to hold a given pressure ratio across a given cross sectional area theoretically. However, from a practical point of view, it is much simpler to install a diaphragm of a given thickness and then increase the pressure ratio across it until it bursts naturally. Using the diaphragm of a given thickness at a slightly lower pressure ratio should ensure that it does not burst naturally, but upon application of a bursting mechanism, it should burst instantly.

Due to the high pressure ratios required to produce a shock wave with a high enough Mach number to induce transonic flow, a diaphragm thickness was found that was capable of withstanding a pressure of 14 bar on the one side while a vacuum of up to 0.15 bar was drawn on the other side.

After running a few experiments, it was found that two pieces of 300 micron sheet and two pieces of 100 micron sheet were required to hold the pressure difference, while at the same time not being too thick for the pricker to burst. It was further discovered that the two 100 micron sheets needed to be placed on the pricker side of the diaphragm. This meant that upon activation of the pricker, the 100 micron sheets would rupture and reduce the overall strength of the diaphragm far enough to cause the thicker 300 micron sheets to rupture. The rupturing of the diaphragm was a bit unreliable however, with some tests not rupturing at all. In addition some tests simply leaked for a while and then ruptured which meant that the pressure ratios set would have changed.

When the same combination was subjected to the same conditions with the 300 micron sheets on the pricker side, a neat hole was punched through the diaphragm, but the whole barrier did not rupture as planned.

A completely reliable rupturing needed to exist.

5.1.1 Pneumatic pricker

The reliability problems were due to the pricker having been designed for the original shock tube which operated at 4 bar driver pressure. This pricker was pneumatically actuated by air pressure regulated to 6 bar. An upgrade of the pricker was required in order to get reliable and instant rupturing of the diaphragm and so the pressure limitation was removed, and the full 15 bar pressure was used to actuate the pricker.

At the same time, the piston driving the pricker as well as its housing were removed and upgraded. The housing was bored out to a larger inner diameter, while a new piston was machined. The combination of a higher actuation pressure, as well as larger piston area meant that the pricker actuated with a much greater force and was capable of rupturing the thick diaphragm consistently and reliably.

5.1.2 Second diaphragm station

The requirement of vacuuming the driven section of the shock tube and the decision to use a diaphragm at the end of the shock tube meant that a suitable diaphragm needed to be found. It was established that the 50 micron sheet was capable of holding a vacuum of 0.1 bar on the one side, with Johannesburg's atmospheric pressure of 0.83 bar on the other side. It was also known that a diaphragm of this thickness would rupture with approximately 2.5 bar of pressure being applied to it, ensuring that the test section and tubing were not exposed to unnecessarily high pressures for an excessive amount of time. The diaphragm, in effect, acted like a high volume flow rate one-way valve making it ideal for use at this position in the tube.

5.2 Pressure Ratio versus Mach Number

Theoretically, we are able to predict the Mach number of a shock wave produced from a given pressure ratio. Of course theoretical predictions do not necessarily translate into reality and so these predictions needed to be validated.

The shock wave equations from section 0 predict the following for a shock wave propagating into a driven pressure of 0.83 bar at 20 ºC. All pressures are absolute pressures.

Table 5.1 Pressure ratio required to achieve a theoretical test Mach number

P4 (bar)	P1 (bar)	P4/P1	Shock Mach No'	Flow Mach No'
8.46	0.83	10.20	1.61	0.70
9.15	0.83	11.03	1.64	0.72
9.93	0.83	11.97	1.66	0.74
10.79	0.83	13.00	1.69	0.76
11.80	0.83	14.21	1.72	0.78
12.87	0.83	15.51	1.75	0.80
14.07	0.83	16.95	1.77	0.82
15.40	0.83	18.56	1.80	0.84
16.89	0.83	20.35	1.83	0.86
18.55	0.83	22.35	1.86	0.88
20.42	0.83	24.61	1.90	0.90
22.53	0.83	27.14	1.93	0.92
24.90	0.83	30.00	1.96	0.94

In the case of a shock tube producing a shock wave, the Mach numbers shown in Table 5.1 are only likely to be achieved just downstream of the diaphragm. Taking losses from the bursting of the diaphragm as well as disturbances causing shock wave attenuation into account, it is reasonable to assume that the pressure ratio required would be higher.

With the pressure transducers on the shock tube located at approximately 31 meters from the diaphragm station, any losses that occur as the shock wave propagates along the length of the tube should be noticeable.

Due to the fact that the maximum pressure obtainable from the compressor in the Mechanical Engineering laboratory is 15 bar, and considering that the driver for the shock tube has a non-zero volume, the actual attainable maximum pressure at the apparatus is approximately 14.3 bar once equilibrium had been reached. The 15 bar pressure could be obtained in the event that the

compressor was left running during pressurising of the driver, but this was considered impractical. As a result, it became necessary to determine the shock wave Mach number at the test section given the available pressure of approximately 14.3 bar.

A test run at a driver pressure of 14.2 bar into atmospheric pressure of 0.83 bar at 23º Celsius, created a shock wave Mach number of 1.71 where theoretically a Mach number of 1.77 should have been produced. This meant that the flow behind the shock wave would have been Mach 0.77, where theoretically it should have been Mach 0.82.

It therefore became clear that a significant amount of energy was being lost as the shock wave propagated along the length of the tube. Given the fact that the industrial steel tubing was not smooth inside, had a welded seam running the length of it, and the fact that over the 31 meters many tube joints existed, it was not surprising. It was desirable to understand where the losses were occurring, and whether anything could be done to improve the efficiency of the tubing.

From an expense point of view changing the type of tubing making up the shock tube was not practical. Improving the efficiency across each joint was much more feasible and so an attempt was made at understanding where the losses were occurring.

5.2.1 Examining joint losses

Each joint had a few features that needed to be examined in order to understand whether an improvement in efficiency could be achieved.

Each flange was accurately machined and included two reamed 8mm locating holes where a dowel pin could be fitted. This would have ensured that each flange was accurately aligned to the other. However, during manufacture of the driven section tubing nothing was done to ensure that the flange was accurately aligned with the tube. At the same time, each length of tubing differed slightly, with its cross section being a slightly different shape, or the welded seam being in a slightly different position. As a result, despite the fact that the flanges were accurately aligned with one another, the tubing did not necessarily align, and this lack of alignment would undoubtedly cause losses as a shock wave passed through. Short of remanufacturing the driven section lengths, this feature had to be accepted.

Due to the need to ensure that a vacuum could be drawn along the full length of the driven section, each joint had a rubber gasket to aid in sealing it. These gaskets are approximately 1.5mm thick and made from rubber insertion material. The gaskets were cut out by hand, and so while every effort was made to ensure that they fitted properly, they were not perfect. At the same time, upon tightening of the bolts on the flanges of the tubing, the gasket would have been compressed and could have caused a slight protrusion. In the event that the gasket did not protrude that much, a possible indent could exist at the joint. Since the gasket material was approximately 1.5mm thick, any discrepancy would have caused a gap or protrusion of approximately this thickness, and so, it was decided to examine whether a different method of sealing the joints would yield a better efficiency.

A section of the driven tubing was chosen where four consecutive lengths of the same dimension were placed. Each length then had a pressure transducer placed at its midpoint, thus allowing the shock wave Mach number to be determined in three different places, and effectively across three different joints. This meant that across the first joint, an initial Mach number could be found and compared to the Mach number found across the second and third joint.

Tests were then run at 13.5 bar driver pressure into the driven section, both having an atmospheric pressure of 0.83 bar followed by 13.4 bar into a vacuum of 0.23 bar. Each test was run twice to get an average value to ensure that the calculated losses were consistent. The values are displayed in Table 5.2.

Each flange has been machined with accuracy and so their faces have a good surface finish. As a result, it was decided that removing the rubber gasket and replacing it with another form of sealant would potentially improve the joint. Sikaflex was decided upon due to its properties and the fact that, similar to silicon, it starts off liquid and then sets to a flexible but firm consistency.

To start off, a single flange had a thin bead of Sikaflex applied to it, and was then clamped up only to be taken apart immediately in order to gauge how much the sealant spread upon clamping. After that, the joint was wiped clean and resealed, along with another two consecutive joints, and the Sikaflex allowed to set. Of course, due to the liquid nature of the sealant, the flanges being joined were virtually in complete contact with one another, so the joint was undoubtedly closer and had fewer imperfections.

The same tests were run, as described before, in order to understand the effects on the efficiency of the joint after the sealing method had been changed.

Table 5.2 Comparison of Mach numbers across joints

	Vacuum			Open		
	Mach Number Across Joint			Mach Number Across Joint		
	1	2	3	1	2	3
Before	2.07	2.06	2.03	1.65	1.63	1.62
	2.08	2.05	2.02	1.66	1.64	1.63
Ave	2.08	2.06	2.03	1.65	1.64	1.62
Difference	**0.02**	**0.03**		**0.02**	**0.02**	
After	2.06	2.04	2.03	1.66	1.64	1.63
	2.08	2.07	2.05	1.66	1.65	1.63
Ave	2.07	2.06	2.04	1.66	1.64	1.63
Difference	**0.01**	**0.02**		**0.02**	**0.02**	

Table 5.2 shows the difference in Mach number across various joints before and after the joints were re-sealed using the new method.

It is fairly clear to see that for the tests run into the driven section at atmospheric pressure, no improvement was found in the losses over each joint. For the tests run into the vacuumed driven section, an improvement of Mach 0.01 per joint loss was found, and therefore over 15 joints, an improvement in shock wave Mach number of approximately 0.15 could be expected. Given the amount of time and effort to reach this level of improvement meant that redoing all of the joints in this manner was not feasible.

As a result, it was decided that the main losses in Mach number occurred as a result of the tubing used, and the alignment of the joints along the length, rather than the method employed to seal the joints, and so, nothing could realistically be done about it.

In order to get the Mach number at the test section to the required value, given the limit of 14.3 bar in the driver, two options were available.

Firstly, the test section could be moved closer to the driver section, thereby removing a large percentage of the total losses, but at the same time drastically reducing the testing time available. Since one of the main purposes of the shock tube was to maximise testing time, this method was considered counterproductive and abandoned.

The second option was to evacuate the driven section further, and thus increase the pressure ratio across the diaphragm, while leaving the driver pressure at the maximum available. In order to

achieve this, a small amount of additional sealing was required due to small leaks that were discovered at higher vacuum. All of the leaks discovered were in the welds holding the flanges onto the driven tubing lengths. These leaks were fixed by drawing a large vacuum in the section, and then smearing Sikaflex around the affected area, while the vacuum pulled some amount of the sealant in to the hole. With all the leaks fixed, a final vacuum of 0.12 bar was achieved.

With the new higher vacuum pressure available, two of the pressure transducers were replaced in the cleanup section of the shock tube in order to determine what shock wave Mach number could be achieved under the higher vacuum conditions.

Tests were run and shock wave Mach numbers capable of producing the transonic flow in the uppermost region of the transonic window were easily attainable.

With the optical system, as described in section 2.3, set up and tested, a photo was taken to ensure that the shock waves produced would appear with the required sensitivity, and that the shape was approximately what was expected. The first shock wave image is shown in Figure 5.1 with the wave travelling from right to left.



Figure 5.1 First shock wave image

The curvature seen in the shock wave in the upper half of the image was due to the slotted floor not being installed. The apparent thickening of the shock wave in the lower part of the image is due to the in-plane curvature created in the shock wave, perpendicular to the flow direction and is due to the slotted nature of the lower wall. Other disturbances behind the incident shock wave are due to the complex reflections occurring because of the nature of the layout of the test section.

These disturbances are to be expected, especially early on in the testing time window, however due to the relatively long testing time available, features like these would disappear early on in the test flow.

It was decided that the shock tube was complete and testing of the actual test piece could take place.

6 Testing Procedure and Precautions

In order to set up and run the shock tube in the correct manner, it is recommended that the following procedures and precautions are considered.

6.1 Test Section Set Up Procedure

Slotted wall set up and installation:

Select the desired open area ratio and thus the correct slot thickness to provide that ratio.

Loosely install all of the floor members onto their supports.

Starting on one edge, measure the required gap between members using a vernier.

Set each corresponding member at the correct distance from the previous one, tightening the bolts as you go.

Once complete, re-measure all of the gaps to ensure that they are set correctly.

Pull the hinge pin out of the door, and remove the door.

Remove the bolts securing the door hinge mounting plate in position and remove the plate.

Carefully install the slotted wall position. Angling the slotted wall laterally in the direction that the slot mountings are ground down will help clear the side walls inside the test section.

Once in position, install the securing bolts after wrapping them with PTFE tape.

Reinstall the hinge plate but do not tighten the bolts.

Replace the door and install the hinge pin.

Close the door and tighten one of the door securing plates by hand.

Tighten the hinge plate bolts, and, after removing the door securing plate again, check that the door opens and closes freely.

Precautions:

Check that there is enough clearance between the outer slot and the test section wall for the test piece mounting upright.

Do not force the slotted wall into place as this could damage the test section wall or the slotted members.

Using your fingers, ensure that there is no step between the test section entry and exit upper and lower walls and the slotted walls.

6.2 Test Piece Set Up Procedure

The test piece needs to be set up in the correct configuration for the test required. It must be decided whether the upper or lower surface is to be tested, and at what angle of attack.

Due to the design of the mounting of the test piece, each surface has its own customised upright to support it. The correct upright must be fitted to the model.

With the model and mounting structure removed from the test section, the bolts that secure the angle of attack must be nipped up but not tightened.

Install the mounting system into the test section, with the aerofoil section not installed, to allow the mounting to fit around the slotted wall.

Tighten the mounting system to the test section.

Install the aerofoil section by gently separating the uprights, and allowing the pins in the aerofoil to click into position.

Making use of a bubble inclinometer, measure the longitudinal angle that the test section is installed at.

Making use of a bubble inclinometer, measure the angle of attack using the flat side of one of the uprights and set the angle of attack relative to the angle of the test section, rather than the earth.

Gently tap the uprights to give the desired angle of attack.

Gently separate the uprights and remove the aerofoil, taking care not to change the angle of attack.

Remove the mounting system carefully to allow access to the angle of attack securing bolts.

Tighten the bolts carefully, ensuring that the angle of attack is not altered.

Reinstall the mounting back into the test section, and reinstall the aerofoil.

Check the angle of attack with the bubble inclinometer.

Once everything is confirmed as being correct, the doors can be closed and the securing plates tightened into position.

Precautions for set up of the test piece:

Ensure the correct uprights are used for the correct surface

Ensure that the angle of attack is measured on both uprights, as a small amount of twisting is possible due to the tolerances in manufacture.

Ensure that the angles measured with the bubble inclinometer are on reliably flat portions of the test section and model. Measuring the angle of attack directly with the model will yield errors.

Ensure that the model is tightened to the test section properly before measuring the angle of attack to ensure that there is no play in the setup.

The brass model is easily damaged and the thin trailing edge must not be handled.

Ensure no tools or bolts are left inside the test section.

6.3 Shock Tube Set Up Procedure

Once the desired Mach number has been chosen, the corresponding diaphragm material can be installed at the diaphragm stations. In the event that the desired Mach number is low enough that firing the shock wave into a vacuum is not required, the thin diaphragm at the downstream end need not be installed.

At the upstream diaphragm station:

Open the station by removing all the bolts and sliding the driver backwards.

Ensure that the pneumatic pricker is free moving and is in its fully retracted position.

Smear a small amount of axle grease on the area where the diaphragm will rest to help keep it in position.

Close the driver onto the driven section and install all the bolts.

Slowly tighten each bolt opposite one another to ensure that the two flanges align correctly. Ensure that the bolts are adequately tight.

At the downstream diaphragm station:

Open the station by removing all the bolts and sliding the last driven section away.

Install one sheet of 50 micron diaphragm material. Apply some axle grease to hold it in position if necessary.

Close the station by sliding the last driven section back into position.

Slowly tighten each bolt opposite one another to ensure that the two flanges align correctly. Ensure that the bolts are adequately tight.

6.4 Optics Set Up

Making use of a candle or similar heat source, set the sensitivity of the schlieren system to desired level.

Leaving the room, take a test photograph to ensure that the sensitivity is still correct. This step is required due to the fact that the floor on which the optical system is mounted warps when it is stepped on.

Remove the heat source from the schlieren system.

6.5 Data Acquisition System Set Up

Connect and switch on the various components of the data acquisition system and the optical system.

Start the data acquisition software and ensure it is communicating with the various components.

Allow the system to stand for approximately ten minutes to heat up adequately.

Set the required delay time on the delay box as well as the type of trigger signal required to trigger it.

Push the test button on the delay box to ensure that the light source is being triggered.

Set up the data acquisition software with the correct pre-trigger time, sample rate, trigger values and recording time required for the test in question.

6.6 General Set Up Precautions

Ensure nothing is near the end of the shock tube.

Check that each transducer is being read correctly and has reached a steady value.

Do not leave anything inside the tube that is not supposed to be there.

Ensure that the doors are correctly tightened and that all of the bolts are in position.

6.7 Testing Procedure

Once the shock tube, data acquisition system and optical systems have been set up correctly, the testing procedure can commence.

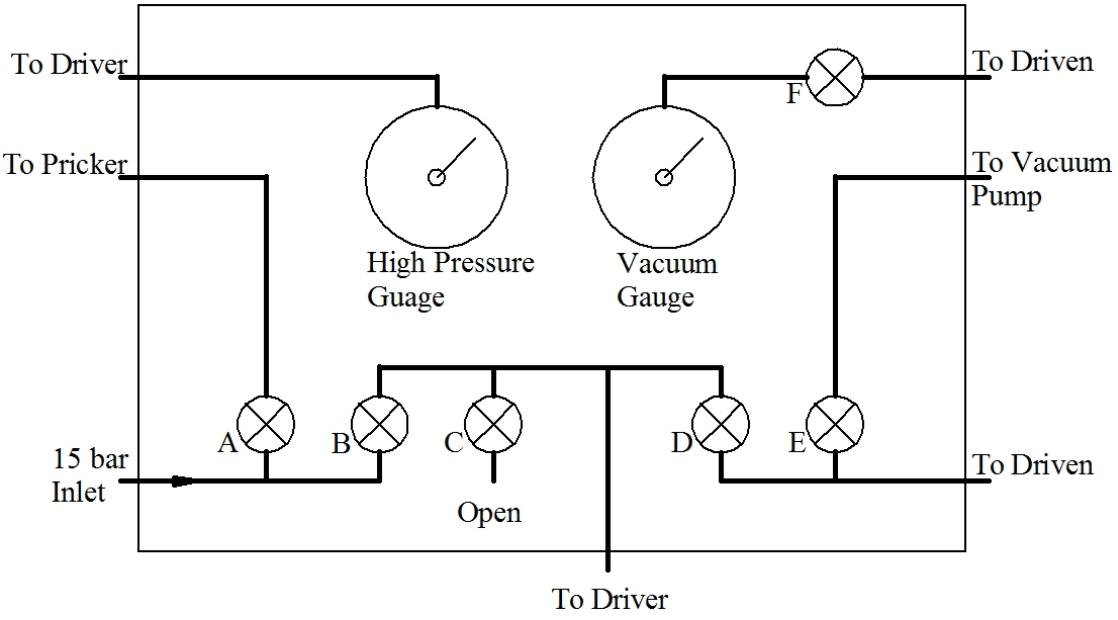


Figure 6.1 Schematic layout of the control board

Ensure that all handles on the control board are set to *closed* and that the high pressure air valve is open, pressurising the line to the control board only.

If the testing Mach number requires the shock wave to be fired into a vacuum, open the valves E and F and start the vacuum pump.

Observe the vacuum gauge and ensure that the pressure is dropping.

Once the pressure is nearing the required value, arm the trigger box and data acquisition software, turn off the lights in the testing room and close and arm the door locks into the room.

Allow the vacuum pressure to overshoot slightly and close valve E and turn off the vacuum pump.

Very carefully open valve D in order to set the vacuum pressure accurately.

Once set, close valve D and valve F.

Blow the whistle to warn bystanders that a test is imminent, and put on hearing protection.

Open valve B and observe the increase in pressure on the pressure gauge.

Once the gauge nears the desired value, blow the whistle again and open the camera shutter.

As the pressure gauge reaches the required pressure, quickly open valve A to fire the shock tube.

Close the camera shutter.

Close valve B.

Very gently open valve F to relieve the vacuum in the gauge.

For tests not requiring a vacuum, simply ensure that the valves for controlling all aspects relating to the vacuum (E and F) are closed, and run the test in the same manner.

Running Precautions:

It is extremely important to ensure that the handle isolating the vacuum gauge (valve F) is closed whenever the shock tube is fired, or the gauge will be damaged.

Ensure that the testing room doors are locked during firing.

If the shock tube does not fire correctly and the driver is left pressured, open the valve C to purge the pressure before opening the diaphragm station. Always wear hearing protection in this scenario because the weakened diaphragm could rupture at any time.

7 Results

The results take the form of both numerical and experimental results, while a comparison is made between the two in order to establish whether the shock tube is operating as it was designed. Due to the nature of the study, more emphasis was placed on the results obtained experimentally, while the numerical results were used solely as a validation tool.

7.1 Computational Fluid Dynamics

As stated previously, the aerofoil section used during testing is the same type that Ansys used to validate their numerical models for the transonic test range during the design of the computational fluid dynamics package, Fluent. As a result, great confidence can be had in the numerical results obtained when the setup of the study in question is the same as that which was used during their validation phase. The mesh layout shown in Figure 7.1 is identical to that used during their validation. In addition, the same mesh was used to create some of the numerical results found in the Ph.D thesis submitted by Roohani (2010). The mesh extends to approximately ninety chord lengths from the aerofoil in question thus ensuring that the boundary of the mesh has no affect on the flow features produced by the aerofoil.

The mesh consists of quadrilaterals with decreasing dimensions as they approach the aerofoil in order to provide greater definition where a large amount of detail is required.

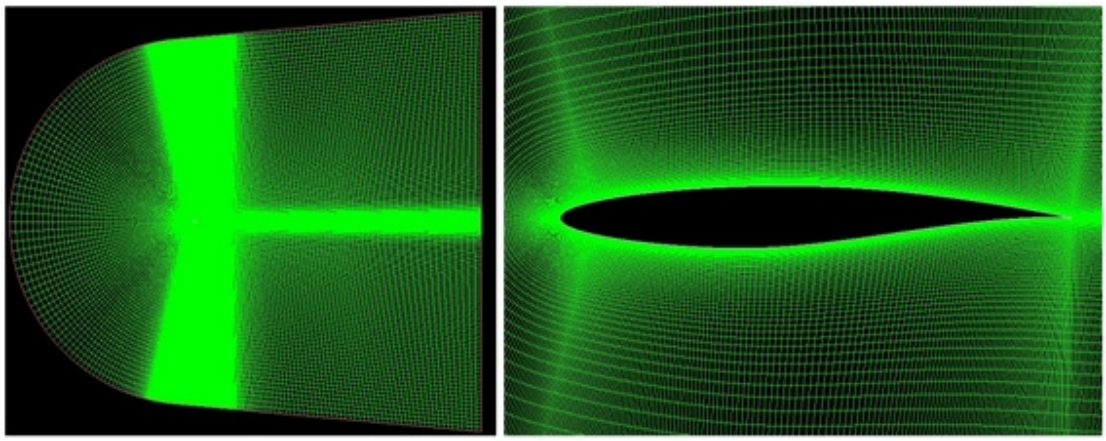


Figure 7.1 Layout of mesh

The number of iterations that were completed for each test was dependent on the shape of the residual graphs and the solution was accepted as converged once the residuals indicated no major change with additional iterations. Convergence tended to be in the region of 15000 to 30000 iterations.

The setup of the numerical results corresponded to the setup validated by Fluent during the development of the software package. The viscous model type was Spalart-Allmaras while the solution was set to steady state, two dimensional with a coupled solver. Finally, the formulation was set to implicit.

Numerical results were computed as shown in Table 7.1 to provide the greatest coverage of the range of Mach numbers to be tested in the wind tunnel as well as to gain a better understanding of the behaviour of the aerofoil at Mach numbers that were not tested.

Table 7.1 Available CFD tests

Angle of Attack	**Available Mach Numbers**			
0°	0.834	0.86	0.88	
2.79°	0.73	upto	0.94	in 0.01 increments
5°	0.83	upto	0.9	in 0.01 increments

7.1.1 Numerical Results

Due to the fact that the primary purpose of the study is the validation of the operation of the wind tunnel that was designed, the numerical results will not be discussed in depth on their own, but rather with specific reference to the tests carried out. Therefore results in section 7.1.1 are presented so as to develop a better understanding of what to expect from the experimental test results.

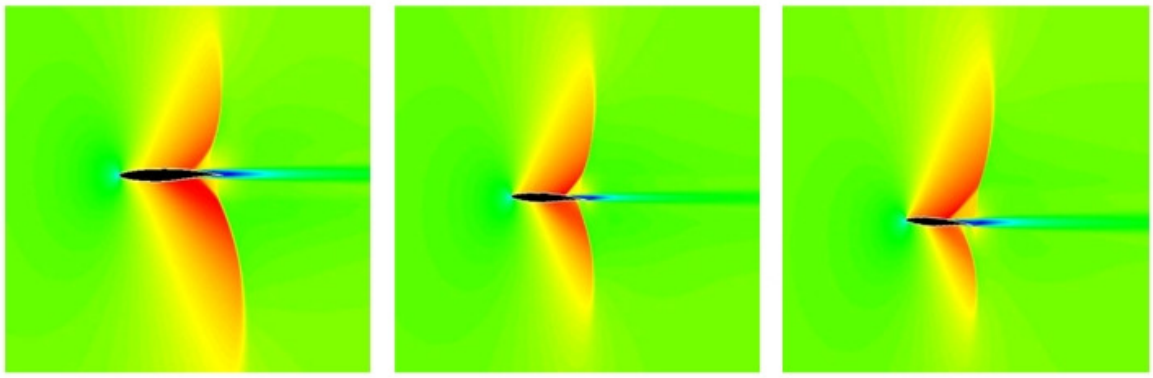


Figure 7.2 CFD at Mach 0.88 at 0º, 2.79º and 5º angle of attack

Contours of Mach number are plotted in Figure 7.2, with the model set at different angles of attack. It is apparent that with an increase in angle of attack, the shock wave on the lower surface weakens while that on the upper surface gets stronger. The increase in strength on the upper surface ultimately results in a larger lambda shock system forming, while on the lower surface the lambda shock system gets smaller.

In general, it is apparent that the numerical results include the stagnation point at the leading edge of the aerofoil as well as the wake region trailing downstream. The shock waves are very apparent in the contours of Mach number and it is easy to see that the numerical results are highly sensitive to small changes in the flow conditions.

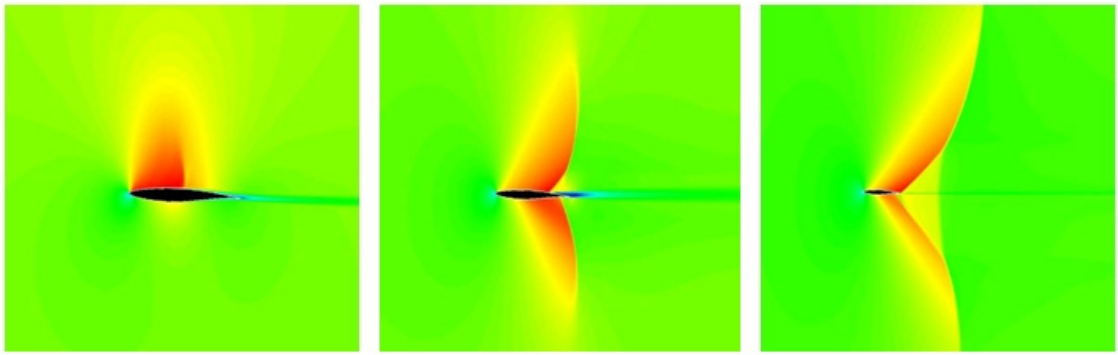


Figure 7.3 CFD at 2.79º at Mach 0.73, 0.83 and 0.93

The series in Figure 7.3 shows how the shock waves increase in strength with an increase in flow Mach number. Additionally, it is apparent that an increase in Mach number results in the shock waves forming further downstream on the aerofoil. As expected, the higher the flow Mach number, the further the shock waves extend into the surrounding flow.

It is apparent that the numerical results produced will be an extremely valuable tool in validating the correct functioning of the wind tunnel.

7.1.2 Fluent Results Validation

During the development of the Fluent CFD package, it was necessary for the developers to validate the results obtained in the transonic Mach range to ensure that the package was yielding the correct solutions. The RAE 2822 aerofoil was chosen for the validation, due to the fact that there was a reasonable amount of data available pertaining to the shock wave position, static pressure coefficients and the lift and drag coefficients. The available data was created in the RAE 8 x 6ft transonic wind tunnel (North Atlantic Treaty Organisation - Fluid Dynamics Panel, 1979).

Among other validation cases of different test setups and aerofoils, Fluent made use of the 9th test case detailed in the Agard AR-138 Report (North Atlantic Treaty Organisation - Fluid Dynamics Panel, 1979) in which the RAE 2822 model was subject to Mach 0.73 flow at 2.79 degrees angle of attack. Comparison was made to results obtained using the Fluent software. Of particular interest to the study in question was the shock wave position on the aerofoil.

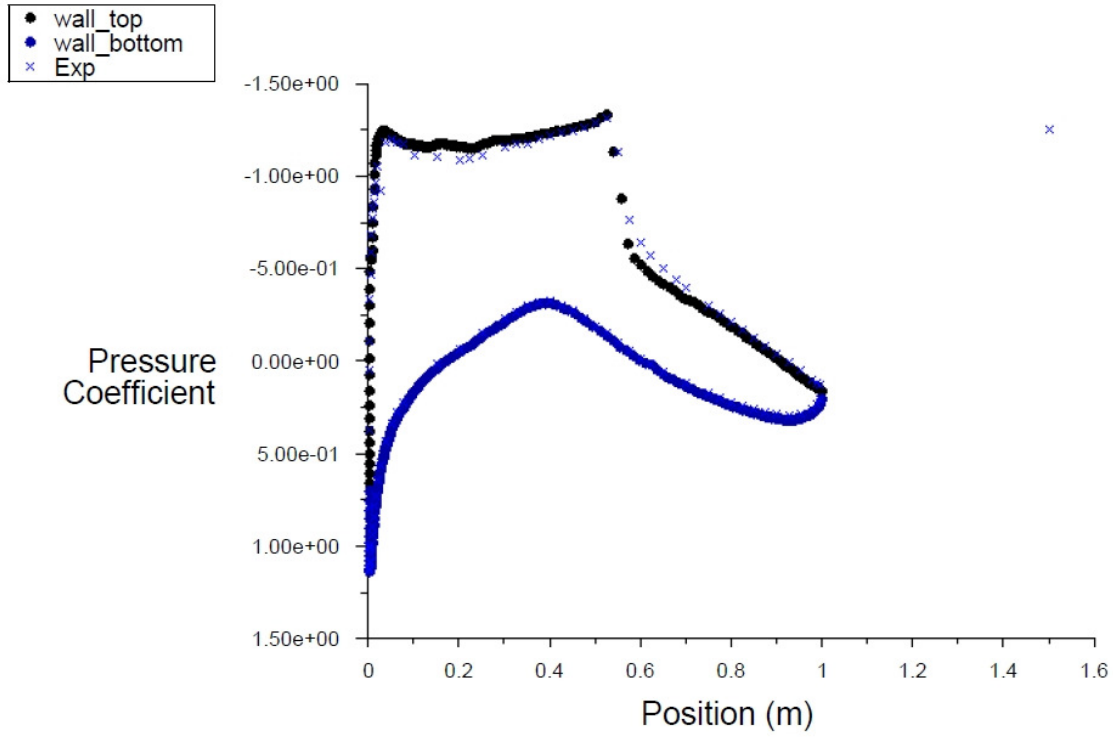


Figure 7.4 Comparison of numerical and experimental pressure coefficient by Fluent (Fluent Inc., 2006)

The shock wave position is considered to be the position on the aerofoil where the pressure coefficient increases rapidly, and so, from Figure 7.4, it is seen at approximately 52 % of the aerofoil chord length. It is apparent that the experimental and numerical results match up extremely well, with very little variance in the predicted shock wave position. As expected, at the relatively low Mach number, no shock wave is seen on the lower surface of the aerofoil.

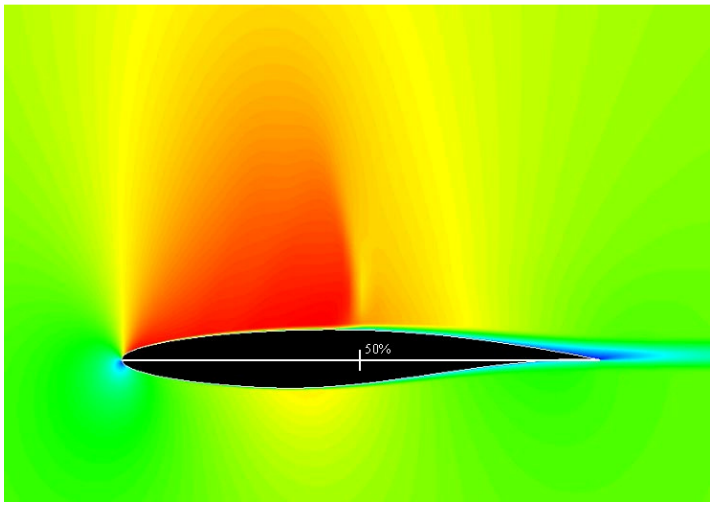


Figure 7.5 Mach 0.73 and 2.79˚ angle of attack

As expected, Figure 7.5 shows the shockwave at approximately 50 % chord. Fluent stated during their validation that they obtained accuracy in shock wave position of 96%, and so a small amount of variance in the shock wave position can be expected. However, it can be said that there is great confidence in the results obtained through the use of the Fluent software.

7.2 Wind Tunnel Test Results

Due to the complexity of the testing procedure and time constraints for the study, a limited number of tests needed to be performed in a range that would provide the greatest proof that the wind tunnel was operating correctly. It was therefore decided that the core of the results would be made up of tests run at a Mach number in approximately the middle of the transonic range. The Mach number chosen was 0.83.

Angles of attack of 0, 2.79 and 5 degrees were chosen to allow data to be collected at various angles of attack, thus providing insight into the performance of the wind tunnel with various test piece configurations. The core of the testing was carried out at an angle of attack of 2.79 degrees. The reason for the angles chosen was to match up with the angles of attack found most commonly in the literature.

The final testing program was carried out as shown in Table 7.2.

Table 7.2 Summary of testing carried out

50% Open Wall						
AoA	0º		2.79º		5º	
Mach No	Time Delay Upper (ms)	Time Delay Lower (ms)	Time Delay Upper (ms)	Time Delay Lower (ms)	Time Delay Upper (ms)	Time Delay Lower (ms)
0.73			21	21		
			24			
			25.5			
0.83	1.61					
	3					
	6					
	9	9	9	9	9	9
	12	12	12	12		
	15	15	15	15	15	15
			18	18		
	21	21	21	21	21	21
		23	24	24		
	27		27	27	27	27
	30	30	30	30		
	33		33	33		
	40		36	36		
			39	39		
				42		
			45	45		
0.91				10		
				15		

10% Open Wall						
AoA	0º		2.79º		5º	
Mach No	Time Delay Upper (ms)	Time Delay Lower (ms)	Time Delay Upper (ms)	Time Delay Lower (ms)	Time Delay Upper (ms)	Time Delay Lower (ms)
0.83			15	15	15	15
			21	21	21	21

7.2.1 Initial Photographs

Upon the first firing of the shock tube, initial photographs were taken to ensure that a planar shock wave was being correctly formed, that the schlieren system was working adequately, that all instrumentation was taking readings, and that the readings made sense.

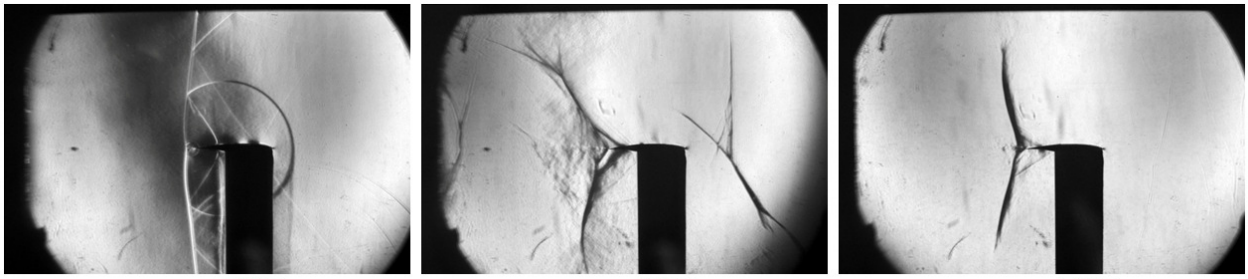


Figure 7.6 Shock tube start-up process

As the incident shock wave travelled over the test piece (0.06ms), a circular reflected wave started propagating outwards from it. The first image in Figure 7.6 is at 0.06ms after the incident shock wave arrived at the leading edge of the test piece. The incident shock wave is now no longer a vertical line as revealed by the schlieren image, but slightly curved due to the obstruction it has encountered. The lower half of the incident shock wave also appears thicker than the upper half and this is because the lower half has been curved in the plane of the image due to the two uprights that it has passed through. Thus the left edge of the thick part of the incident shock wave would be the part of the wave that passed through the centre of the uprights and so experienced their effects the least, while the right edge of the wave is the portion closest to the two windows. This portion would have lost a small amount of energy passing over the uprights, and so has slowed the wave slightly causing the in-plane bending seen. Other wave features are also visible in the image and are due to the complex reflections and refractions of the wave throughout the slotted wall and plenum chamber regions of the test section. Their exact composition and source is of little interest except that they need to have disappeared by the time semi-steady state flow has been set up.

At 1.45ms the incident shock wave is positioned 0.91 meters from the leading edge of the test piece. Some complex flow features are clearly visible and are likely due to all of the reflected

shock waves and other flow features interacting with the transonic flow that they are in. Again their composition is of little interest.

At 4.45ms the test section is largely free from the previously seen flow features and the transonic shock waves are clearly visible on the trailing edge of the test piece.

The images will be discussed in more detail later on, however, it can be seen that the schlieren setup was capable of detecting the incident shock wave as well as the transonic shock waves that formed subsequently. In addition, the delay system was working as planned.

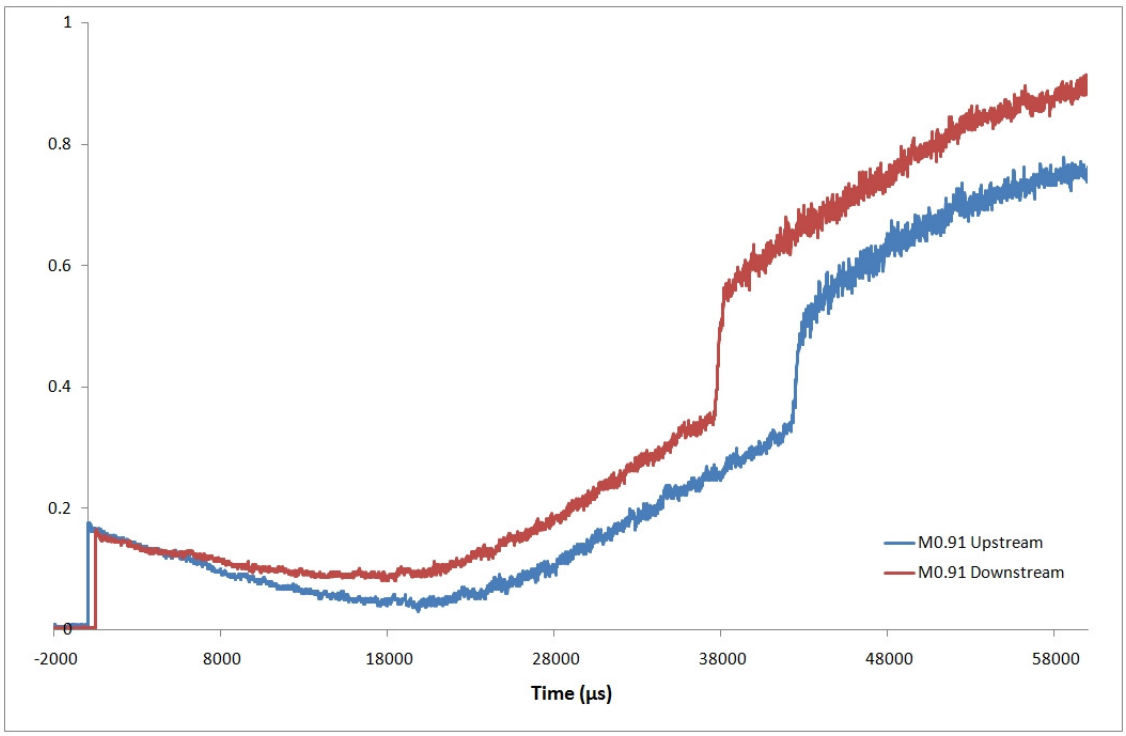


Figure 7.7 Pressure trace produced during testing at Mach 0.91

The pressure trace shown in Figure 7.7 clearly shows the pre-trigger time as set on the data logger (horizontal lines before the activation time of 0µs), and then the two pressure spikes as the shock wave passes over each pressure transducer. When inspected closely, the spikes are not perfectly vertical as is predicted by the theory that the shock wave is considered a discontinuity in the flow properties. Although the shock wave is an extremely short distance in thickness, the pressure transducers are a few millimetres in diameter, and since pressure readings are taken every two microseconds, approximately three readings can be taken while the shock wave passes over.

Once the incident shock wave has passed, the pressure transducers take readings of the now increased pressure of the flow which will eventually return to their zero value after a sufficient amount of time. Features such as the return of the reflected shock wave off the end of the shock tube can be seen on the pressure trace. In the example shown in Figure 7.7 the reflected wave is seen at approximately 38000 microseconds on the trace recorded by the downstream pressure transducer. The upstream pressure transducer then registers the reflected wave at approximately 42000 microseconds, showing that the wave is moving upstream in the shock tube. Once this feature reached the test section a small amount of time before reaching the downstream pressure transducer, the testing window was over.

For the sake of clarity and in order to compare the test results with the numerical results, the upper and lower pictures were combined to produce a picture with no support mechanism as shown in Figure 7.8.

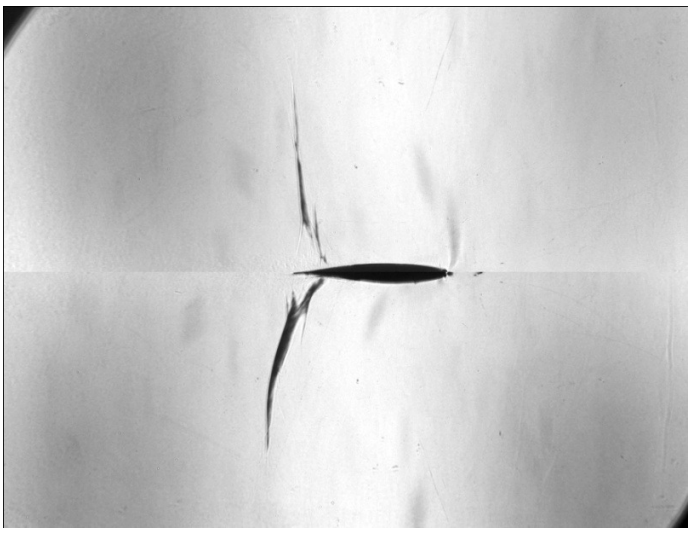


Figure 7.8 Example of joined image

7.2.2 Testing at Mach 0.83

Testing carried out at Mach 0.83 was performed using various layouts, angles of attack and time delays. The testing was performed for delay times starting soon after the passage of the shock wave, and continued on until it was clear the flow had become unsteady and unusable. Once

again, the upper and lower test pictures have been combined to create a single image containing no test piece support in order to identify the flow feature more easily. All testing images display the delay time starting when the incident shock wave passed the upstream pressure transducer.

2.79º Angle of Attack, Open Walled Tests: 50% Open Area Ratio

The test images obtained during testing at 2.79º angle of attack with the open walls were combined to more easily identify specific flow features as well as the progression of the flow throughout the time window.

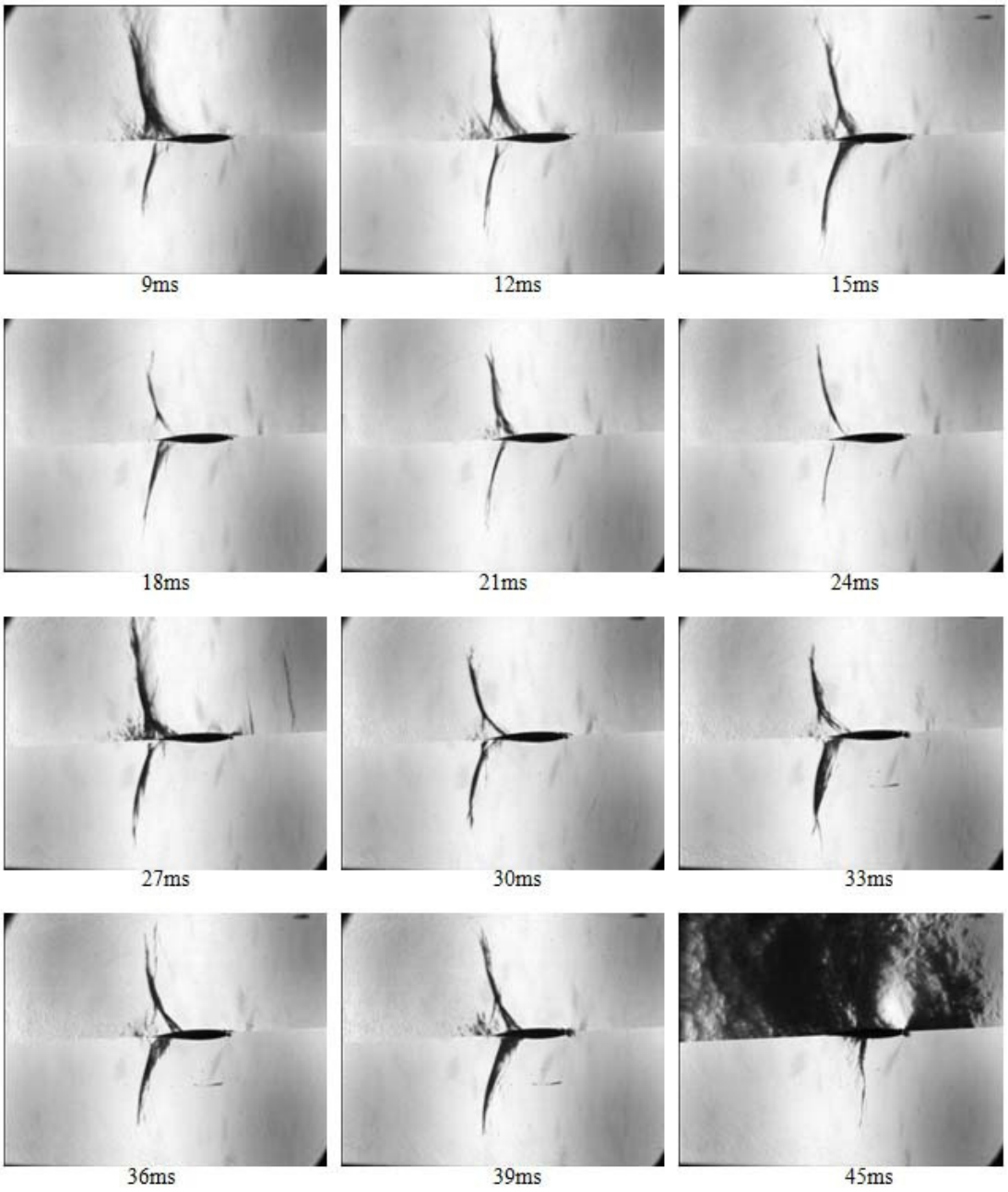


Figure 7.9 Mach 0.83 at 2.79º with open walls

From the sequence shown in Figure 7.9, it can be seen that the testing flow is established soon after the passage of the shock wave, remains semi-steady and then breaks down somewhere between 39 and 45 milliseconds. The region where the flow is semi-steady is from approximately 12 milliseconds to approximately 39 milliseconds. During this time duration, the transonic shock

wave position on the test piece and the general shape of the shock wave varies by only a small amount. Some of this variance can be accounted for by the fact that each half of each image was obtained by means of a separate test and so some discrepancies in Mach number are always going to occur.

One of the most notable features of the transonic shock wave formed on the test piece is the fact that it appears a lot thicker than the incident shock wave that was seen earlier. The reason for this apparent thickness is the in-plane bending of the wave between the two windows of the test section. The test section is certainly not uniform from one window to the other due to the slotted nature of the upper and lower walls and as a result, it is unlikely that the flow will be perfectly uniform across the test section either. Thus if one was to take a chord wise slice through the test piece and its associated flow features, the shock wave would appear extremely thin. However, as you moved from one slice to the next slowly making your way across the test section, small variance would occur in the shock wave shape and position on the test piece. However this variance would be slight and would be contained within the bounds of the shock wave as seen in the original image. The effect on the final result is thus relatively small and for the purposes of this study, can be ignored.

Each of the shock waves in this series of images has a lambda shock pattern displayed fairly close to the surface of the test piece. This shock pattern forms due to the shock induced separation that occurs on the test piece due to the separation of the boundary layer. At the point where the boundary layer separates, an oblique shock wave is formed. This oblique shock wave extends until it meets the normal shock wave which was the cause of the separation in the first place. At this point, a trailing shock forms and extends back towards the now separated flow, the formation of which is due to compatibility conditions downstream of the system needing to be satisfied. (Ben-Dor, Igra, & Elperin, 2001) The finer details of this type of system are beyond the scope of this study, however, this type of system is known as a lambda shock system, due to the shape of the interaction of the three shock waves. More details of the system can be found in section 2.1.

Downstream of the lambda shock system, a significant turbulent region can be seen and this is due to the separation of the flow as previously explained.

Comparison to Numerical Results

With the flow features surrounding the shock wave formation on the test piece clearly identified and understood, a comparison of the features displayed during physical testing can be made with those features predicted by the numerical results.

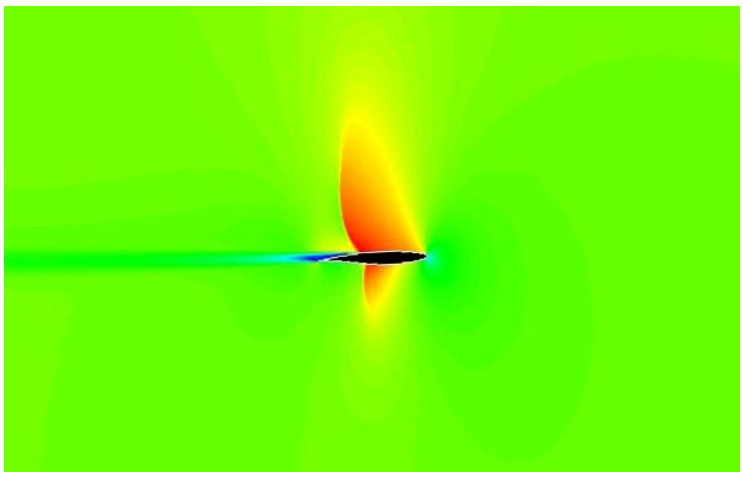


Figure 7.10 CFD at Mach 0.83 and 2.79º angle of attack

Upon initial inspection of the result shown in Figure 7.10 it is clear that the numerical and experimental results contain similar features. Two defined transonic shock waves are clearly visible extending outwards from the surface of the aerofoil into the surrounding flow. A turbulent wake region is also visible, as is a lambda shock pattern on the upper surface of the aerofoil. The lambda shock pattern is not visible on the lower surface however, and this is made more evident by the fact that the turbulent wake region appears mainly to originate from the upper surface of the model. This makes sense since the lambda shock pattern is associated with boundary layer separation. On the lower surface, no lambda shock pattern is seen, and so no boundary layer separation is predicted.

Since the experimental setup did not contain any instrumentation that would allow the actual testing Mach number to be known, it is difficult to accurately compare the experimental results with the numerical results without first establishing that the Mach number of the two results is comparable within a range of M0.05. As a result, since there was confidence that the numerical result was very accurate, simply overlaying the numerical onto the experimental result and

finding the closest match for the range of time delays meant that the experimental Mach number could be predicted with a fair degree of confidence.

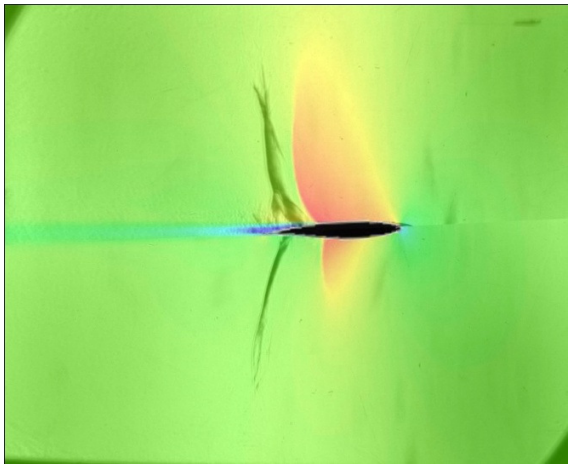


Figure 7.11 CFD Mach 0.83 overlaid onto experimental Mach 0.83

Initially a test picture taken in approximately the middle of the testing time window was chosen for the comparison. The theoretical testing Mach number based on pressure ratios across the diaphragm was M0.83. A numerical result at the same Mach number was thus overlaid onto the experimental image in order to compare the transonic shock wave shape, chord wise position and general flow features around the aerofoil. It is quite apparent that the numerical and experimental results are similar, but do not compare to a degree of accuracy that is acceptable.

Since it is known that an increase in Mach number results in downstream movement of the transonic shock waves on the aerofoil, it is clear that the numerical result is at a Mach number that is lower than that of the test result. It is therefore clear that while the theory predicts the Mach number to be a certain value, this value is not necessarily reflected in the final result. The possible reasons for the discrepancy is that during testing, boundary layer growth effectively reduces the cross sectional area of the section resulting in an increase in Mach number of the subsonic flow.

In order to establish the actual test Mach number, overlays of numerical results with an increasing Mach number were then created. The experimental result generated at 21ms delay was chosen since it fell in approximately the middle of the testing time window.

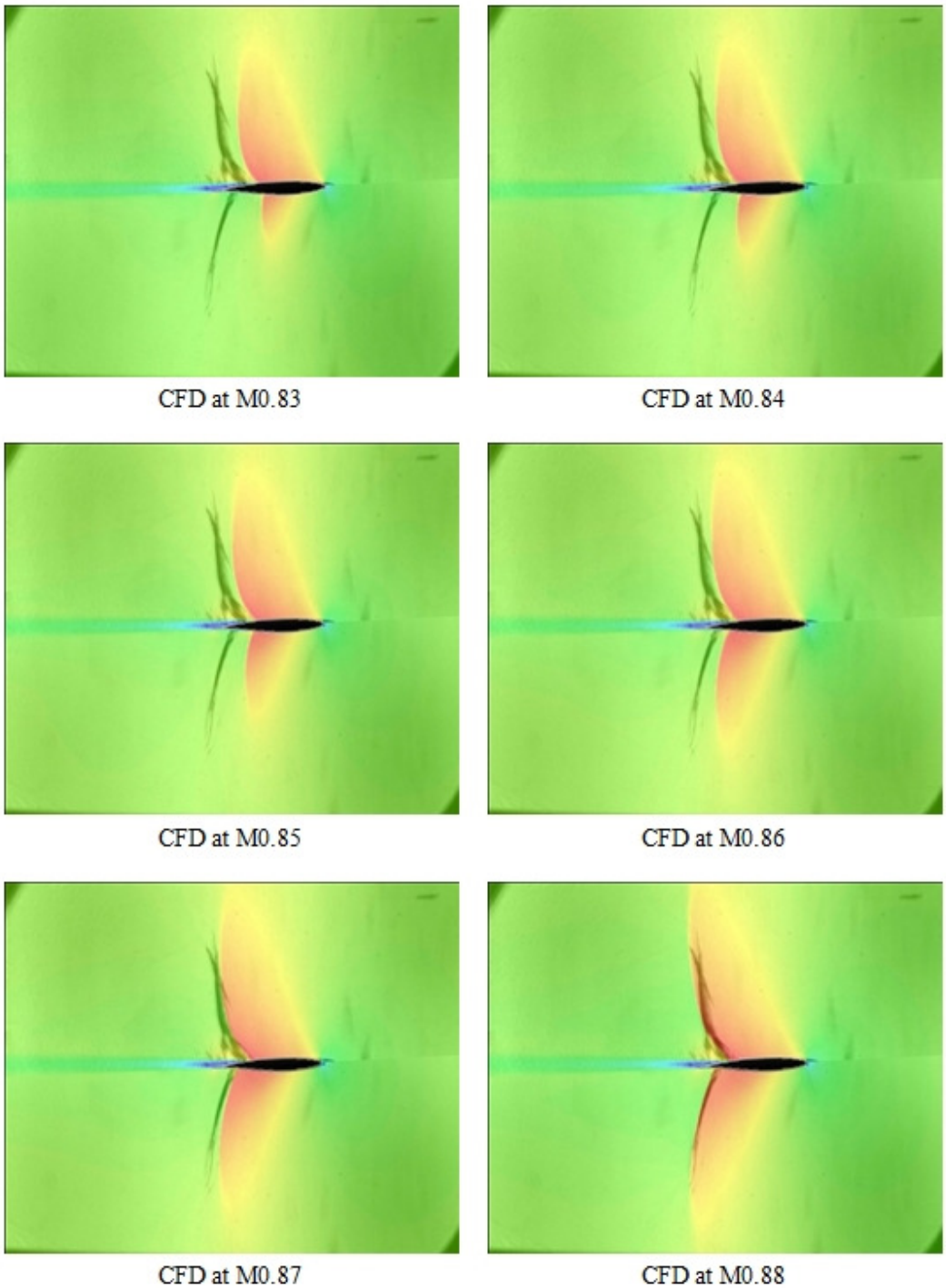


Figure 7.12 Overlay of different CFD Mach numbers onto Mach 0.83 experiment at 2.79º angle of attack

As the numerical results increase in Mach number, the chord wise position of the transonic shock waves gets closer while the shock wave shape appears to match up more closely too. At M0.88 for the numerical results, the experimental and numerical results appear to match very closely. Thus, the numerical result obtained at a Mach number of 0.88 was compared to the experimental results as shown in Figure 7.13 and Figure 7.14.

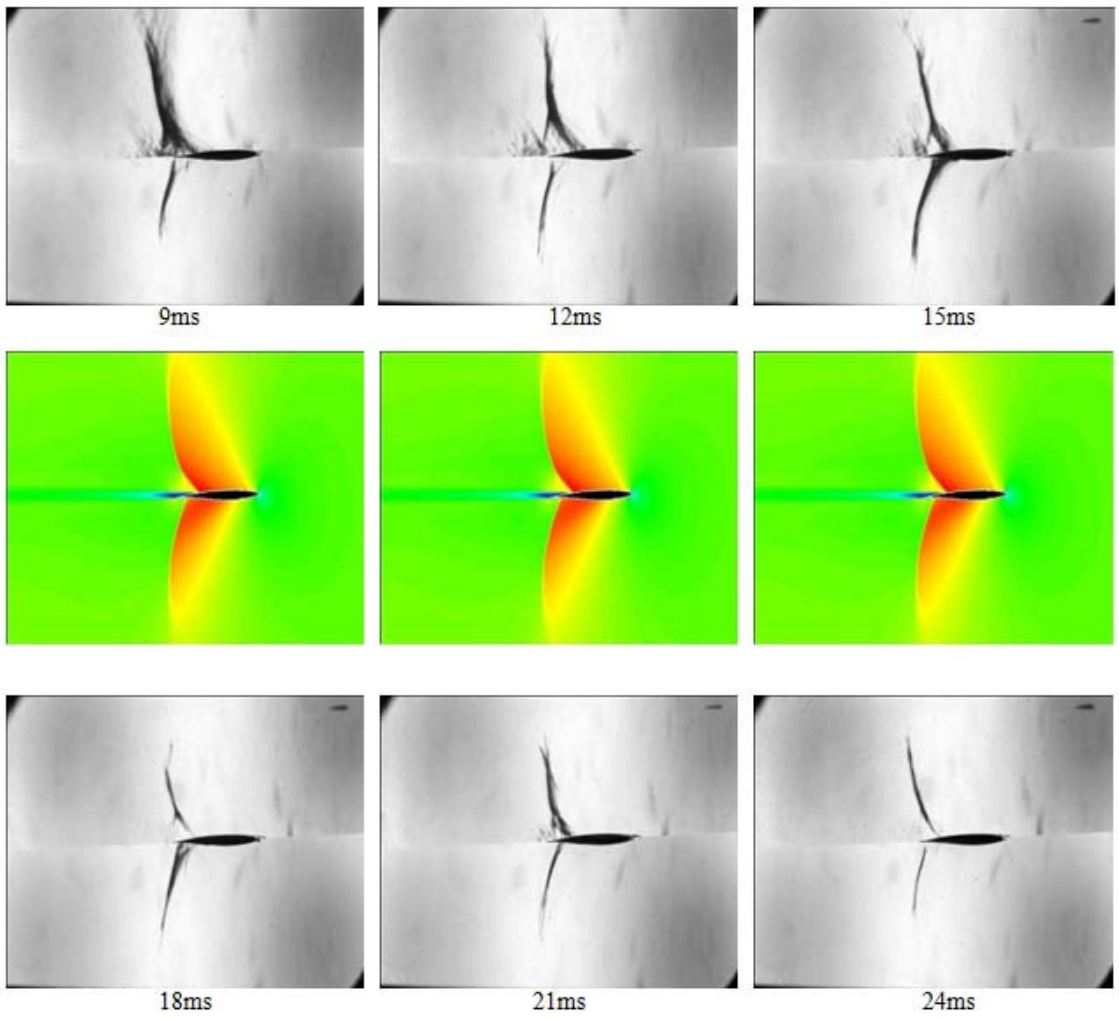


Figure 7.13 CFD at Mach 0.88 compared to experiment at 2.79º angle of attack (9-24ms)

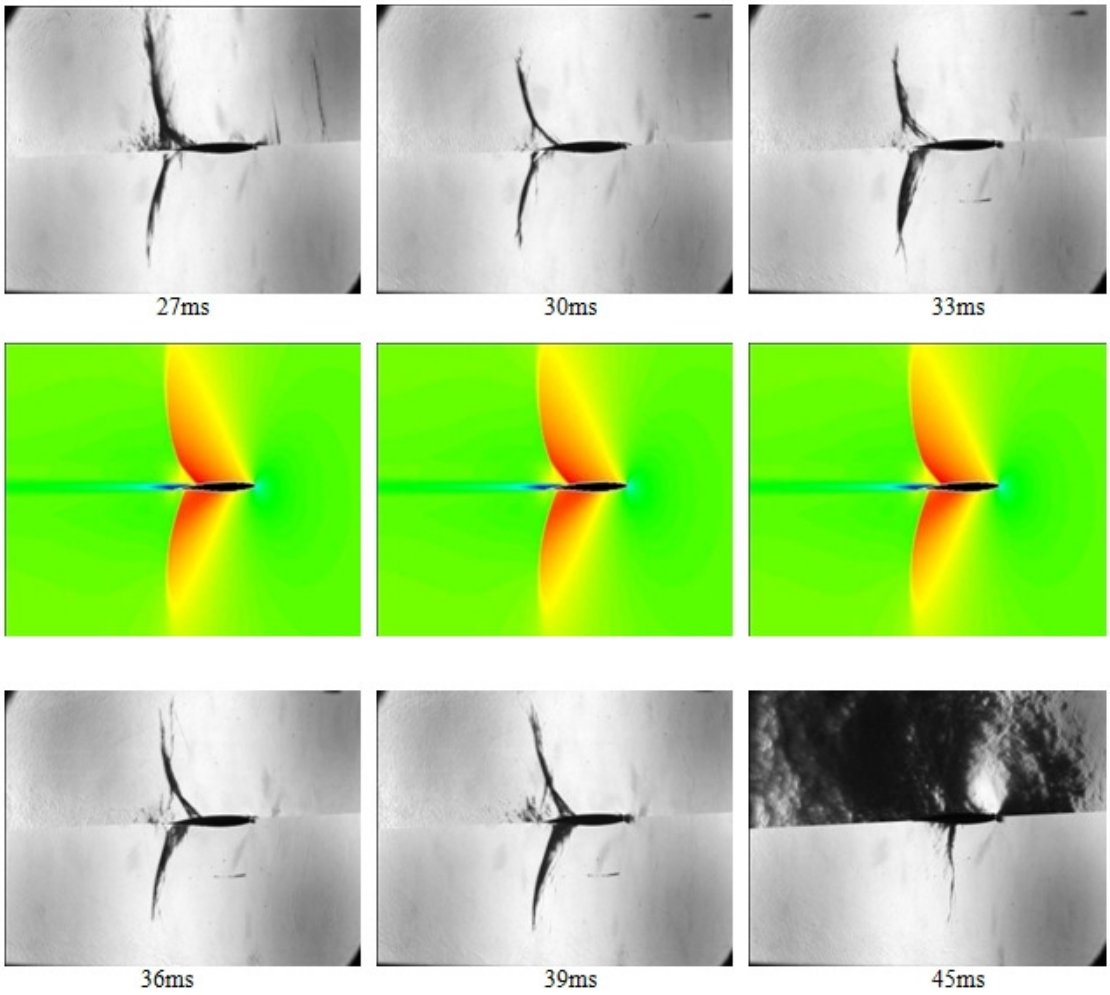


Figure 7.14 CFD at Mach 0.88 compared to experiment at 2.79º angle of attack (27-45ms)

From Figure 7.13 and Figure 7.14 it is apparent that the numerical results obtained at a Mach number of 0.88 match very closely with the experimental results throughout the testing time window. It is therefore safe to assume first of all that the testing Mach number is higher than theoretically predicted, and second of all that the testing flow Mach number is relatively constant throughout the testing time window, provided the flow is not in the process of being established or broken down. The increase in Mach number from the theoretical to the actual value equates to a 6% rise.

General Observations

Since the numerical testing simulates results obtained in free stream flow with no imposed boundary conditions like those found in wind tunnel testing, it represents the type of result that is obtained by a correctly functioning wind tunnel.

As discussed previously, testing by means of a wind tunnel imposes boundary conditions close to the model being tested, and these boundary conditions are not found when the body is in free stream flow. However, from the comparison of the experimental and numerical results, the imposed boundary condition appears to have very little to no affect on the results being generated.

Two key concerns with testing in the transonic flow region are that shock reflection off the nearby wind tunnel wall will occur and interfere with the airflow around the model, and that the transonic shock waves will be artificially bent as they approach the wind tunnel wall such that they meet it at ninety degrees. From the comparison of the numerical and experimental results, neither of these two features is apparent. The shock wave shape matches very closely with the shape predicted in the numerical result, and it matches across the full distance that the experimental shock wave is visible. There appears to be no interference from any reflected shock waves since there is no visual indication of any interference, as well as the fact that the experimental and numerical results match up well in almost all aspects.

One slightly noticeable difference between the experimental and numerical results is the distance that the transonic shock waves extend outward from the aerofoil. In the numerical results, the shock wave is visible for a greater distance than is visible in the experimental results. However, the visualization mechanism in the numerical results is also a lot more distinct than in the experimental results. The optical system also has a practical limit in sensitivity and so, as the shock waves weaken, they become less visible. This slight discrepancy is expected and thus does not reflect that the experimental and numerical results are vastly different from one another.

2.79º Angle of Attack, Closed Wall Tests: 10% Open Area Ratio

In order to establish whether the correct wall open area ratio had been chosen, testing was done with a significantly more closed wall. It was of interest to compare the results obtained with the 50% open wall and those obtained with the 10% open to establish whether any significant difference in the result was noticed.

Due to time constraints, testing was not carried out for as many time delays as in the 50% open walled case. From the time delays available, a clear comparison could still be made however. The initial test at a delay of 9ms was carried out using only the lower surface, since, as shown previously, the image shows only the starting process of the flow and comparison to actual data is meaningless.

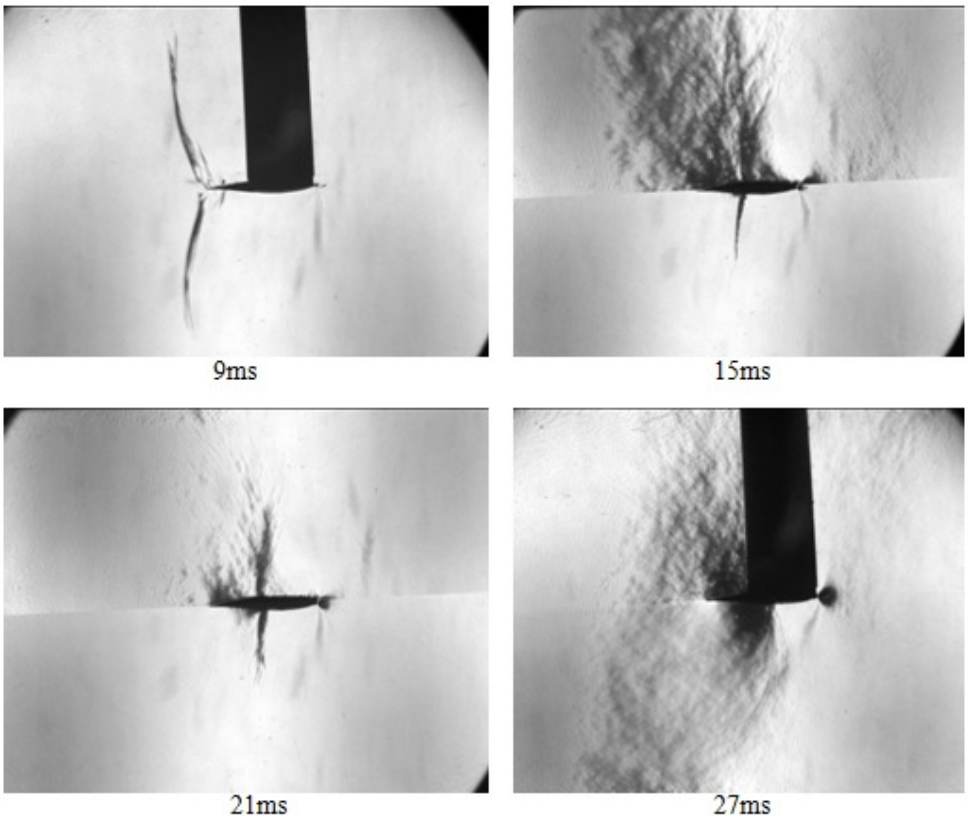


Figure 7.15 Mach 0.83 at 2.79º angle of attack with closed walls

The initial observation from the images in Figure 7.15 is that at 9ms delay, transonic shock waves are clearly visible. As before, the shock waves are set up very close to the trailing edge of the aerofoil in the early stages of the flow establishment. At the next available time increment, the shock waves have moved far upstream of their starting position. The shock wave on the lower surface of the aerofoil became a lot less prominent, while the flow on the upper surface has degenerated to the point where no features are clearly visible. At 21ms the lower shock wave is largely unchanged from before, while the upper shock wave is slightly more visible. Again, however, the features of the flow on the upper surface are not nearly as defined as the features found in the testing carried out with the 50% open walls.

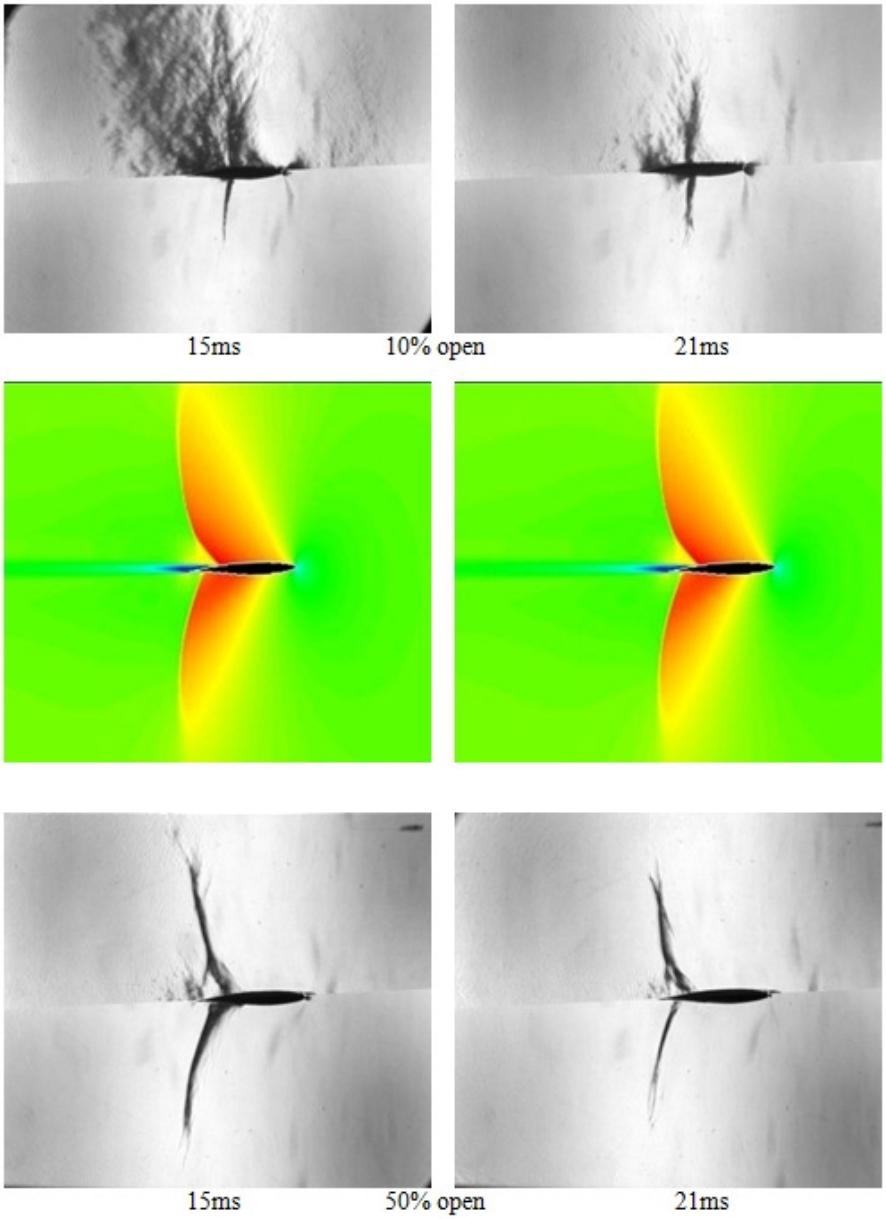


Figure 7.16 Comparison of Mach 0.88 CFD to results at 10% and 50% open wall (5º angle of attack)

From the comparison images found in Figure 7.16 it is clear that while the 50% open wall produces flow features that are very similar to those predicted by computational fluid dynamics, the 10% open wall produced results that compare very poorly to both the CFD and the 50% open wall tests. The transonic shock waves produced from the 10% open wall testing are vastly

different from the shock waves that were expected. Their chord wise position is also a lot further upstream on the aerofoil than would be expected for testing at this Mach number.

With an increase in testing delay time, the shock wave position and shape vary very little, indicating that the flow in the test section had reached a semi-steady condition. Later on in the sequence shown in Figure 7.15 at a delay of 27ms, the lower surface still exhibits this vastly different flow and thus it was decided to abandon the testing at this stage.

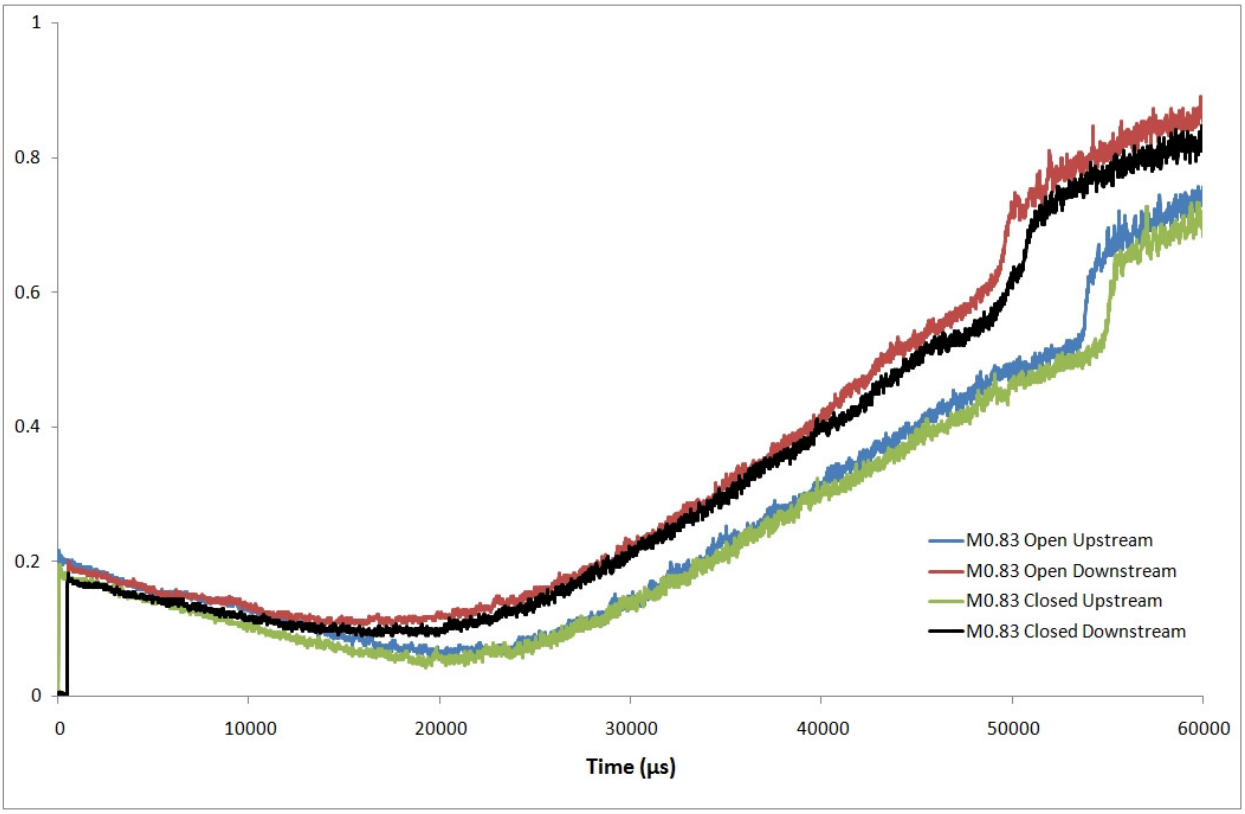


Figure 7.17 Pressure trace at Mach 0.83 and 2.79º angle of attack with open and closed walls

Figure 7.17 contains an overlay of the pressure traces from the testing carried out for both the 50% open and 10% open wall cases. It is quite apparent, due to the similarity in pressure trace shape, features and times between major events such as the passing of the incident shock wave and the arrival of the reflected shock wave, that the two tests occurred under almost identical circumstances, from a flow point of view, upstream of the test section. It can thus be concluded that, all other aspects being the same, the test section walls were the influence on the flow around the aerofoil and thus the formation of the transonic shock waves and other flow features.

5º Angle of Attack, Open Wall Tests: 50% Open Area Ratio

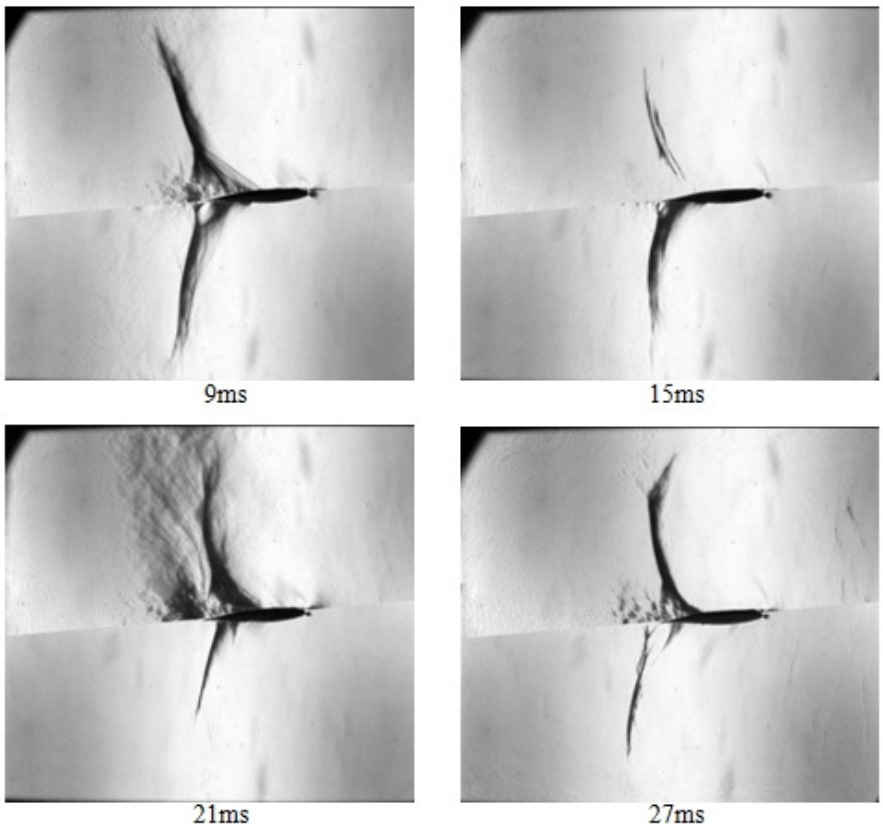


Figure 7.18 Mach 0.83 at 5º angle of attack with open walls

From the sequence shown in Figure 7.18 it can be seen how the testing flow is again established soon after the passage of the shock wave. As before, the shock waves on the test piece are seen to be fairly thick in some of the images. This is due to the non-uniform nature of the test section as one passes from one window to the next, due to the slotted upper and lower walls causing in-plane bending of the shock wave. As in the results for the test piece at 2.79 degrees angle of attack, this shock wave thickness will not affect the results and can be largely ignored.

Generally, the shock waves formed on the upper surface of the model appear to extend further into the surrounding flow region in almost all of the images than those seen during testing at 2.79 degrees angle of attack. This is due to the fact that the higher angle of attack leads to a higher

Mach number over the upper surface of the aerofoil which in turn leads to a stronger normal shock wave forming. This fact is further emphasised by the clear formation of lambda shock systems on the upper surface, whereas virtually no lambda shock system is seen on the lower surface. As stated previously, the lambda shock system is a result of the strong interaction between the normal shock wave formed on the surface and the boundary layer that is found along the surface. Once the normal shock wave reaches the required strength, the interaction between it and the boundary layer causes the boundary layer to separate and the lambda shock system to establish. No lambda shock system is seen on the lower surface of the aerofoil because the normal shock wave is not of the required strength.

A clear wake region is seen resulting from the significant lambda shock system on the upper surface of the aerofoil whereas almost no wake is seen from the lower surface. Again this is due to the relative strengths of the shock waves on each surface and their resulting interaction with the boundary layer that is formed along each surface.

Comparison to Numerical Results

With the flow features surrounding the shock wave formation on the test piece clearly identified and understood, a comparison of the features displayed during physical testing can be made with those features predicted by the computational fluid dynamics results.

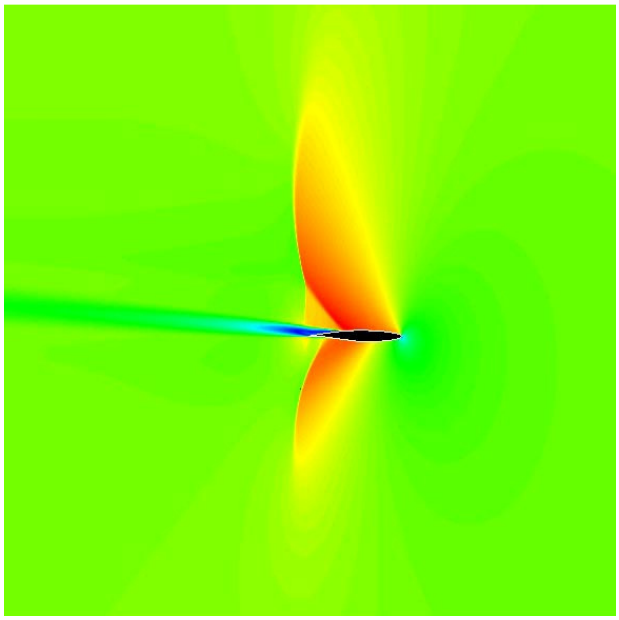


Figure 7.19 CFD at Mach 0.88 and 5º angle of attack

Upon initial inspection of the result shown in Figure 7.19 it is clear that the numerical and experimental results contain similar features. The two well defined transonic shock waves are visible extending outwards from the surface of the aerofoil into the surrounding flow. These waves extend further out into the flow than the waves seen in the numerical results from testing at 2.79 degrees angle of attack. A turbulent wake region (dark to light blue) is also visible, as is a lambda shock pattern on the upper surface of the aerofoil. The lambda shock pattern is barely visible on the lower surface however, and this is made more evident by the fact that the turbulent wake region appears to originate predominantly from the upper surface of the model. This makes sense since the lambda shock pattern is associated with boundary layer separation. On the lower surface, the lambda shock pattern is barely visible since there is very little boundary layer separation caused by it and so its contribution to the turbulent wake region is extremely small.

Once again, due to the lack of instrumentation in the test section of the wind tunnel, the actual Mach number of the flow can only be estimated. Thus, as done previously, numerical results were overlaid onto the experimental results in order to be able to accurately determine what the experimental Mach number was. A series of numerical results of varying Mach number were overlaid onto a given delay time and the closest match chosen. Since for the 2.79 degree angle of attack tests, a Mach number of 0.88 was found to match most accurately with the results, it is expected that the exercise will yield a similar result. Hence only numerical results from flow

close to M0.88 were used in order to refine the process. The overlaid results can be seen in Figure 7.20.

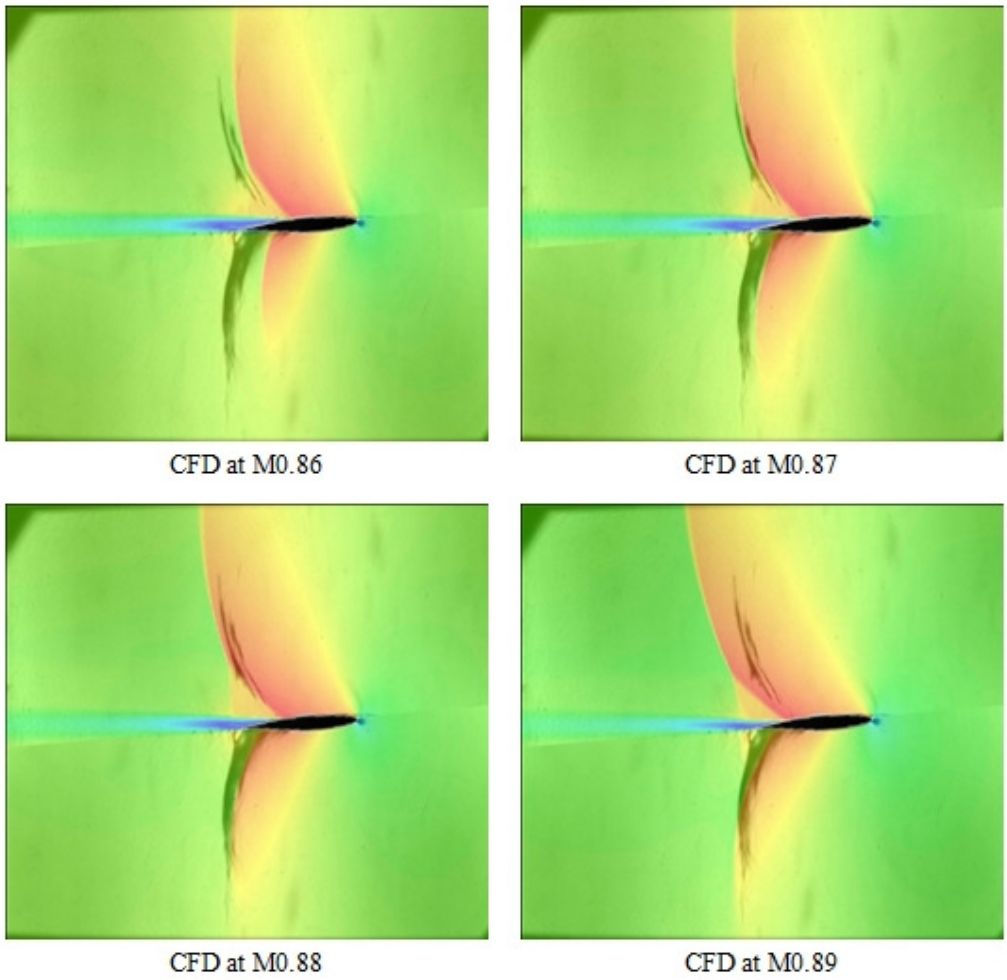


Figure 7.20 Overlay of different CFD Mach numbers onto Mach 0.83 experiment at 2.79º angle of attack

Again, comparing chord wise position of the transonic shock waves, their corresponding shape and the proportions of the lambda shock system, it is a relatively simple process to establish a CFD Mach number that appears to reproduce the experimental results with the least difference in the aforementioned features. As before, the chord wise position of the transonic shock waves moves downstream with an increase in Mach number, while the size of the lambda shock system also increases. These clear effects and the fact that all of the flow features are relatively sensitive

to a change in Mach number mean that it is not difficult to establish with confidence which CFD result corresponds the best to the experimental results.

As the numerical results increase in Mach number, the chord wise position of the transonic shock waves gets closer while the shock wave shape appears to match up more closely too. At M0.88 for the numerical results, the experimental and numerical results appear to match very closely and so further comparisons were made using this Mach number.

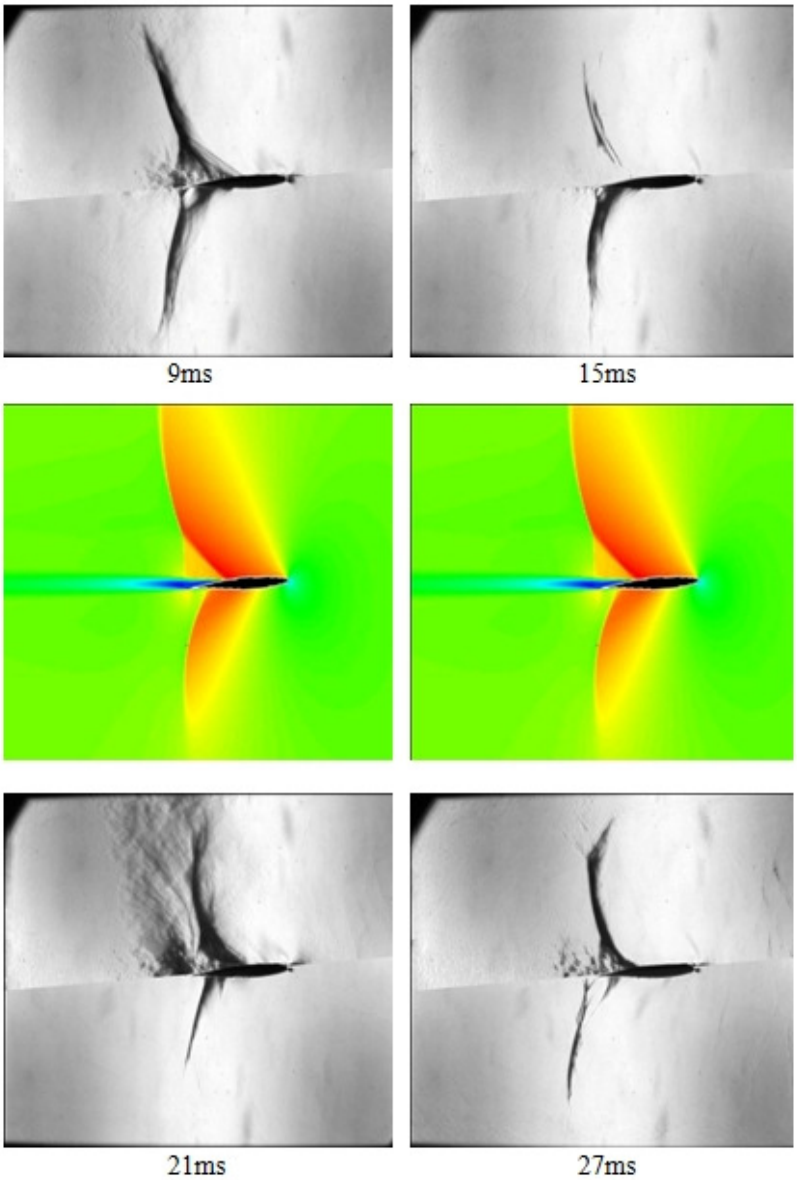


Figure 7.21 CFD at Mach 0.88 compared to experiment at 5º angle of attack

From the images contained in Figure 7.21, it is apparent that the numerical results obtained at a Mach number of 0.88 match very closely with the experimental results throughout the testing window. The sequence shows that the testing flow is semi-steady throughout the time delay window and again that the actual testing Mach number is higher than theoretically predicted. The increase in Mach number from the theoretical to the actual value equates to a 6% rise.

General Observations

Again, it is desired that the wind tunnel test results indicate as little interference from the upper and lower walls as possible, since the purpose of the wind tunnel is to simulate airflow in an unbounded region. As discussed previously, testing by means of a wind tunnel imposes boundary conditions close to the model being tested, and these boundary conditions are not found when the body is in free stream flow. However, from the comparison of the experimental and numerical results, the imposed boundary condition appears to have very little or no affect on the results being generated.

That said, there are some features contained in the higher angle attack results that are worth noting.

From the numerical results, it is clear that the transonic shock waves extend much further from the aerofoil than in the results at a lower angle of attack. This fact means that the transonic shock waves formed during experimentation will be required to approach the boundary walls very closely. This is not an ideal feature since complex flow features are set up very close to the slotted walls and are likely to interact with the shock waves being formed.

Despite the abovementioned fact, again, the experimental and numerical results show similarities that are well within the requirements for a wind tunnel that is producing the required results.

Inspecting the image in Figure 7.21 at 9ms delay, the transonic shock wave position on the aerofoil is almost identical to that predicted by the numerical results. In addition, the lambda shock system appears in the same position and is of the same proportion to that predicted numerically showing that the flow features around the aerofoil are being recreated correctly. The wake flow is clearly visible and as expected can be seen originating mainly from the upper surface of the aerofoil where the lambda shock system is found.

Interestingly, as the transonic shock waves approach the upper and lower walls of the test section, they are seen to disappear quite quickly. This is due to the shock cancelling effect the slotted walls create to ensure that no shock reflection occurs off the wall. In addition, the upper transonic shock wave is seen to approach the upper wall at an angle and even as it nears the wall, it does not bend to meet it at 90 degrees as would occur under normal circumstances, again showing that the slotted wall feature is operating as planned.

The image, in Figure 7.21, at a delay of 15ms shows clear agreement between the numerical and experimental result. Although the upper surface image is slightly light, due to the lower sensitivity of the optical system, it is clear that the shock wave shape, position and resulting lambda shock system match the same features predicted numerically very accurately. The shock wave and resulting flow features formed on the lower surface of the aerofoil show similar agreement. Only a very small lambda shock system was predicted numerically for the lower surface and it is clear from the image that only an extremely small system was created experimentally.

Inspection of the image at a time delay of 21ms shows similar agreement between numerical and experimental results. However, the shock wave on the upper surface has a slight amount more curvature than that predicted numerically, and so, while it originates on the upper surface of the aerofoil at approximately the same chord wise position, the slight increase in curvature means that it terminates slightly further upstream as it nears the upper slotted wall. This discrepancy appears to be a one off problem and with the lack of instrumentation inside the test section, it is difficult to know whether or not it is due to a slight change in the flow properties produced during that particular test run. However, the discrepancy is still small and so while it is not ideal, it does not represent a failure of the experimental setup. The shock wave found on the lower surface of the aerofoil matches the numerical result almost identically, further proving that the experimental setup is functioning correctly at a 5 degree angle of attack and after a delay of 21ms.

The image produced at a time delay of 27ms again shows similar flow features to those discussed previously. The upper transonic shock wave again closely matches the numerical results in curvature, position and relative proportions of the lambda shock system. A notable feature, however, is found as the upper transonic shock wave approaches the upper slotted wall. A slight kink is formed and is likely due to the complex interactions between the flow set up through the slotted wall boundary and the transonic shock wave itself. Again, this feature is not of enough concern to conclude that there has been a failure in the experimental setup. The lower shock wave

is seen to have formed slightly further downstream from its predicted position, and this can be attributed to the slight Mach number increase in the flow due to the longer time delay, as seen previously.

Generally, across the full time delay sequence, the flow features reproduced experimentally match up very closely with those features predicted numerically. As discussed, a few slight discrepancies in the results were seen, but none were severe enough to conclude that the experimental setup and layout had failed in any way. No apparent shock reflection off the slotted walls could be seen and in all images, except that at a time delay of 27ms, the shock waves did not appear to have their shape or curvature artificially influenced by the nearby slotted wall.

5º Angle of Attack, Closed Wall Tests: 10% Open Area Ratio

As previously shown in the results for 2.79 degrees angle of attack, the 10% open wall had a large effect on the experimental results. In order to establish whether the correct wall open area ratio had been chosen, testing was again done with the significantly more closed wall. It was of interest to compare the results obtained with the 50% open wall and those obtained with the 10% open wall to establish whether any significant difference in the result was noticed at the new angle of attack.

Due to time constraints, testing was not carried out for as many time delays as in the 50% open wall case. From the time delays available, a clear comparison could still be made however.

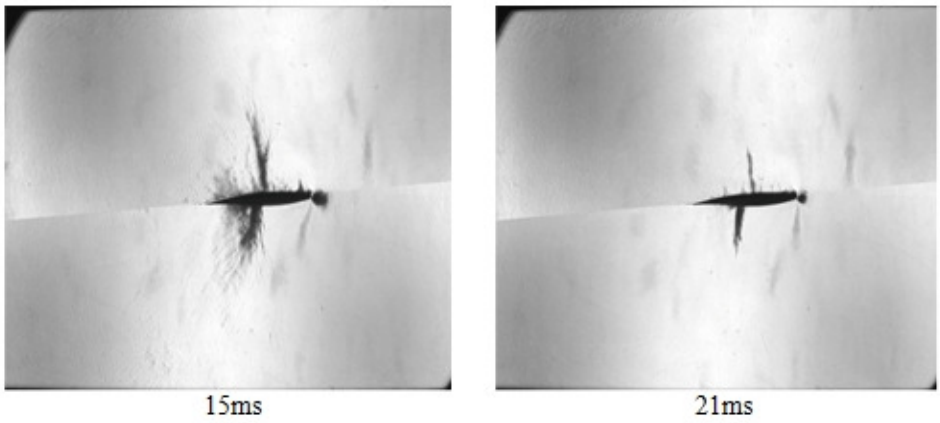


Figure 7.22 Mach 0.83 at 5º angle of attack with closed walls

Testing was performed at 15ms and 21ms delays only and is seen in Figure 7.22. However at these time delays acceptable images were found when testing with the 50% open walls. As such, a good comparison of the effect of the more closed slotted wall is available.

The initial observation from the images in Figure 7.22 is that at 15ms delay, small transonic shock waves are clearly visible. However these shock waves are not well defined and contain none of the features seen previously in the testing with 50% open walls. The shock waves off both the upper and lower surfaces of the aerofoil are not a smooth, well defined line as before, but rather have a jagged, spiky appearance. In addition, the shock waves barely extend a chord length away from the aerofoil. There is also no sign of a lambda shock system being set up and consequently there is very little evidence of a turbulent wake region downstream of the model. In general, the shock waves lack any of the features seen previously during the 50% open wall testing.

The image obtained at a delay of 21ms is largely similar to that obtained at 15ms showing that the flow is steady at this stage in the testing time window. However, the lack of the expected features once again is obvious with both upper and lower shock waves appearing nothing like the shock waves formed when testing with the 50% open wall. Lambda shock systems are similarly not visible.

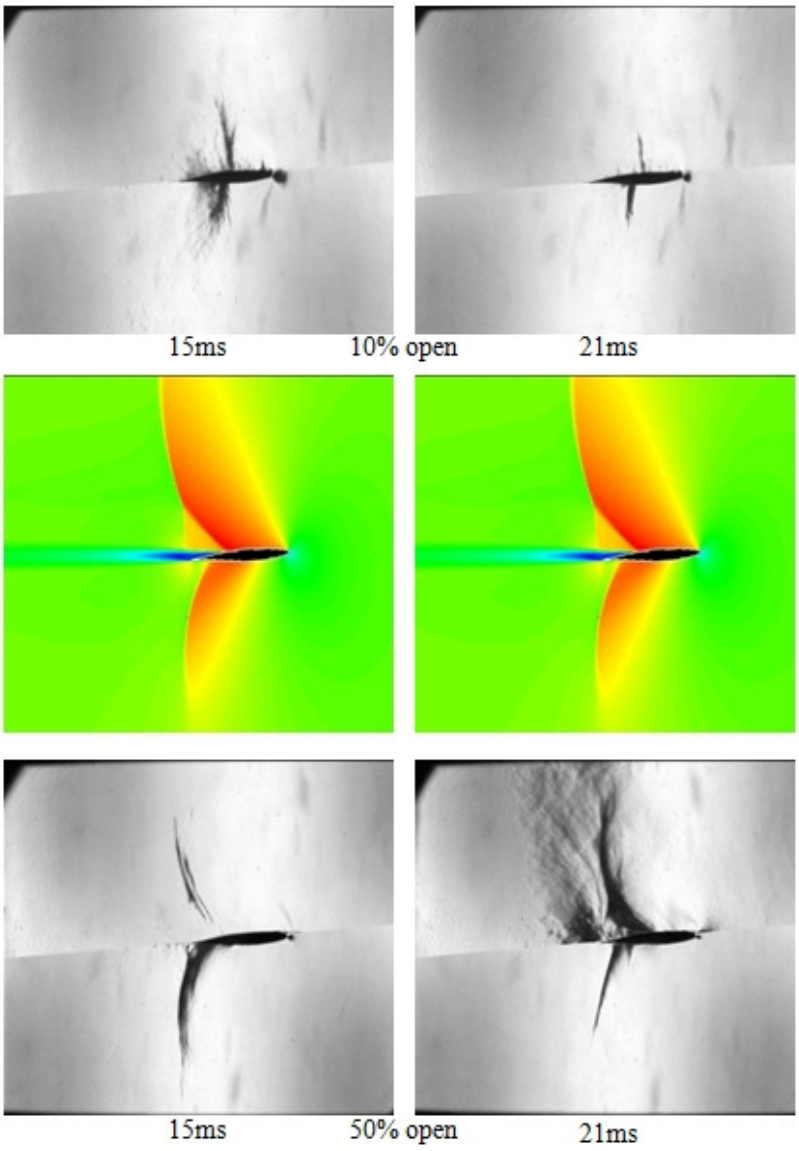


Figure 7.23 Comparison of Mach 0.88 CFD with results at 10% and 50% open wall (5º angle of attack)

As seen with the 10% open wall testing at an angle of attack of 2.79 degrees, the transonic shock waves that are formed are a lot further upstream on the model than those predicted numerically. In general, it is clear that the numerical and experimental results have very little in common with one another. Chord wise position of the transonic shock waves differs greatly as does the shape and composition of the shock waves themselves. A large lambda shock system is predicted to form on the upper surface of the aerofoil and this would normally result in a fairly significant

wake region downstream. However, neither a lambda shock system nor its corresponding wake region is evident in the experimental imagery.

Since the images obtained at a delay of 15ms and 21ms vary by only a small amount from one another, it is safe to assume that similar images would be obtained throughout the testing time window, and so it is clear that no further testing is required to prove that the 10% open wall does produce results that are acceptable.

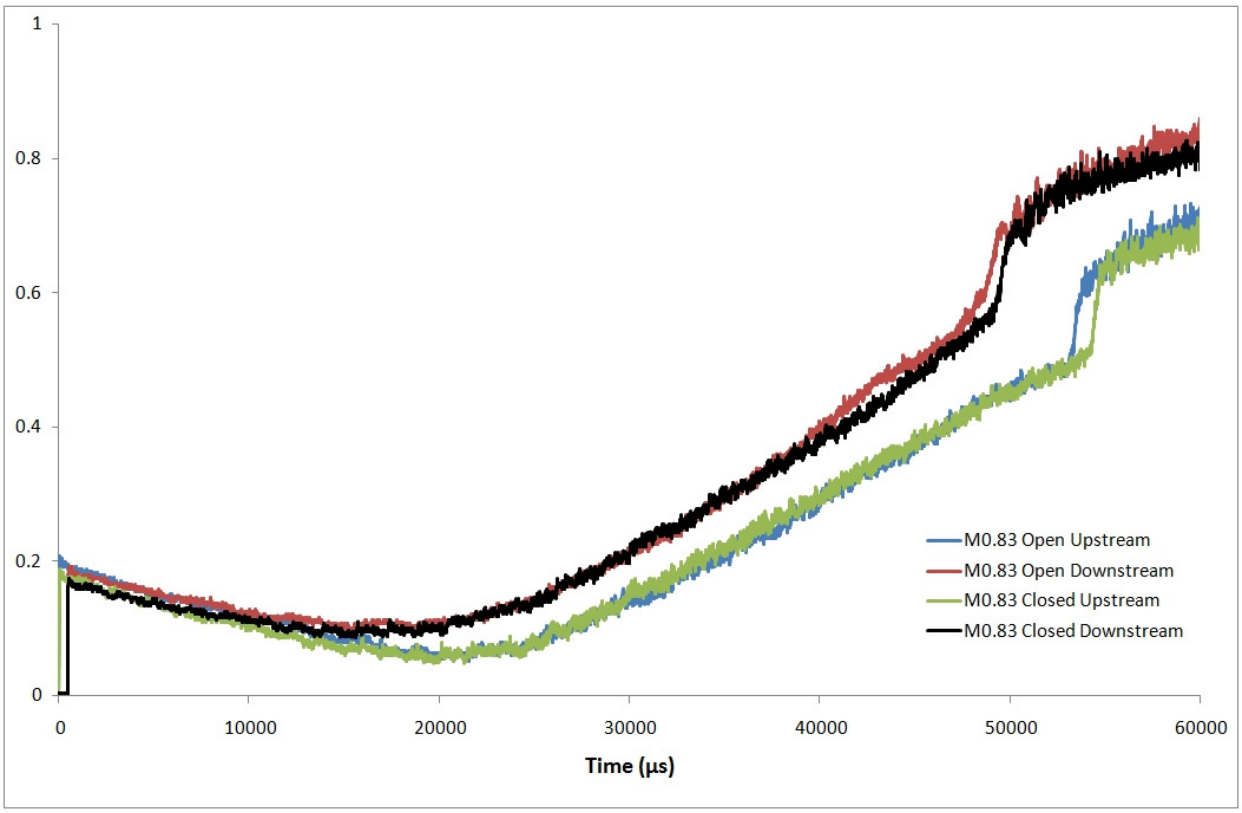


Figure 7.24 Pressure trace at Mach 0.83 and 5º aoa for open and closed walls

Figure 7.24 contains an overlay of the pressure traces from the testing carried out for both the 50% open and 10% open wall cases. It is quite apparent due to the similarity in pressure trace shape, features and times between major events, such as the passing of the incident shock wave and the arrival of the reflected shock wave, that the two tests occurred under almost identical circumstances from a flow point of view upstream of the test section. It can thus be concluded that, all other aspects being the same, the test section walls were the influence on the flow around the aerofoil and thus the formation of the transonic shock waves and other flow features.

0º Angle of Attack, Open Wall Tests: 50% Open Area Ratio

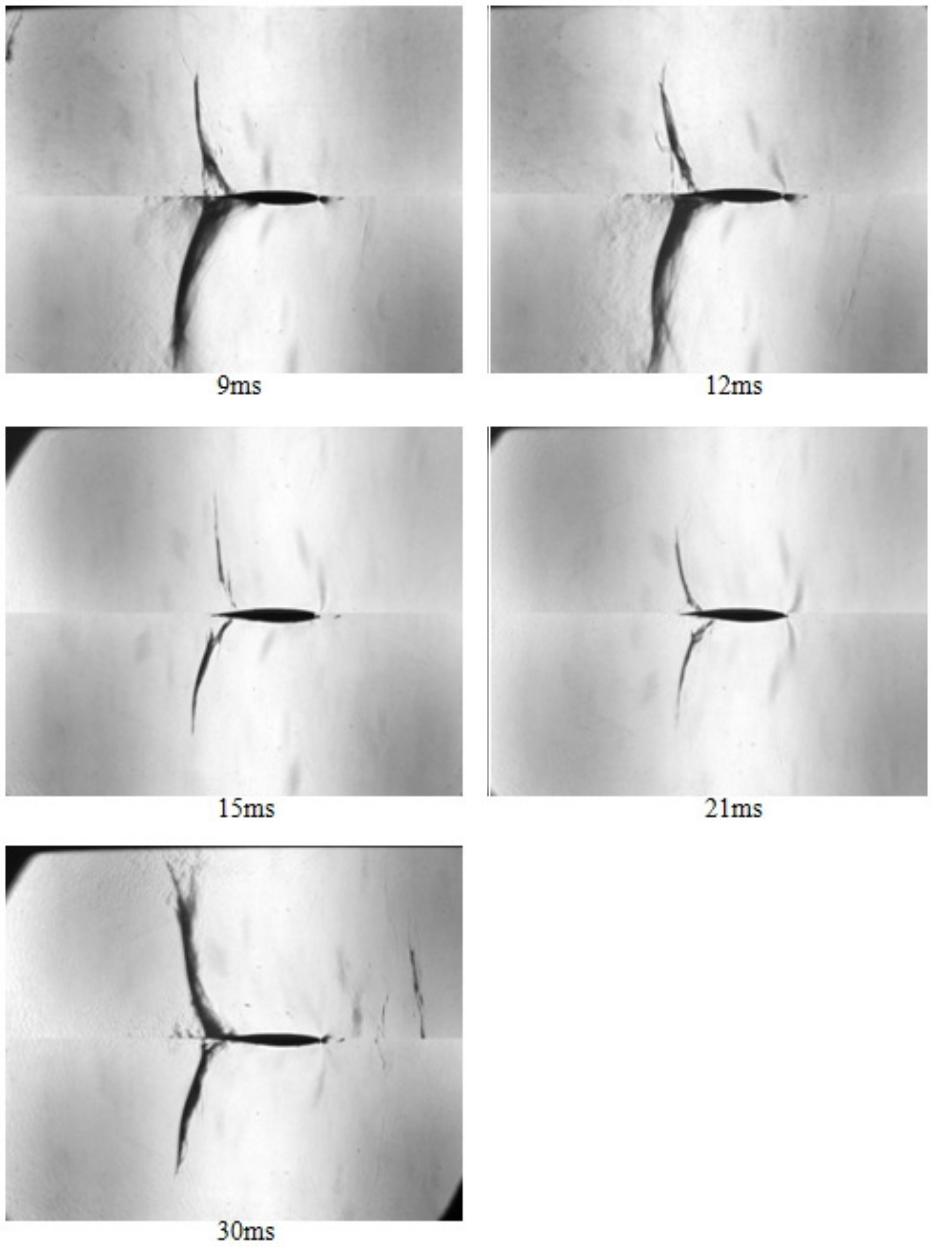


Figure 7.25 Mach 0.83 at 0º angle of attack with open walls

Once again, from the sequence shown in Figure 7.25, the testing flow is set up a short time after the passage of the shock wave.

Again, the transonic shock waves appear relatively thick in the sequence, and this is explained by the in-plane bending of the shock wave across the test section as explained previously.

The sequence clearly displays the presence of the lambda shock pattern on both the upper and lower surfaces of the aerofoil. The shock system exists due to the features explained previously. Interestingly however, the lambda shock system is more prominent on the lower surface at 0 degrees angle of attack than that seen previously at 2.79 and 5 degrees angle of attack. The reason for the increase in prominence of the lambda shock system on the lower surface is the slight increase in Mach number of the flow passing over the lower surface at the lower angle of attack. This slight increase results in a stronger normal shock wave forming. The slight increase in strength of the shock wave results in a greater interaction between the boundary layer and the normal shock wave, which results in a more prominent separation of the boundary layer on the lower surface. This, of course, results in a more prominent wake region which in turn results in a more obvious lambda shock pattern.

Conversely, the Mach number of the flow on the upper surface is slightly lower, resulting in a decrease in the normal shock wave strength with the ultimate effect of a slightly less prominent lambda shock wave system.

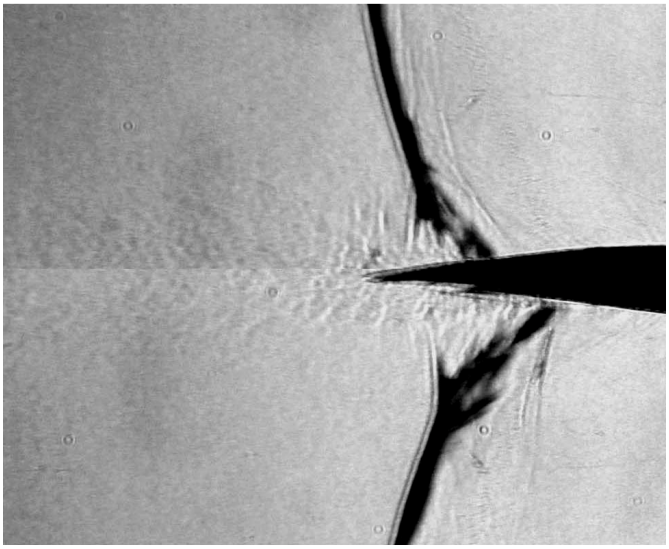


Figure 7.26 High contrast image showing wake region and lambda shock systems

Downstream of the lambda shock systems, a significant turbulent region can be seen in Figure 7.26 and this is due to the separation of the flow as explained previously. However, at the now

lower angle of attack, the wake region is slightly reduced in thickness and is also produced more equally between the upper and lower surface of the aerofoil.

Comparison to Numerical Results

As before, it is useful to make a comparison between the features displayed during physical testing and those features predicted by the computational fluid dynamics results.

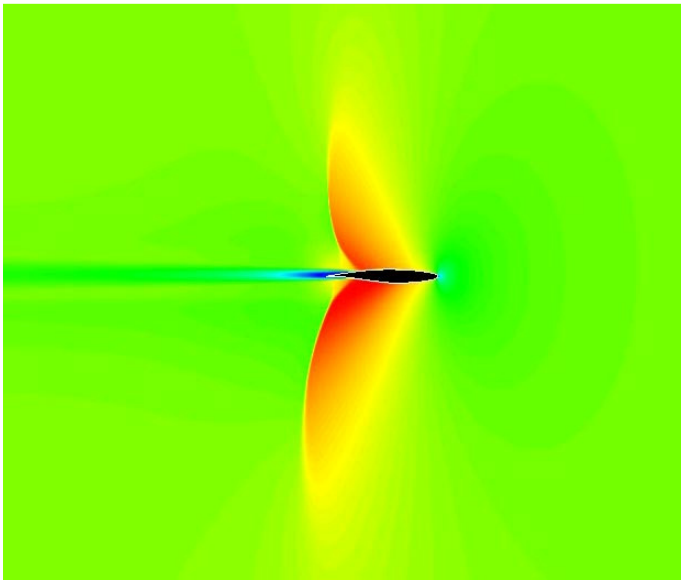


Figure 7.27 CFD at Mach 0.88 and 0º angle of attack

Inspecting the numerical result shown in Figure 7.27, it is clear that similar flow features are found in both the numerical and the experimental result. The two, well defined transonic shock waves are clearly visible extending outwards from the surface of the aerofoil into the surrounding flow and a turbulent wake region is also visible. Lambda shock systems are now visible on both the upper and lower surface of the aerofoil and the resulting wake region is seen to be being produced much more symmetrically than that seen previously on the 2.79 and 5 degree angle of attack results. As explained previously, the wake region and the lambda shock system go hand in hand and so the presence of the system on both upper and lower surfaces would explain the more symmetrical wake region.

The numerical result shows the lower shock wave extending further into the flow and being slightly more defined than the upper shock wave. This is due to the increase in the Mach number

on the lower surface as can be seen by the larger region of dark red when compared to the region on the upper surface.

Again, with the experimental setup's lack of instrumentation that would allow the actual testing Mach number to be known, comparison of experimental results with numerical results obtained at different Mach numbers is able to provide some insight into the achieved experimental Mach number. From the testing at 2.79 and 5 degrees angle of attack, it was found that a Mach number of M0.88 for the numerical results provided the closest match between experiment and CFD. Since the testing being discussed was carried out at the same theoretical Mach number, it is reasonable to assume that numerical results at approximately M0.88 will again provide the most similar results between the two tests. However, to ensure that this was the case, overlays of the numerical onto the experimental results were again performed. Since it was unlikely that the Mach number would vary drastically from the testing at 2.79 and 5 degrees angle of attack, the exercise was only carried out for numerical Mach numbers of M0.86 and M0.88.

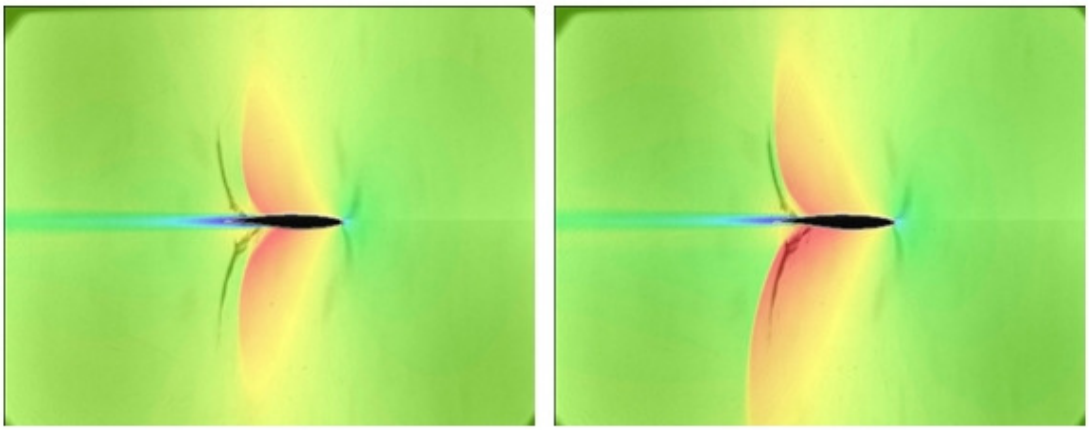


Figure 7.28 Overlay of different CFD Mach numbers onto Mach 0.83 experiment at 0º angle of attack

Once again a Mach number of 0.88 in the numerical results matched most closely with the experimental results. Overlaying the numerical results at M0.88 onto the experimental results throughout the testing range clearly shows accurate agreement between the two.

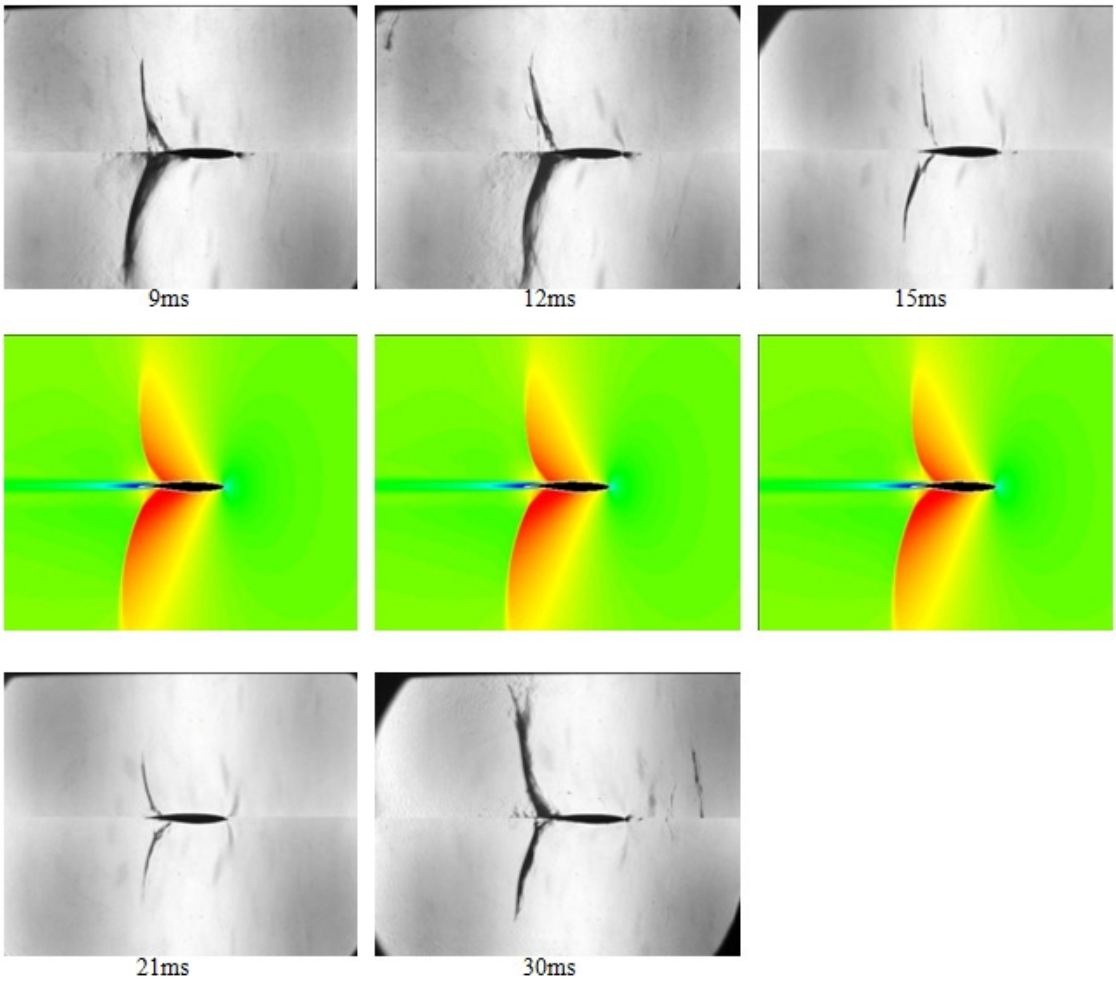


Figure 7.29 CFD at Mach 0.88 compared with experiment at 0º angle of attack

The images shown in Figure 7.29 show that the testing Mach number is higher than that predicted theoretically as well as that the flow Mach number during the testing window is relatively constant, except during the times when the flow is being established or broken down. Again, the increase in Mach number from the theoretical to the actual value equates to a 6% rise.

General Observations

Once again, in order to show the correct functioning of the wind tunnel, experimental results that closely match the numerical results needed to be obtained. As discussed previously, testing by means of a wind tunnel imposes boundary conditions close to the model being tested when these

boundary conditions would not exist in free stream flow. However, from the comparison of the experimental and numerical results, the imposed boundary condition appears to have very little to no affect on the results being generated.

In Figure 7.29, the results show neither shock wave bending due to the proximity of the wall nor shock wave reflection back onto the aerofoil. Again, the shock wave shape matches very closely with the shape predicted in the numerical result, and it matches across the full visible span of the experimental shock wave. There appears to be no interference from any reflected shock waves since there is no visual indication of any interference as well as the fact that the experimental and numerical results match up well in almost all aspects.

Initially, at 9ms delay, the experimental shock wave position is slightly further downstream than that shown by the numerical result. However, this image is very early in the testing time window and is during the time that the flow is being established. This discrepancy is not unexpected, but just shows that the testing flow has not yet reached its steady state Mach number.

The image obtained at 12ms delay shows an improvement in the shock wave position agreement while at 15ms the two results match almost perfectly.

At a delay of 21ms, there is a slight change in the shock wave position on the lower surface of the aerofoil, while the upper shock wave position is virtually unchanged. The reason for the slight upstream movement of the lower shock wave is explained by the fact that each image is composed of two test runs, both of which occur under slightly differing conditions. The lower surface test was run at a slightly lower Mach number than the upper surface test, and thus, a slight upstream movement of the shock wave is acceptable.

The image shown for 30ms shows the shock waves slightly further downstream than the CFD results. This is explained by the slight increase in flow Mach number as the testing time increases. This increase in flow Mach number is caused by the slight thickening of the boundary layer along the length of the shock tube and results in a decreasing flow area with time, thus causing the flow Mach number to increase slightly.

Generally, all of the experimental images from 12ms upwards show the formation of the lambda shock system as previously discussed. The position, shape and layout of the shock system closely resemble the system predicted numerically. The only images where the lambda shock system cannot be said to closely resemble the numerical result are those at 9ms and 30ms, where the lambda shock system is difficult to define visually in the experimental result.

7.2.3 Testing at Mach 0.73

In order to ensure that the wind tunnel was operating correctly across the full transonic range, testing was carried out at the lower end of the Mach range. Due to the low Mach number chosen for the testing, it was expected that the transonic shock waves would be very weak and, as a result, it was decided that testing at an angle of attack of 2.79 degrees would yield images that were likely to contain at least a single transonic shock on the upper surface of the aerofoil.

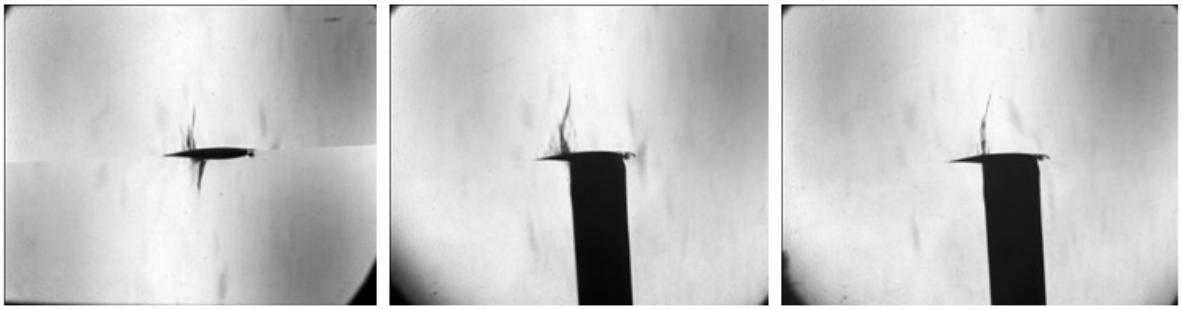


Figure 7.30 Mach 0.73 at 2.79º angle of attack with open walls

Testing was carried out using time delays that would fall in approximately the middle of the testing window.

Due to the angle of attack and the low Mach number, it was expected that a transonic shock wave would only form on the upper surface of the aerofoil. As a result of this, for the sake of completeness, the testing was performed largely only on the upper surface of the aerofoil, with only a single delay time on the lower surface.

The most prominent feature of all of the test images is that while a transonic shock wave is visible, it does not extend far outward from the surface of the aerofoil and lacks the clear form that was shown in the images from testing at Mach 0.83. Across the testing time delays, the shock waves are not as apparent as before, and also appear slightly spiky in form.

As expected, no lambda shock system is visible due to the relative weakness of the normal shock wave being produced.

Interestingly, in the image from a time delay of 21ms, a very small shock wave has appeared on the lower surface of the aerofoil. It extends only a small distance into the surrounding flow.

Comparison to Numerical Results

As before, it is useful to make a comparison between the features displayed during physical testing and those features predicted by the computational fluid dynamics results.

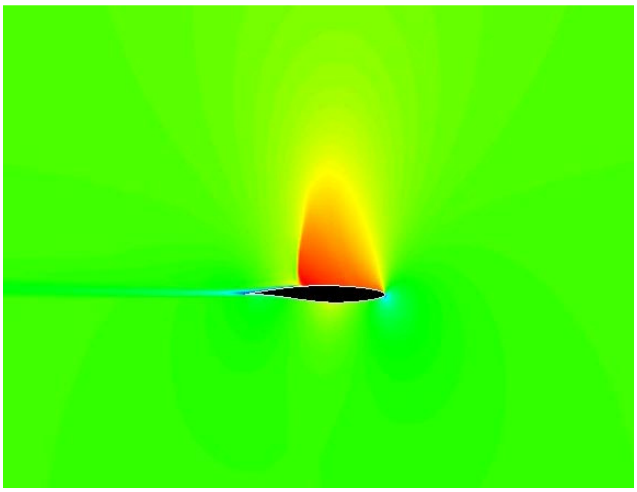


Figure 7.31 CFD at Mach 0.75 and 2.79º angle of attack

The most obvious feature of the image in Figure 7.31 is the lack of any transonic shock waves on the lower surface of the aerofoil. Due to the fact that the aerofoil is at an angle of attack of 2.79 degrees, it is expected that any shock wave that formed on the lower surface would be of a lower strength than that found on the upper surface. Since the shock wave on the upper surface does not extend very far into the flow and the fact that it is visibly quite a weak shock wave, it is unsurprising that no shock wave would form on the lower surface.

However, upon inspection of the flow around the lower surface of the aerofoil, it is apparent that there is a region of high subsonic flow as indicated by the yellow area. Thus, while the image shows no distinct shock wave on the lower surface, one would form if the flow Mach number were to increase slightly.

The wake region downstream of the aerofoil is seen as a thin line with very little dark blue indicating a lack of turbulence. This result is not unexpected since the shock wave formed on the upper surface of the aerofoil is weak and does not have any lambda shock systems associated with it.

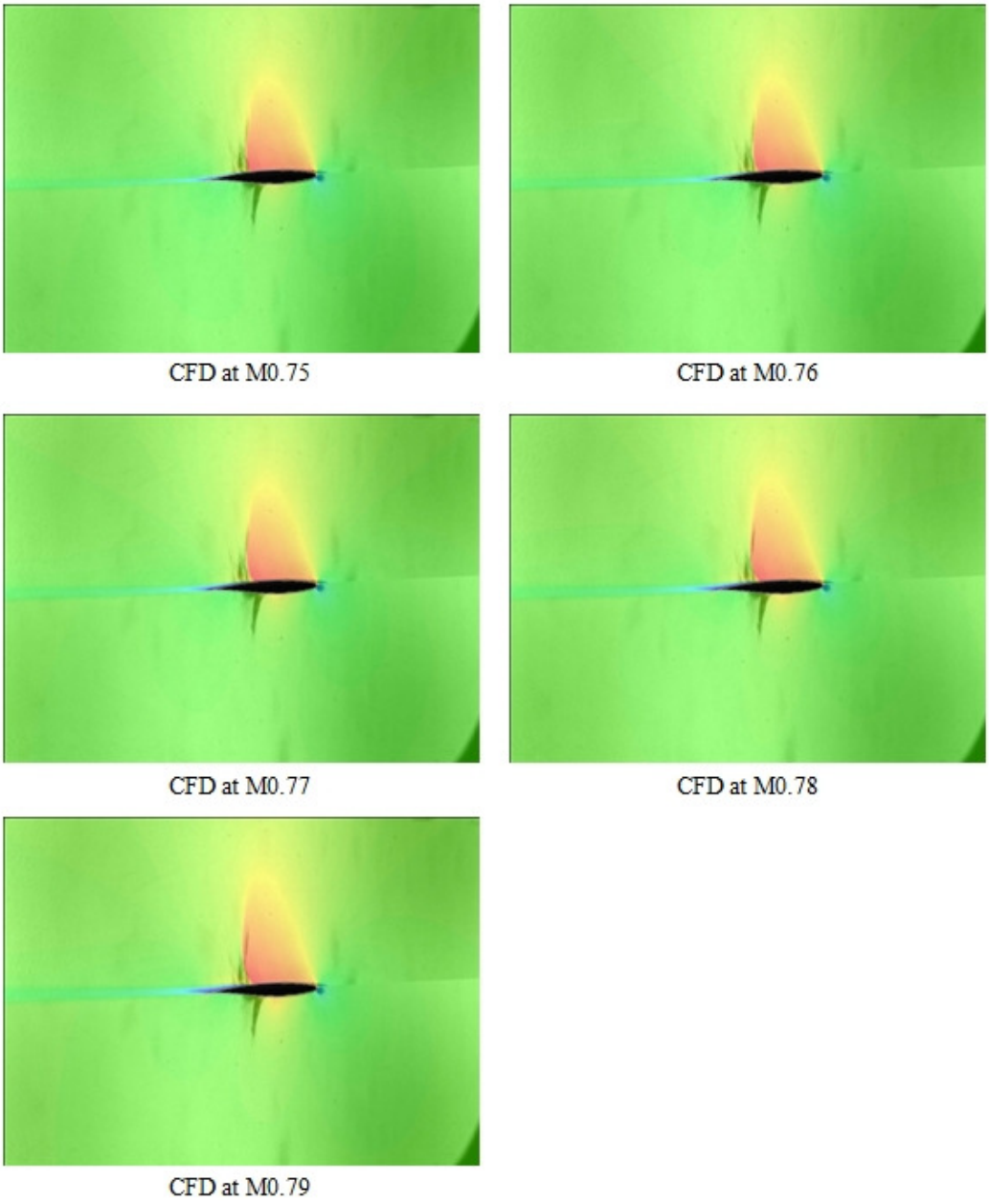


Figure 7.32 Overlay of different CFD Mach numbers onto Mach 0.73 experiment at 2.79º angle of attack

Since the testing was carried out at a theoretical Mach number of 0.73, from the results previously presented, it is expected that a higher Mach number from the numerical testing would provide the closest match.

It is clear that the chord wise position of the transonic shock wave on the upper surface in the numerical results does not change drastically with a change in flow Mach number. However, the transonic shock wave shape does change, as does the relative size of the wake region. These facts make an exact comparison slightly more difficult to generate. However, based on shock wave shape, the numerical test at Mach 0.75 shows the closest correlation to the experimental results. The numerical result at M0.75 does not, however, show a transonic shock wave forming on the lower surface of the aerofoil and this feature is only apparent at approximately M0.78. However, at M0.78 the shock wave on the upper surface has a shape that is different from that found experimentally and so confidence is had that M0.78 is not the Mach number that the test took place at, despite the formation of a small transonic shock wave on the lower surface in the experimental results.

It is quite apparent that as the experimental Mach number approaches that at which transonic shock waves would form, the setup becomes quite sensitive to any discrepancy in Mach number. As a result, it shows that in order for accurate testing to be performed under such conditions, the requirement for instrumentation in the test section is ever more important. However, this small discrepancy in the result does not indicate a failure of the wind tunnel, and is in fact proof that the wind tunnel is capable of producing acceptable results even at the lower end of the transonic Mach number range.

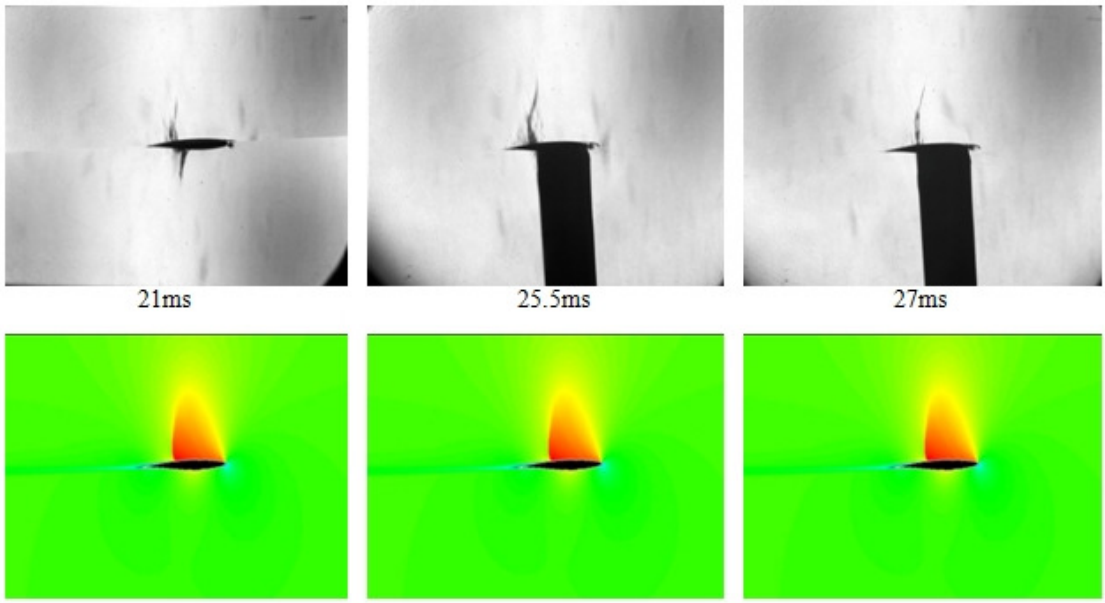


Figure 7.33 CFD at Mach 0.75 compared to experiment at 2.79º angle of attack

The images shown in Figure 7.33 show that the testing Mach number is higher than predicted theoretically, as discussed previously, and that depending on whether the upper or lower surface is being used as the means to establish correlation between the experimental and the numerical results, the Mach number will vary between M0.75 and M0.78. This equates to a range of between approximately 3 to 6% higher than theoretically predicted. That said, the shock wave on the upper surface correlates well with the numerical result obtained at M0.75 and not at M0.78.

General Observations

From the images seen in Figure 7.33 the transonic shock wave on the upper surface of the aerofoil matches the Mach 0.75 numerical result almost exactly. The reason that it is said to match most closely, is because of the shape of the shock wave. The change in chord wise position of the shock wave, especially near to the surface of the aerofoil, is very small with an increase in Mach number. However, further out into the flow, the shock wave position has a more significant change with an increase in Mach number. At the same time, the curvature of the shock wave near the surface of the aerofoil also increases with an increase in Mach number, and these features are used to make the comparison. The extent to which the shock wave propagates into the surrounding flow as well as the curvature and chord wise position of the wave itself, show very close correlation with the numerical result. Interestingly, since the sensitivity of the optical system needed to be increased slightly in order to capture the weak shock waves expected to be produced at the lower Mach number, the extent to which the shock wave propagates outwards matches up with the numerical results to a greater degree than seen previously at the higher Mach number testing.

In addition, a feature not seen previously in the higher Mach number testing is the thin wake region trailing downstream of the aerofoil. The reason this region is now visible is due to the lack of boundary layer separation caused by the stronger shock waves found in the higher Mach number testing.

7.2.4 Testing at Mach 0.91

In order to ensure that the wind tunnel was operating correctly across the full transonic range, testing was carried out at the higher end of the Mach range. Due to the high Mach number

chosen, there was concern that the wind tunnel would choke. This concern was made even more real by the fact that all of the testing performed thus far had resulted in a higher than expected obtained Mach number. Testing at a theoretical Mach number of 0.91 would likely result in an actual test Mach number of approximately M0.96 which results in the setup becoming extremely prone to choking.

In order to establish whether the wind tunnel was working adequately, it was initially decided that testing would be done on the lower surface of the aerofoil which could be expected to produce a slightly weaker shock wave than the upper surface at 2.79 degrees angle of attack.

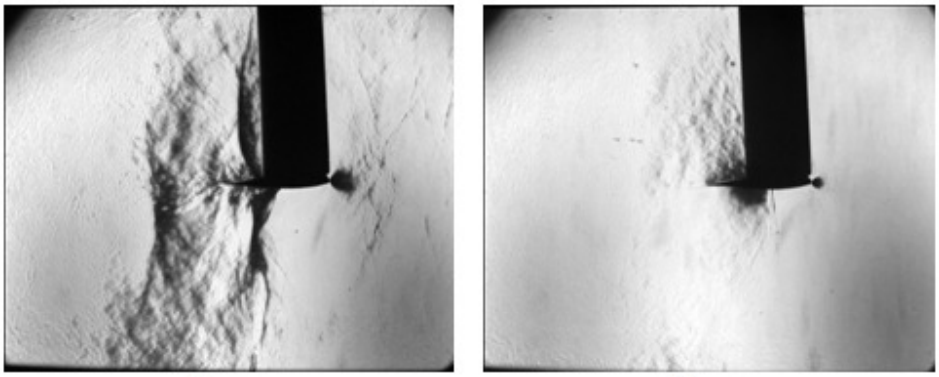


Figure 7.34 Mach 0.91 at 2.79º angle of attack with open walls

Testing was carried out using two time delays, with the initial delay showing the establishment of the testing flow. Due to the high Mach number involved, it was expected that the testing time window would be shorter due to the reflected shock wave and the contact surface arriving faster than before. Thus, the second time delay of 15ms was chosen.

Upon inspection of the image taken at 10ms delay, it is apparent that the transonic flow has been set up and that the transonic shock waves are forming on the upper and lower surfaces of the aerofoil. The flow contains a fair amount of disturbances which is not ideal, but due to the fact that the image was taken after only a short time delay, it is not unreasonable that the flow has not cleared up and become more uniform. A large portion of the visual disturbances are likely caused by the separation of the boundary layer formed along the windows of the test section.

However, once the image at a time delay of 15ms is inspected, it is clear that the wind tunnel is not operating as expected. The transonic shock waves that were initially seen forming on the

upper and lower surfaces in the previous image have now disappeared. There is a feature on the lower surface of the aerofoil, but this feature is not in line with what is expected at this Mach number. Interestingly, the features on the aerofoil bear great resemblance to the features seen during testing at the lower end of the transonic window, near Mach 0.73. As such, despite the lack of instrumentation in the test section capable of determining the actual flow Mach number, it is apparent that the flow Mach number is not at nor higher than the theoretically produced Mach 0.91.

While this is an unexpected result, it is not an unreasonable result and simply shows that testing at the upper end of the transonic window has additional difficulties.

As shown before, all of the testing has resulted in a test flow Mach number higher than that predicted theoretically when considering the pressure ratio across the diaphragm. This test flow Mach number equated approximately to a 6% increase in Mach number from theoretical predictions. Thus, for the test case at Mach 0.91, it is not unreasonable to assume that the Mach number being produced is in the region of Mach 0.96 which is very high subsonic. As the testing flow approaches sonic, the decrease in cross sectional area required to make the flow become sonic gets increasingly small. Thus, at a high subsonic Mach number, only a very small decrease in the cross sectional area is required in order for the wind tunnel to choke.

From the images seen in Figure 7.34, the wind tunnel is initially seen operating as expected at 10ms delay. However, only a short amount of time later, the flow has changed completely and no transonic shocks are visible. It is therefore safe to assume that by the time the image was taken at 15ms delay, the wind tunnel has choked somewhere upstream of the test section resulting in testing flow of a Mach number which was much lower than expected. The reason for the sudden change during the time delay between 10ms and 15ms is likely due to the build up of the boundary layer with time. An increase in boundary layer thickness will result in an effectively reduced cross sectional area and, as discussed earlier, the cross sectional area does not need to change by much in order for the system to choke.

From the explanation given, it is safe to assume that testing of the upper surface of the aerofoil under the same conditions would yield very similar results and thus it was decided to abandon the very high Mach number testing at this stage.

Furthermore, it is clear that any form of comparison to the numerical results would yield an unsurprising lack of correlation between the two. As a result of this fact, the exercise was not carried out.

Comparison of Pressure Plots

Due to the fact that the results obtained represent the upper limit of the Mach number that the wind tunnel is capable of producing, it is of interest to see whether any indications of what has changed during the operation of the tunnel can be seen in the pressure traces obtained during the testing in question. As a result, the pressure trace produced during the experimental run that produced the image in Figure 7.34 at a time delay of 15ms was overlaid with the pressure trace obtained during testing at Mach 0.83, where the results were very good.

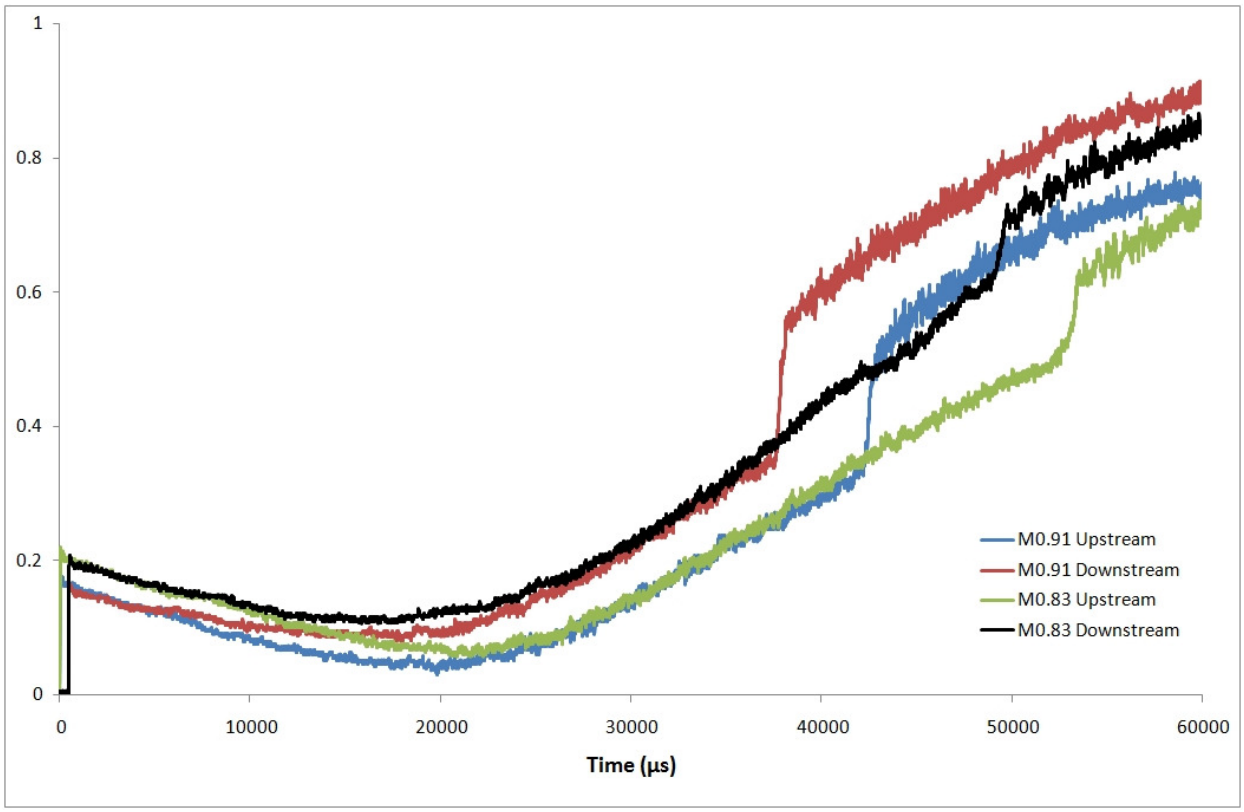


Figure 7.35 Pressure trace overlay for testing at M0.91 and M0.83

It is apparent from the image in Figure 7.35 that the testing at Mach 0.91 exhibited largely the same features in the pressure plot as those found in the pressure plots created during testing at Mach 0.83. The main difference between the two pressure plots is that the one created during testing at Mach 0.83 takes longer before the arrival of the reflected wave, and the spike in pressure upon arrival of the reflected wave is larger on the Mach 0.91 test. These features are in line with what is expected from the pressure plot since at Mach 0.91 everything will happen at a smaller time delay and with slightly greater intensity.

There are, not unexpectedly, slight differences in the gradients of the graphs at various points and other similar discrepancies, but there are no other major differences between the two pressure plots. There are certainly no apparent differences that would indicate that the wind tunnel is not operating correctly.

7.2.5 Predicted versus actual testing time

Theoretical testing times based on the various arrivals of wave features at the test section were predicted using Kasimir3. Of course, there are a number of assumptions present in the results that are displayed by the program and, as such, the effect of these assumptions needs to be clarified in order to establish how the actual testing time related to the predicted theoretical testing time.

One of the key assumptions made by the Kasimir3 program is that there are no losses incurred during the passage of the incident shock wave or any of its associated reflected shock waves. The same applies to the passage of the contact surface and the resulting flow itself. Due to the fact that the shock tube in question is more than 40 meters long and constructed from very rough construction tubing, this assumption is quite poor. As shown previously, the incident shock wave experiences great losses at each joint in the tubing, as well as along each length of tubing it needs to propagate through. Hence it is safe to assume that the reflected wave off the end of the shock tube and the contact surface will experience similar losses.

Theoretical testing time was calculated by taking the time at which the incident shock wave passed through the test section and subtracting it from the time at which the reflected shock wave and contact surface arrived in the test section. As discussed previously, the shock tube is considered to be optimised when the contact surface and the reflected shock wave arrive in the test section simultaneously. Of course, it is clear that this theoretical optimisation is only true

provided all the assumptions made in the process are true, which is not the case. As such, it is of interest to establish what the approximate testing time was, based on the pressure traces obtained during the various tests performed.

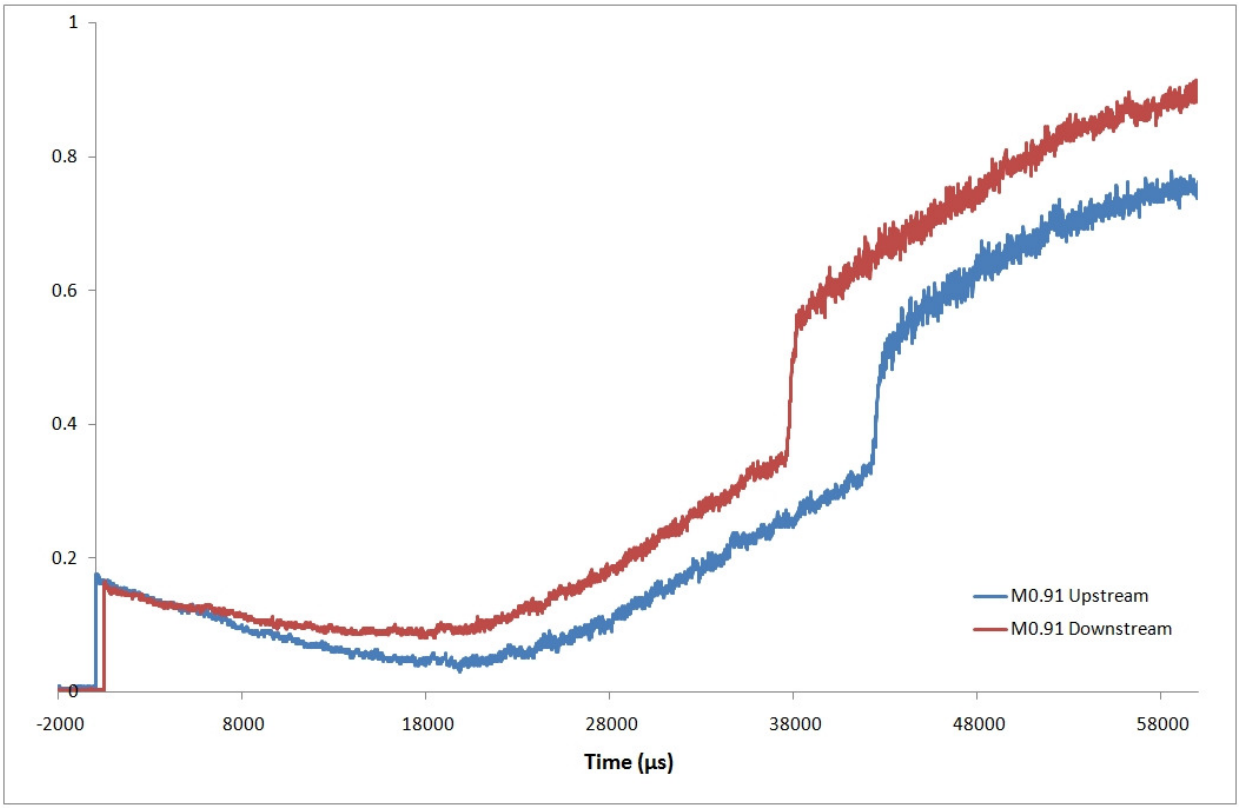


Figure 7.36 Pressure trace for flow at M0.91

At time 0ms, the incident shock wave has reached the upstream pressure transducer and after another few milliseconds, reaches the downstream transducer. At this point, and at an incident shock Mach number of 1.91, the shock wave is 1.4 milliseconds from the leading edge of the test piece. This will signal the start of the testing time. The reason for the delay between the two vertical spikes from each pressure transducer is the fact that they are spaced 300mm apart. Using this known spacing, and the time delay between each spike, the shock wave velocity is simple to calculate.

After a short amount of time, the steady readings from the two pressure transducers become slightly disturbed and the pressure reading starts to increase. This feature is first seen on the downstream pressure transducer, and then on the upstream one, indicating that the feature causing

the disturbance is travelling from the test section, upstream towards the transducers. This feature is the reflected shock wave that originated at the test piece as the incident shock wave passed by. The reflected wave can be seen in its early stages in Figure 7.6 at 0.06ms.

After some time, there is another pressure spike, and again the downstream pressure transducer registers the spike before the upstream transducer does. This is the reflected shock wave off the end of the shock tube, and clearly signals the end of the available testing time. Of course, by the time the downstream transducer has registered the reflected shock wave, it has already passed through the test section. Thus the available testing time will be from when the incident shock wave has passed over the test piece until when the reflected shock wave enters the test section and destroys the flow. Theoretically this should be met with the simultaneous arrival of the contact surface which would similarly destroy the testing flow.

Naturally, the features that are shown in Figure 7.36 are occurring in the cleanup section upstream of the test section. Thus, simply taking time readings off the pressure trace would yield an incorrect testing time value. However, since the distance from the pressure transducers to the test piece is known, the testing time can still be calculated from the pressure traces since it is clear that the start of the test window will be upon passage of the incident shock wave through the test section, and the test flow will break down upon the return of the reflected shock wave.

The test window is calculated as the time difference between passage of the incident shock wave over the test piece and the passage of the reflected shock wave over the test piece. From the pressure trace, both of these wave velocities can be calculated, and with the knowledge of the distance from the transducers to the test piece, the exercise becomes trivial.

Table 7.3 Theoretical and experimental testing times

	Testing Time (ms)	
Flow Mach No'	**Kasimir**	**Experiment**
M0.73	26.3	39.0
M0.83	24.9	37.8
M0.91	22.7	25.2

The testing times found using Kasimir3 are based solely on theory for the testing position chosen and do not take any form of losses into account while assuming that the end of the shock tube is a solid wall. Experimentally, there are significant losses that occur throughout the system and the end of the shock tube consists of a weak diaphragm which ruptures when exposed to a sudden

increase in pressure. Clearly the two situations are significantly different. However Table 7.3 contains results that are both expected and unexpected.

The Kasimir3 predictions show an obvious decrease in testing time with an increase in flow Mach number which is reasonable, given the increased Mach number of the incident shock wave and resulting flow. The experimental testing times follow a similar trend although the difference between testing times at Mach 0.73 and 0.83 is a lot smaller than that between Mach 0.83 and 0.91.

Clearly the testing times predicted by Kasimir3 are lower than the experimental testing times, since they are predicted assuming a solid boundary at the end of the shock tube, which is a poor assumption. The rupturing of the diaphragm at the end of the shock tube would drastically affect the reflected shock wave and thus would result in much greater testing times being experienced experimentally.

The experimental testing times are not much lower than the testing times predicted by Kasimir3 for the optimal test position shown in Table 4.1. In addition the testing times are high in comparison to similar facilities in existence and the resulting images demonstrate that the testing time is more than adequate to set up the semi-steady, transonic flow required to produce accurate transonic wind tunnel tests.

8 Conclusions

A transonic wind tunnel was designed, constructed and calibrated making use of the principles of operation of a shock tube in order to create transonic flow. Simple transonic testing was performed on a test piece with well documented flow characteristics in the transonic flow regime, in order to validate the functioning of the wind tunnel. A numerical study was carried out on the same test aerofoil in order to compare computational fluid dynamics results with the experimental results.

Upon completion of the finished shock tube, calibration was carried out in order to establish how the shock tube functioned. It was found that due to the rough internal surfaces of the industrial tubing used to create the lengths of the wind tunnel, as well as their corresponding joints, that the incident shock wave Mach number needed to be much higher than originally predicted. This resulted in the requirement for a significant vacuum to be drawn in the driven section of the shock tube. It was established that under the vacuum conditions, the pressure ratios needed to create the incident shock wave of the required strength were easily obtainable.

A diaphragm of the required thickness was then found in order to predictably and reliably activate the shock tube at the required pressure ratios. Once the shock tube had been calibrated, actual testing was relatively simple to perform.

Initial images taken of the establishment of the flow showed a distinct reflected shock wave off of the test piece as well as other shock reflections occurring off the various surfaces in the test section. After approximately 4.45ms, these reflections had largely disappeared and clear transonic shock waves were seen on the aerofoil. The flow around the aerofoil was largely clear of unwanted features. During testing, it was found that images taken at a time delay of approximately 9ms showed that the flow had been established correctly, but had not yet reached the semi-steady state that was seen at slightly later time delays.

Numerical results were created at various Mach numbers and at 0º, 2.79º and 5º angle of attack, corresponding to the angles of attack that were tested experimentally. The numerical results were created using Mach number increments of M0.1 in order to ensure that a discrepancy in the

experimental Mach number would not result in the inability to make a comparison between the numerical and experimental results.

Experimental testing occurred under various flow, test piece and test section conditions. A key aspect of the design of the wind tunnel was the design of the test section upper and lower walls to ensure that shock wave cancellation took place while simultaneously ensuring that the wind tunnel did not choke at too high a test Mach number.

A slotted wall layout was chosen over a perforated wall due to flow conditions expected during testing. Two key features of the perforated wall type were its inability to function correctly with an increase in boundary layer thickness and the fact that it was likely that each perforation would create slight disturbances which would propagate outward into the region around the test piece. Both of these features did not suit the test section design and expected flow conditions and so choosing the slotted wall eliminated these features.

A wall boundary with easily changeable geometry and layout was created so that the effects of varying the open area ratio of the wall could be established. The testing carried out clearly demonstrated that at a wall open area ratio of 50%, the results produced throughout the transonic Mach number range, and for various test piece angles of attack, correlated very well with the numerical results. Testing carried out at an open area ratio of 10% showed extremely poor correlation with the numerical results, showing that the correct selection of wall open area ratio was vital in obtaining useful experimental data.

The numerical results showed a noticeable downstream movement of the transonic shock waves with an increase in flow Mach number. At the same time, with an increase in angle of attack, a relative strengthening of the shock wave on the upper surface of the model along with a relative weakening of the shock wave on the lower surface was seen. Both of these features were reproduced through experimental testing using the 50% open wall layout.

The numerical results showed the formation of a lambda shock system when the transonic shock waves reached a given strength. These lambda shock systems generally resulted in distinct wake regions trailing downstream of the aerofoil. Again, the experimental results accurately reproduced these lambda shock systems and their corresponding wake regions when testing was performed with the 50% open walls.

The numerical and experimental results correlated well with one another when the transonic shock wave shape was considered. For the most part, the shape, chord wise position, and extent to

which the shock wave propagated into the surrounding flow domain correlated extremely well when the experimental results using 50% open walls were compared with the numerical results.

Due to the lack of instrumentation in the test section, the actual flow Mach number could only be found theoretically. Upon comparison with the numerical results however, it was found that in all testing cases, numerical results at a higher Mach number showed the best correlation between the two. This was a clear indication that the testing Mach number was in fact higher than predicted. However, the numerical results at the higher Mach number correlated with the 50% open wall test results extremely well. It was decided that the increased Mach number was due to the boundary layer growth with time, during the testing. Despite these facts however, the flow was at a semi-steady state for the majority of the testing time window, once the flow had been established.

The upper and lower limits of the testing Mach range were established. Since the only method of studying the flow around the test piece was using schlieren, it was clear that testing at a Mach number at which transonic shock waves did not form would be of little interest. Testing was carried out at a theoretical Mach number of 0.73 and showed that weak transonic shock waves had formed on both upper and lower surfaces. Comparison of the experimental result to the numerical result at M0.75 showed a good correlation of the image on the upper surface of the aerofoil. The numerical results however showed that a small transonic shock wave would only form on the lower surface of the aerofoil at approximately M0.78. Therefore it was concluded that at the lower end of the testing Mach range, the experimental setup became quite sensitive for the establishment or non-establishment of transonic shock waves. It did not indicate a failure of the experimental setup however.

Testing at the upper limit of the transonic Mach range showed a limitation in the experimental setup. Testing was carried out at a theoretical Mach number of M0.91. As was the norm with the test results, it was expected that the actual Mach number achieved would be in the region of Mach 0.96. At a Mach number this close to unity, the experimental setup was extremely prone to choking. The experimental results initially showed that the transonic flow was being established as before. However later on in the testing time window, no transonic shock waves could be seen, indicating that the wind tunnel had choked. It was therefore clear that testing at a high subsonic Mach number was not possible.

The testing performed at 5º angle of attack resulted in very strong transonic shock waves forming on the upper surface of the aerofoil. These strong waves extended further out into the flow domain, very close to the slotted walls. No shock wave reflection was seen to occur at the wall

and the shock waves did not get artificially bent due to the proximity to the wall. This showed that the slotted walls were operating as expected when laid out with the 50% open area ratio.

The theoretical testing time predicted by the Kasimir3 program was found to be lower than the testing time found during experimentation. It was decided that this fact was partially due to the losses experienced by the incident shock wave and its resulting flow features as it propagated down the shock tube. However, the main cause for the increase in testing time was the assumption that the end wall of the shock tube was a solid boundary, where the experimental setup had a weak diaphragm that would burst under only a small increase in pressure. This fact meant that the reflected shock wave would be weakened when compared to the theoretical shock wave and so would arrive back at the test section at a later time instant than predicted.

The testing times experienced during experimental testing were found to be more than adequate to establish semi-steady flow. The shock waves and corresponding flow features set up on the test piece varied very little in shape, chord-wise position and composition once the initial flow establishment had taken place, showing that the flow Mach number had little variance during the testing time window.

In general, the wind tunnel operated as designed, provided the test section open wall layout was correctly selected at 50% open and that the Mach number did not exceed a theoretical Mach number of approximately M0.9.

During the experimental work, it became evident that the experimental setup could be improved upon in the future.

Since each test time delay required two tests to obtain a single image, it is clear that a high speed camera would be hugely useful in reducing the number of tests required. Two tests would be required to obtain upper and lower images for all time delays throughout the testing time window. In addition, it would be simple to establish the exact moment at which the testing flow broke down and thus testing times would be easy to predict.

Placing instrumentation into the test section would also be beneficial in determining the velocity variation throughout the test section, as well as determining the actual Mach number of the flow for a given test run. It is essential that the correct instrumentation of the test section takes place in order to further develop the facility by gaining a greater understanding of the properties of the flow throughout the test section.

It is thus recommended that the abovementioned suggestions are implemented for future studies in order to obtain the best possible results from the minimum number of test runs when making use of the facility.

References

Alshabu, A., & Olivier, H. (2008). Unsteady wave phenomena on a supercritical airfoil. *AIAA Journal, Vol 46, No. 8* , 2066-2073.

Ben-Dor, G., Igra, O., & Elperin, T. (2001). *Handbook of shock waves, Vol. 2.* Academic Press.

Bernt, S. B. (1955). *Ph.D Thesis - On the influence of wall boundary layers in closed transonic test sections.* Pasadena: California Institute of Technology.

Bruhn, E. F. (1973). *Analysis and Design of Flight Vehicle Structures.* Jacobs Publishing Inc.

Doyle, G. K. (1998). *Ph.D Thesis - Shock wave interactions with porous beds.* Johannesburg: University of the Witwatersrand.

Fluent Inc. (2006). *Fluent 6.3 Validation Guide.* Fluent Inc.

Geiger, F. W., & Mautz, C. W. (1949). *The shock tube as an instrument for the investigation of transonic and supersonic flow patterns.* Washington D.C.: Engineering Research Institute, University of Michegan.

Glass, I. I. (1959). *Shock Tubes, Part I: Theory and Performance of Simple Shock Tubes.* UTIA Review, No. 12, Institute of Astrophysics, University of Toronto.

Goethert, B. H. (1961). *Transonic Wind Tunnel Testing.* Pergamon Press.

Jang, H. K., Kim, M. S., Kwon, J. K., Kim, B. J., & Kwon, S. B. (2004). *Transonic double wedge airfoil flow in shock tube.* Kyungpook National University.

Kasimir3. (1993). *Shock tube simulation program.* RWTH Aachen.

North Atlantic Treaty Organisation - Fluid Dynamics Panel. (1979). *Agard Adivsory Report No. 138.* London: Agard.

Olivier, H., Reichel, T., & Zechner, M. (2003). Airfoil flow visualization and pressure measurements in high-Reynolds-Number Transonic Flow. *AIAA Journal, Vol 41, No. 8* , 1405-1412.

Rabinowicz, J. (1957). *Ph.D Thesis - Aerodynamic studies in the shock tube.* Pasadena: California Institute of Technology.

Rohani, H. (2010). *Ph.D Thesis - Aerodynamic effects of accelerating objects in air.* Johannesburg: University of the Witwatersrand.

Settles, G. S. (2001). *Schlieren and Shadowgraph Techniques: Visualizing Phenomena in Transparent Media.* Springer-Verlag.

Skews, B. W. (2007). *Compressible Flow - Course Notes.* Johannesburg: School of Mechanical Engineering, University of the Witwatersrand.